

Report No. MTI-68TR61

DESIGN MANUAL

EXTERNALLY-PRESSURIZED STEAM-LUBRICATED JOURNAL-BEARINGS

edited by
s.b. malanoski

Contract No. N00014-65-C0214

MTI Project No. 10495

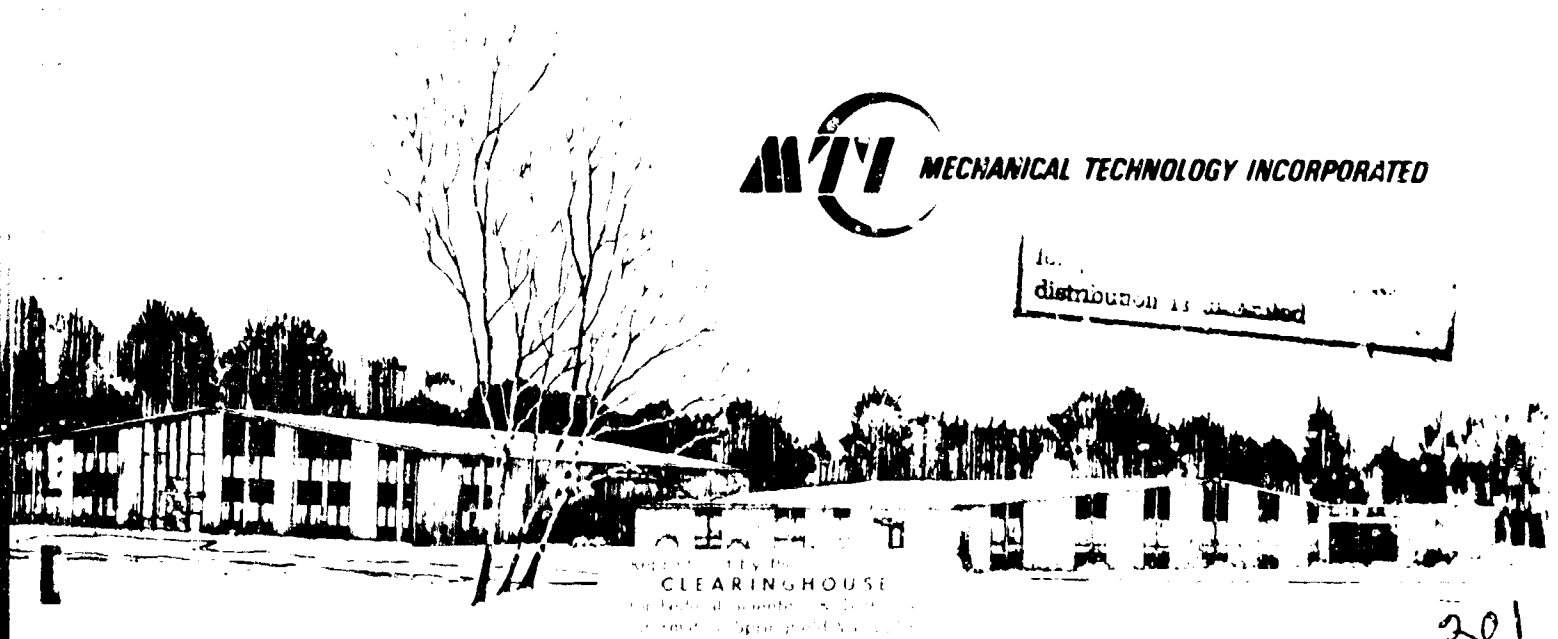
December 1968

DDC
REFORMED
FEB 27 1969
RESERVED
B

AD 682990



distribution is restricted



MTI
CLEARINGHOUSE
for technical documents and drawings
in mechanical engineering

NO. MTI-68TR61

DATE: Dec. 30, 1968

TECHNICAL REPORT

DESIGN MANUAL EXTERNALLY-PRESSURIZED, STEAM-LUBRICATED JOURNAL BEARINGS

Editor: S. B. Malanoski

Contributors: J. Bjerklie S. F. Murray

J. Lund F. K. Orcutt

S. B. Malanoski C. H. T. Pan

Editor

Stanley B. Malanoski

Walter G. Smith

Approved

Prepared for

Office of Naval Research
Department of the Navy

Prepared under

Contract N00014-66-C0214
MTI No. 10495

Reproduction in Whole or in Part is Permitted
for any purpose of the U.S. Government

MTI
MECHANICAL TECHNOLOGY INCORPORATED
MTI

968 ALBANY - SHARER ROAD LATHAM, NEW YORK -- PHONE 785-0922

GENERAL
TABLE OF CONTENTS

	<u>Page</u>
FORWARD	iii
CHAPTER I DESIGN PROCEDURES	1
CHAPTER II SUMMARY OF EXPERIMENTAL RESULTS	25
CHAPTER III BEARING DESIGN METHODS AND DATA	59
CHAPTER IV EXPERIMENTAL EVALUATION OF THREE STEAM PROCESSING UNITS	127
CHAPTER V THERMAL DESIGN GUIDE	157
CHAPTER VI SUGGESTED MATERIALS	178

FOREWORD

High pressure steam supply is an economical means to achieve process fluid lubrication. This prospect is particularly attractive for rotating power conversion machinery in which the steam turbine provides the driving power. The obvious advantages are:

- Elimination of the oil lubrication system saves maintenance requirement, improves reliability, avoids fire hazards, and reduces nuisances such as oil-vapor fouling and noises.
- Use of steam bearings in hot zones minimizes temperature gradients and the associated mechanical problems.
- Cost for generating high pressure steam is relatively modest.

Considerations in the design of steam bearings are quite similar to those in the design of gas bearings. In fact, if the steam can be maintained at a superheated state at all times, every aspect known of the gas bearing would be directly applicable. However, if the supply steam is either saturated or slightly wet, additional complications arise due to the possibility of liquid-vapor phase changes. Consequently material problems related to erosion and corrosion must be resolved, thermodynamic properties become important, and heat transfer effects are of utmost importance. Under the sponsorship of the Office of Naval Research, a number of research and development studies have been carried out at MTI with the aim of establishing practicable guidance for the design of steam-lubricated bearings with a saturated supply. This document consolidates the pertinent findings related to the design of steam-lubricated journal bearings.

This manual consists of six chapters, the titles of which are listed on the preceding page. All but the first chapter is written as a complete, topical report. The first chapter entitled, "DESIGN PROCEDURES", contains an illustrative design problem, and brings together the essential contents of the other five chapters to give a cohesive account of the latest information on the design of steam-lubricated externally-pressurized journal bearings.

CHAPTER I
DESIGN PROCEDURES

CHAPTER I
TABLE OF CONTENTS

	<u>PAGE</u>
INTRODUCTION	3
Functions and Requirements	3
Related Problems and Their Solutions	4
Design Parameters	5
PRACTICAL DESIGN EXAMPLE	9
REFERENCES	20
NOMENCLATURE	21
INDEX	23

INTRODUCTION

By definition, a bearing is a machine part which supports a load and allows a journal to turn, or rotate. An externally-pressurized steam-lubricated journal bearing is such a part that performs with the use of a high pressure steam supply. Thus, when designing an externally-pressurized, steam-lubricated bearing one must be aware of not only the bearing design itself, but also the rotor and the external steam supply and related hardware.

The overall bearing design should be influenced by the functions and/or requirements of the bearing, such as load-carrying capacity and stiffness; the related problems that can arise during operation, such as steam erosion, thermal distortion and shaft instabilities; and previous solutions of these problems based on theoretical and experimental experiences such as material selection and choice of mechanical design. Thus, the objective of this chapter is to outline design procedures, utilizing a practical design example with reference to the other five chapters of this manual which cover experimental experiences, bearing performance, thermal design, bearing materials, and steam processing.

Functions and Requirements

The function of the externally-pressurized, steam-lubricated, journal bearing is to carry applied radial, and moment loads, while maintaining a steam film between the sleeve and the journal. The bearing is to be designed to withstand thermal distortions, angular misalignment, momentary overloading and to avoid instabilities. Geometrical simplicity is desired to avoid excessive manufacturing costs. Because the bearing is externally-pressurized, the designer must concern himself with the external steam supply system and related hardware such as filters, separators and traps, and furthermore since the lubricant is steam one must deal with high temperature materials and mechanical design concepts.

Upon stating the functions and requirements of a bearing, one immediately becomes aware of the problems that can arise - thermal stresses, instabilities, material erosion, and, etc.

Related Problems and Their Solutions

The externally-pressurized steam bearing has the normal problems associated with rotor-bearing systems, the problems of externally-pressurized gas bearings, the problems of high temperature bearings and finally its own inherent problems.

Since all gas bearings have relatively low damping characteristics compared to oil lubricated journal bearings, the rotor-bearing critical speeds and response to dynamic load must be given a considerable amount of attention and analysis in design. Another problem that arises is the alignment of the bearings with respect to the rotating shaft. In small machines, this problem may be solved by boring or grinding the bearings in-line. However, in large machines alignment is usually obtained by mounting the bearings on flexures (self-aligning mountings.)

The problems that arise in all externally-pressurized gas bearing systems are of two basic varieties; the first, is related to the design of the external gas supply system which must satisfy the pressure and flow requirements of the bearing, and the second is related to instabilities that can occur in an externally-pressurized gas bearing. There are three instabilities and these are named, 1) lock-up, 2) pneumatic hammer, and 3) hydrodynamic instability, or fractional frequency whirl. All of these instabilities can be avoided by proper design. Lock-up can be prevented by providing for a sufficient number of restrictors in the design, and sizing the bearing to carry all loads while allowing the journal to be displaced a maximum of half the radial clearance. The second instability, pneumatic hammer can be avoided by designing with inherently compensated restrictors. Orifice restriction will provide a bearing with greater stiffness, however, this type of restriction is prone to pneumatic hammer instability and restrictor design and operating conditions must be chosen carefully. The third instability is inherent with hybrid bearings^{*}, and hydrodynamic instability occurs when the shaft speed is in excess of the first rigid body critical speed by a factor of approximately 1.6. The problems of high temperature

*A hybrid bearing is a bearing that has both hydrostatic (externally-pressurized) and hydrodynamic effects.

bearings are essentially thermal distortions and stresses. These are eliminated or curtailed by design - use of self-aligning mounts, proper selection of materials, and the fabrication of the bearing parts with proper clearances.

Additional problems must be considered when the bearing lubricant is high pressure, saturated steam. There are three significant ones; namely, steam hammer instability, material erosion in the restrictor regions, and the steam delivery system, including the piping, filtering, separating and trapping. The first problem, steam hammer, can be avoided by using the "unitized bearing" design, with proper condensate separating and trapping. Just as the use of inherent compensation is the most straight forward step in avoiding pneumatic hammer, the use of the unitized bearing design is the best, first step in preventing steam hammer. The material erosion and wear problem is minimized by designing with the proper materials. The problem of the steam-delivery system is multi-faceted with the major concern being to remove all or nearly all entrained moisture from the supply steam. This can be done by the use of commercial separators. Filters to remove entrained solid particles and effective pressure regulation are additional steam supply system considerations:

Design Parameters and Design Direction

The solution of the externally-pressurized, steam-lubricated journal bearing design problem is quite straight-forward when one considers the appropriate design parameters and available design direction.

Analytical design guidances concerning the bearing performance and thermal design are presented in detail in Chapters III and V respectively.

The bearing performance data is a function of five parameters: the slenderness ratio, L/D , the restrictor coefficient, $\Lambda_g \xi$, the pressure ratio, P_g/P_a , the eccentricity ratio, ϵ , and the squeeze number, σ .

The slenderness ratio is the ratio between the bearing length, L , and the journal diameter, D . A very narrow bearing has a slenderness ratio which approaches zero. A very long bearing has a slenderness ratio approaching

infinity. The typical design range is between one-half and two. Axial spacing and bearing alignment usually dictate a slenderness ratio less than one whereas the thermal design, load-capacity and stiffness requirements dictate a slenderness ratio greater than, or at least equal to, one. A good choice is a bearing with the slenderness ratio equal to one.

The restrictor coefficients, $\Lambda_s \xi$, is the ratio between the flow resistance of the steam film and the flow resistance of the feeding holes. The feeding holes must be designed such that they restrict the flow and produce a pressure drop at the entrance to the film. When the feeding holes are restricted, the bearing possesses stiffness. However, if the restriction is so large that the pressure drop through the feeding holes absorb all the available supply pressure, the downstream pressure approaches the ambient pressure and the bearing stiffness and load capacity approaches zero. It becomes evident that there is an optimum amount of restriction at which the bearing stiffness is a maximum. This optimum value of the restrictor coefficient occurs at approximately, $\Lambda_s \xi = 0.7$.

The third design parameter, the pressure ratio, P_s/P_a is a ratio between the supply pressure and the ambient pressure. This parameter is related to the total pressure drop, $P_s - P_a$, which is important in sizing the bearing to carry a given load. A typical range of the pressure ratio is from 3 to 20. Normal designs have a pressure ratio of approximately 10.

The bearing eccentricity ratio, e , is the ratio of the displacement of the journal center to the radial clearance. If the eccentricity ratio is zero there is no displacement — no load. When the eccentricity ratio is one the journal is touching the bearing — maximum load. In an externally-pressurized bearing the load is nearly linear with displacement up to an eccentricity ratio of 0.5. Normal operation should be at, or less than, an eccentricity ratio of 0.5.

The fifth design parameter, the squeeze number, σ , is the key to the dynamic performance of the bearing. This performance is characterized by the bearing's stiffness and damping properties, and by the stability of the bearing. In most applications, the natural frequencies of the system, such as the critical speeds of the rotor, are predominantly determined by the bearing stiffness, the

response of the system to vibratory forces (usually synchronous with the rotating speed) depend strongly on the damping present in the bearings. Furthermore, the dynamical forces can induce self-excitation and thereby make the bearing unstable. It is, therefore, necessary that data be available to the designer from which both the stiffness and damping coefficients and also the bearing stability can be determined.

Other secondary, bearing design, parameters are the clearance ratio, C/R and the number of feeding planes and feeding holes.

A clearance ratio of one mil/in. is normally a good choice. A decrease in clearance will decrease the steam flow by a factor of the clearance cubed and increase the stiffness linearly. However, a smaller clearance also means that the manufacturing tolerances could be more critical and also the bearing is more sensitive to dirt and distortion.

The question of single plane versus double plane feeding is largely a question of how critical it is to obtain the highest possible load and stiffness. From the standpoints of thermal design and fabrication a steam bearing with a single plane feed is the best choice.

The number and size (diameter) of the feeding holes provide a means to optimum performance. By adjusting these, the optimum value of the restrictor coefficient can be obtained. Normally, the number of holes per feeding plane should be set at a minimum of from 6 to 8. Also, the circumferential hole spacing should be compatible with the axial flow path. The diameter of the feeding holes usually range from 0.030 to 0.120 inches.

The bearing thermal design data is a function of one primary parameter, $L/D\sqrt{\Delta}$. L/D is the slenderness ratio, previously discussed. And Δ is a parameter composed of the clearance ratio, the bearing and shaft wall thickness, and the thermal conductivity of the steam, the shaft material, and the bearing material. This parameter is a derivative of the heat transfer analysis performed on the "unitized bearing". The unitized bearing is a particular bearing design which consists of a dual-manifold arrangement. This arrangement

includes a jacketing steam header to control the bearing and shaft temperature with little loss of heat from the steam in the separate steam header which supplies the bearing film. The jacketing header is filled with condensing steam above the supply header pressure. The shaft and bearing temperatures are thus maintained close to the supply steam saturation temperature because this condensation of steam in the jacketing header supplies the heat losses.

The basic guide to minimize the formation of condensation and thus minimize evaporation within the steam film which in turn enhances the protection against steam hammer instability is to minimize the clearance ratio, the shaft and bearing wall thickness and the thermal conductivity of the shaft material, and to maximize the slenderness ratio and the bearing thermal conductivity. A typical operating range of $L/D\sqrt{\Delta}$ is from 0.75 to 4.0. Experience indicates that one should design with $L/D\sqrt{\Delta} \geq 2$.

Important empirical experiences obtained in MTI's development studies in steam bearing lubrication are reported in Chapters II, IV and VI. Many items must be considered in a complete steam bearing design study such as the steam delivery system, and the bearing and shaft materials.

The steam delivery system should consist of a steam processing unit to dry the supply steam prior to its entering the bearing supply header and an effective trapping arrangement to remove the separated condensate from the steam supply. An independent steam line is also necessary to supply the steam to the jacketing manifold of the unitized bearing which in turn satisfies the environmental and shaft heat loads.

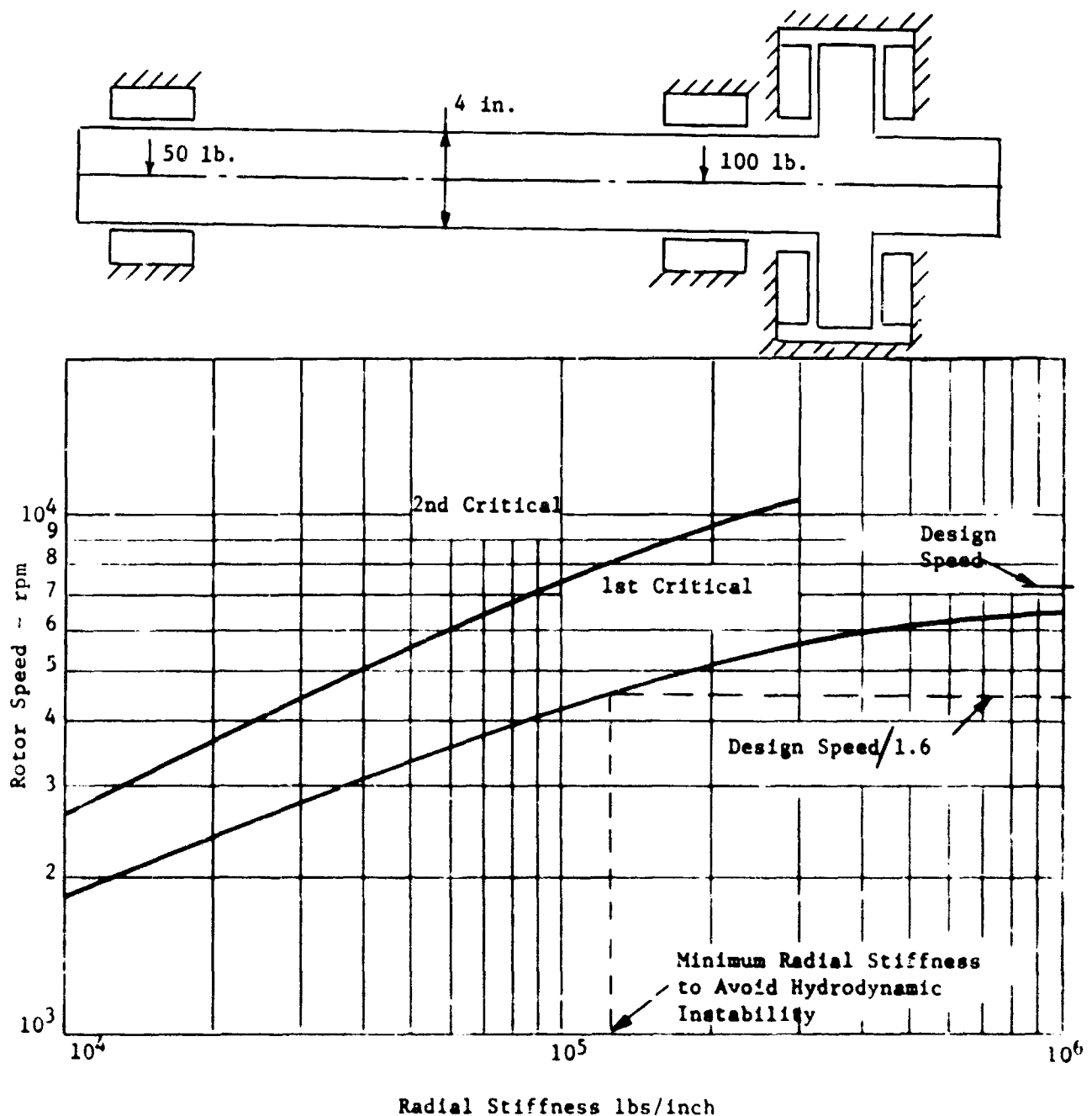
Based on the overall results of the material studies at MTI a chrome carbide coating sprayed on 400 series stainless steel appears to be the best material choice for both the bearing and shaft materials in a steam bearing design. This choice provides the best protection against steam erosion and wear due to sliding.

An index of terms for easy reference, related to the bearing functions and requirements, design problems and their solutions, and design parameters has been included at the end of this Chapter.

The essentials of the next five Chapters are utilized in the following practical design example.

Practical Design Example

A sketch of a bearing-rotor system is shown below. The journal outside diameter is 4 inches. The problem is to design a saturated steam-lubricated journal bearing to carry the 100-lb. load and operate at 7200 RPM. A critical speed map prepared for this rotor configuration indicating the first and second critical speeds as a function of bearing radial stiffness is also shown below.



Other operating conditions are:

ambient pressure, 14.7 psia

maximum supply pressure, 200 psig

maximum flow available, 150 lb/hr/bearing

From the critical speed map it is obvious that one must operate above the first critical and in order to avoid hydrodynamic instability the bearing stiffness should be 2×10^5 lb/in., or greater. Hydrodynamic instability occurs at approximately 1.6 times the lowest shaft critical speed.

Assume and $L/D = 1$, and single-plane feeding from Design Chart - 2 in Chapter III, $CK/(\Delta p LD) = 0.32$ at $\Lambda_s \xi \sim 0.7$. From Chapter II it is advised to use a 0.75 correction factor if one operates near the optimum $\Lambda_s \xi$ value. With the maximum supply pressure, $\Delta p = 200$ psig, and an assumed value of $C/P = 1$ mil/in the radial stiffness is

$$K = \frac{\Delta p LD}{C} (0.32) (0.75),$$

$$K = \frac{200(4)(4)}{2} (0.24) (10^3),$$

$$K = 384,000 \text{ lb/in; } \Delta p = 200 \text{ psi}$$

$$K = 200,000 \text{ lb/in; } \Delta p = 104 \text{ psi}$$

For the same conditions and assumptions as above the load-capacity is,

$$W = \Delta p L D e (0.32) (0.75),$$

$$W_{MAX} = 200 (4) (4) (0.5) (0.24),$$

$$W_{MAX} = 384 \text{ lbs.; } \Delta p = 200 \text{ psi}$$

$$W_{MAX} = 200 \text{ lbs.; } \Delta p = 104 \text{ psi}$$

The value of $\epsilon = 0.5$ is recommended as a maximum value to avoid the danger of lock-up.

In the calculations above, three assumptions were made:

- 1) $L/D = 1$
- 2) Single-Plane Feeding
- and 3) $C/R = 1 \text{ mil/in}$.

An $L/D = 1$ is suggested as a first choice. From the standpoint of the thermal design and for maximum load-capacity and stiffness an $L/D > 1$ is better. However, the above calculations indicate that the bearing with $L/D = 1$ has sufficient load-capacity and stiffness. Axial spacing and bearing alignment usually dictates an $L/D < 1$. From a load-capacity and radial stiffness standpoint an $L/D = 1$ would be acceptable. From a thermal design standpoint an $L/D < 1$ is not recommended. Usually the bearing flow is higher for a smaller L/D as will be shown in subsequent calculations. Therefore, use $L/D = 1$, subject to an acceptable result for flow.

Double-plane feeding is normally used only when the load-capacity and stiffness requirements are extremely critical since it does lead to a more complicated mechanical design. In this case, single-plane feeding is more than adequate.

A $C/R = 1 \text{ mil/in}$ is normally a good choice. A decrease in clearance will decrease the flow by a factor of C^3 and increase the stiffness linearly. However, a smaller clearance also means that the manufacturing tolerances could be more critical and also the bearing is more sensitive to dirt and distortion.

The radial centrifugal growth is calculated as:

$$\Delta C = 0.0256 \frac{N^2 R^3}{E} \left[\frac{1-2\nu}{1-\nu} + \left(\frac{R_1}{R} \right)^2 \frac{3-2\nu}{1-\nu} \right]$$

It is not anticipated that any exotic shaft base materials will be needed in this case. Therefore, make the calculation for ΔC using steel properties. Of course, such a size shaft (4 in. dia.), should be hollow in order to reduce the weight without compromising too much on rigidity. It is recommended that an initial shaft thickness be calculated from $t/D = 3/32$. Therefore, $t = 3/8"$. With $R = 2$ in. and $R_1 = 1.625$ in., $R_1/R = 0.8125$.

$$\Delta C = 0.0256 \frac{(0.283) (120)^2 (2)^3}{3 \times 10^7} \left[\frac{1-.6}{1-.3} + (0.66) \frac{3-.6}{1-.3} \right]$$

$$\Delta C = 79 \times 10^{-6} = 79 \mu\text{-in.}$$

This change in clearance is essentially negligible, being less than 4% of the nominal radial clearance of 2 mils, and would be taken up by the machining tolerances. However, this calculation must not be played down especially in higher speed applications where a stress estimate should also be made. For this problem the hoop stress at the outer radius is less than 1500 psi.

Next, the bearing steam flow calculation should be made. From Design Chart 7 in Chapter III at $\Lambda_s \bar{G} = 0.7$, $\bar{G} = 0.29$. One must now determine μ and RT . At $P_s = 200 + 14.7 = 214.7$ psia, $\mu = 2.9 \times 10^{-9}$ reyns, $R = 79$ ft/ $^{\circ}R$ and $T = 390^{\circ}F = 850^{\circ}R$, $RT = 3.11 \times 10^8$ in²/sec². At $P_s = 104 + 14.7 = 118.7$ psia, $\mu = 2.7 \times 10^{-9}$ reyns, $R = 80.5$ ft/ $^{\circ}R$ and $T = 340^{\circ}F = 800^{\circ}R$, $RT = 2.98 \times 10^8$ in²/sec². These data have been obtained from Figs. III-2 and III-3.

It becomes obvious that neither μ nor the product RT vary much over the pressure range of from 100 to 200 psi and for design purposes it is sufficient to represent μ by an average value, say $\mu = 2.8 \times 10^{-9}$ reyns, and RT by an average value of 3×10^8 in²/sec². Thus $\mu RT = 0.84$ lb/sec.

The total mass flow to the bearing is then calculated to be,

$$G = \frac{\pi C^3 P_s^2}{6\mu RT \xi} \bar{G},$$

$$G = \frac{\pi (2 \times 10^{-3})^3 (214.7)^2 (0.29)}{6(0.84) (1)},$$

$$G = 66.5 \times 10^{-6} \frac{\text{lb. sec.}}{\text{in.}} = 92.5 \text{ lb/hr}; P_s = 214.7 \text{ psia.}$$

From the above expression, for the same value of $\Lambda_s \xi$, the flow varies directly with the supply pressure squared, the clearance cubed and inversely as $\xi = L/D$. It is obvious from the flow standpoint why the clearance and supply pressure should be minimized and L/D maximized. Since 92.5 lb/hr does not exceed the flow limit of 150 lb/hr, the initial choices of $C/R = 1 \text{ mil/in}$ and $P_s = 214.7 \text{ psia}$ are satisfactory. The use of $L/D = 1/2$, from a flow consideration, would not be acceptable.

The restrictor downstream pressure may be calculated with the aid of Fig. III-4. First calculate $\bar{G}_0 = \frac{G}{\Lambda_s \xi} = \frac{0.29}{0.7} = 0.414$; enter the ordinate of Fig. III-4 with 0.414 and read the abscissa, $P_c/P_s = 0.715$. Therefore, $P_c = 153.5 \text{ psia}$. This will be needed in subsequent thermal design calculations.

The number and diameter of the inherently compensated bearing feeder holes are calculated with the aid of the definition of $\Lambda_s \xi$, Fig. III-5, and a "rule of thumb" based on the spacing between feeder holes and the axial flow path.

Thus,

$$nd = \frac{P_s C^2}{6\mu \sqrt{RT} \xi} \Lambda_s \xi,$$

$$nd = \frac{214.7 \times (2 \times 10^{-3})^2 (0.7)}{6 \times 2.8 \times 10^{-9} \times 1.73 \times 10^4 \times 1}.$$

$$nd = 2.$$

One could use 20-0.1 in. dia. holes, 10-0.2 in. dia. holes, or 30-.067 in. dia. holes, for example. But, before deciding consider the rule of thumb that n should be greater than 4π for single plane feeding and $L/D = 1$. Thus, n should be greater than 12. Select an average value of $n = 20$. Therefore $d = 0.1$ inch diameter.

From Fig. III-5, entering the abscissa with $\frac{d}{5D} = \frac{0.1}{(1)(4)} = 0.025$, the ordinate, $(n5)_{\min.}$ is equal to 7. Thus, the minimum allowable value is $n = 7$. Certainly $n = 20$ satisfies this criterion.

The power requirements are calculated as follows:

$$\begin{aligned} \text{Pump. power} &= \frac{G Q T}{6600} \log_e \left(\frac{P_s}{P_a} \right), \\ &= \frac{66.5 \times 10^{-6} \times 3 \times 10^8}{6600} \log_e \left(\frac{214.7}{14.7} \right), \\ &= 8.1 \text{ HP.} \end{aligned}$$

$$\begin{aligned} \text{Friction Power Loss} &= \frac{\pi^3 L D^3 N^2}{6600 C \sqrt{1-\epsilon^2}}, \\ &= \frac{\pi^3 (2.8 \times 10^{-9}) (4)^4 (120)^2}{6600 \times 2 \times 10^{-3} \sqrt{0.75}}, \\ &= 0.028 \text{ HP.} \end{aligned}$$

These calculations indicate typical bearing power losses for a 4-inch shaft supported on externally-pressurized steam journal bearings operating at 7200 RPM. Notice that the pumping power varies greatly with the supply pressure and the friction power loss has the most variation with the journal diameter and speed.

No detailed design will be given here for the flexure support. Chapter III covers this topic. It should be emphasized, however, the stiffnesses of the flexible support must satisfy two requirements: 1) the radial stiffness

must be higher than the bearing radial stiffness by at least a factor of two, and 2) the angular stiffness must be lower than the bearing angular stiffness by a factor of two.

The bearing angular stiffness is calculated from Design Chart - 9 of Chapter III with $L/D = 1$ and $\Lambda_s \xi = 0.7$, $C K_{ang} / (\Delta p L^3 D) = 0.042$. Allowing a 0.75 correction factor the angular stiffness is calculated as:

$$\begin{aligned} K_{ang} &= \frac{\Delta p L^3 D}{C} \times 0.75 \times 0.042, \\ &= \frac{200(4)^4}{2 \times 10^{-3}} \times 0.0315, \\ &= 8 \times 10^5 \text{ in.-lb/rad.} \end{aligned}$$

It is outside the scope of this present manual to set up a detailed dynamic analysis, but one should be cautioned that such an analysis is usually necessary. It should be standard design practice to perform a dynamic analysis on all gas bearing supported rotors. Such analyses with corresponding computer programs are available and should be a part of the library of all designers active in gas bearing-rotor design.

The usual approach in the bearing-rotor dynamic analysis is to separate the bearing from the rotor — representing the bearing by frequency dependent springs and dashpots. One should refer to Ref. I-1 for a detailed description of the approach to this problem.

For externally-pressurized bearings usually the static characteristics are sufficient if the following inequality is satisfied:

$$N < 0.05 \frac{P_a}{\mu} \left(\frac{C}{R} \right)^2$$

For the present problem,

$$\begin{aligned} N &= 120 < 0.05 \frac{14.7 \times 10^{-6}}{2.8 \times 10^{-9}}, \\ N &= 120 < 262. \end{aligned}$$

If the inequality is not satisfied, the dynamic characteristics that are given in Design Tables 1-6 in Chapter III may be used.

For this problem, use the stiffnesses presently calculated and for the damping values use Design Chart - 15 and Design Chart - 21 from Chapter III for the static, radial damping and static, angular damping respectively.

From Design Chart - 15 in Chapter III, the radial damping at $\Lambda_s \xi = 0.7$ is:

$$\frac{B}{\mu L (R/C)^3} = 3.9.$$

Therefore, allowing a correction factor of 0.75

$$B = 3.9 \times 0.75 \times 2.8 \times 10^{-9} \times 4 \times 10^{-9}$$

$$B = 33 \text{ lb. sec./in.}$$

From Design Chart - 21 in Chapter III, the angular damping at $\Lambda_s \xi = 0.7$ is:

$$\frac{B_{\text{ang}}}{\mu L^3 \left(\frac{R}{C}\right)^3} = -0.2.$$

$$B_{\text{ang}} = -0.2 \times 0.75 \times 2.8 \times 10^{-9} \times 4^3 \times 10^{-9},$$

$$B_{\text{ang}} = -27 \text{ in.lb.sec./rad.}$$

For inherently-compensated bearings, the radial damping component is always positive, thus the bearing will not experience pneumatic hammer. A negative value of the angular damping component (as in the present problem) usually implies pneumatic hammer with flex-mounted journal bearings in exceptional cases. It would take a detailed analysis to investigate this problem, and it will not be presented here. Some appropriate discussion on this problem is given in Ref. 1-2.

The basic bearing design is now completed. However, before finalizing the dimensions the thermal design should be checked.

The "unitized bearing" or dual-manifold design that should be used in the solution of the present problem is shown schematically in Fig. V-1a. Notice that separate supply and jacketing headers are featured in this design.

The first step is to calculate the value of the parameter $L/D\sqrt{\Delta}$, where

$$\Delta = \frac{2}{\left[1 - \left(\frac{r_1}{r_2}\right)^2\right]} \left\{ \frac{1}{\frac{k_s}{k_b} \ln \frac{r_4}{r_3} + \frac{C}{R} \left(\frac{k_s}{k_f}\right)} \right\}$$

It is always wise to design the bearing and the journal from the same material. In Chapter V, it is further noted that k_s should be minimized and as a first choice one should use a 400 series, stainless-steel. From the standpoint of erosion, as discussed in Chapter VI, this choice is highly recommended. Other design recommendations are to set $C/R = 1$ mil/in, and $t/D = 3/32$. Therefore,

$$\begin{aligned} r_1 &= 1.625 \text{ in.} \\ \left[1 - \left(\frac{r_1}{r_2}\right)^2\right] &= 0.34 \\ r_2 &= 2.000 \text{ in.} \end{aligned}$$

$$\begin{aligned} r_3 &= 2.002 \text{ in.} \\ r_4 &= 2.377 \text{ in.} \end{aligned} \quad \ln \frac{r_4}{r_3} = 0.174$$

$$k_s = k_b = 1.1 \text{ Btu/(hr-in-}^\circ\text{F)}$$

$$k_f = 0.00146 \text{ Btu/(hr-in-}^\circ\text{F)}$$

$$\Delta = \frac{2}{0.34} \left\{ \frac{1}{0.174 + \frac{1.1}{1.46}} \right\}$$

$$\Delta = 5.46$$

$$\sqrt{\Delta} = 2.34, \frac{L}{D} \sqrt{\Delta} = 2.34 > 1.75.$$

As discussed in Chapter V, $\frac{L}{D} \sqrt{\Delta}$ should be greater than 1.75 for a single-row design. Experience indicates that in general for supply pressures up to 215 psig this will minimize the chance for film entrance condensation.

Upon entering Fig. V-4 with $\frac{L}{D} \sqrt{\Delta} = 2.34$, one finds $\psi_{so} = 0.085$. From this value one can calculate the allowable heat transfer along the shaft at bearing exit, q_{se} . First, it is necessary to calculate the film entrance saturation temperature. With $P_c = 153.5$ psia (from previous design calculations) the corresponding saturation temperature is 360°F , (From Fig. V-5). The shaft entrance temperature, T_{so} , must be larger by say 10°F . From experience with supply pressures less than 215 psig, the jacketing manifold should be operated at 20 to 30 psig higher than the bearing manifold, yielding a temperature difference of about 10°F . In this case the supply pressure and corresponding saturation temperature are 214.7 psia and 388°F respectively. Therefore, the jacketing header should be supplied with condensing steam at 240 psia with a corresponding saturation temperature of $T_m = 398^\circ\text{F}$. Thus,

$$q_{se} = \frac{2\pi (r_2^2 - r_1^2) k_s (T_m - T_{so})}{\psi_{so} L}$$

$$q_{se} = \frac{2\pi (2^2 - 1.625^2) (1.1) (398 - 370)}{0.085 (4)}$$

$$q_{se} = 772 \text{ Btu/hr.}$$

If the temperature difference, $(T_m - T_{so})$, was 2.8°F rather than 28°F then one would have to house the bearing assembly and allow a heat loss of only 77 Btu/hr. In actuality, the 772 Btu/hr heat loss would be easily satisfied. On the other hand, the 77 Btu/hr heat loss might be more difficult to satisfy. The final result will probably lie between 772 and 77 if one designs with the unitized bearing and encloses the entire assembly from the ambient air.

The significance of the functional relationship of ψ_{so} versus $\frac{L}{D}\sqrt{\Delta}$, (Fig. V-4), is illustrated by the following example. Suppose that $\frac{L}{D}\sqrt{\Delta}$ was such a value as to give a ψ_{so} ten times that of above — thus, $\psi_{so} = 0.85$ at $\frac{L}{D}\sqrt{\Delta} = 1.0$. In order to realize a temperature difference, $(T_m - T_{so}) = 28^\circ\text{F}$ the allowable heat loss would then have to be ten times smaller, or 77 Btu/hr. Practically speaking, this probably could not be accomplished with the present design techniques and therefore the chance of condensation formation leading to steam-hammer instability would be greatly increased.

The thermal design is in satisfactory agreement with the bearing design.

The bearing and shaft base material should be either 410 or 416 stainless steel. The bearing surfaces should have a chrome carbide coating to protect against wear and erosion damage. In our experiences, in order to get good, clean edges around the feeder holes, it was necessary to resort to ultrasonic drilling of the chrome carbide. Another method that has been used with success is to leave a circumferential strip of base material approximately 1/4 inch wide in which the holes may be drilled by normal means. The chrome carbide coating extends axially outward from this strip.

A complete summary of experimental results on the unitized bearing has been written in Chapter II and should be used to direct this design and future designs. Most important is to include a steam processing unit to dry the supply steam prior to entering the bearing supply header and to provide for effective trapping and removal of separated condensate from the steam supply and the jacketing manifold. A commercially available processor and two other processors have been evaluated and reported on in Chapter IV. The commercial processor is recommended for use in the present design.

REFERENCES

- I-1 Lund, J.W., "Calculation of Stiffness and Damping Properties of Gas Bearings," Trans. ASME, Journal of Lubrication Technology, Vol. 90, Series F, No. 4, October 1968, Paper No. 68-LubS-19.
- I-2 "Design of Gas Bearings," Vol. 1, Design Notes, Section 5.8, Hydrostatic Bearing Design, Dynamic Performance and Stability, and Section 6.1, Self-Acting Journal Bearings, Design Manual for RPI-MTI Gas Bearing Design Course, (1966).

NOMENCLATURE

B	Radial damping coefficient, lbs. sec./in.
B _{ang}	Angular damping coefficient, lbs. in. sec./radian
C	Journal bearing radial clearance, in.
D	Journal bearing diameter, in.
d	Feeder hole diameter, in.
E	Modulus of Elasticity, psi
K	Radial stiffness, lbs./in.
K _{ang}	Angular stiffness, lbs.in./radian
k _l	Thermal conductivity of medium γ , Btu/(hr.-in.-°F)
L	Total length of journal bearing, in.
n	Total number of feeding holes
N	Rotor speed, RPS
P _a	Ambient pressure, psia
P _s	Supply pressure, psia
P _c	Pressure downstream of feeding hole, psia
q	Heat rate, Btu/hr.
G	Mass flow, lbs. sec./in.
\bar{G}	$= G / \frac{\pi C^3 P_s^2}{6 \mu R T_s}$ for journal bearing, dimensionless flow
\bar{G}_o	$= \bar{G} / A_s$ for journal bearing, dimensionless feeder hole flow
R	$= 1/2 D$, journal bearing radius, in.
R _i	Inner radius of shaft, in.
r ₁ , r ₂ , r ₃ , r ₄	Inner and Outer radii of shaft and bearing, in.
R	Gas constant, in. ² /sec. ² /°R
T	Total temperature, °R

t_l	Thickness of wall of item "l", in.
W	Bearing load, lbs.
Γ	Weight density, lbs./in. ³
ΔP	$P_s - P_a$, psi
ΔC	Clearance change, in.
Δ	Defined by Eqs. 4 and 5 in Chapter V
ϵ	$= e/C$, journal bearing eccentricity ratio
Λ_s	$= 6\mu\sqrt{RT}/(P_s C^2)$, restrictor coefficient
μ	Gas viscosity, lbs.sec./in. ²
ν	Poisson's ratio ($\nu = .3$ for steel); Frequency, rad./sec.
ξ	$= L/D$, journal bearing, single plane admission $= L_2/D$, journal bearing, double plane admission
σ	Squeeze number
ψ	Defined by Eqs. 10 and 11 in Chapter V

Subscripts

b	= bearing
f	= film
m	= jacketing manifold
s	= shaft
se	= shaft condition at film exit
so	= shaft condition at film entrance

INDEXTo Functions and RequirementsChapter

Load Capacity	II, III
Stiffness	II, III
Damping	III
Flow	II, III
Pressure	II, III
Alignment	II, III
Rotor Response	III
Power Loss	III

To Related Problems

Erosion and Wear	VI
Thermal Distortion	II, V
Condensation	II, IV, V
Instabilities :	
Steam Hammer	II, IV, V
Pneumatic Hammer	III
Hydrodynamic Instability	III
Lock-Up	II, III
Critical Speeds and Unbalance Response	III

To The Solutions Of The Problems

Material Selection	VI
"Unitized Bearing" and Mechanical Design	II, V
Inherent Compensation	II, III
Processing and Trapping	IV
Bearing Selection and Sizing	II, III, V

INDEX (continued)Parameter Range and Initial Design Choice

<u>Parameter</u>	<u>Typical Range</u> Min., Max.	<u>Recommended Value</u>
P_c / P_s	0, 1.0	> 0.546
L/D	1/2, 2.0	1.0
P_s / P_a	3, 20	< 10
$\Lambda_s \xi$.01, 10	0.7
ϵ	0, 1.0	< 0.5
σ	.01, 100	See Chapter III
$C/R \times 10^3$	0.5, 1.5	1.0
n	6, 48	See Chapter III
$L/D\sqrt{\Delta}$	0.75, 4.0	≈ 2.0
τ/D	See Chapter V	3/32

CHAPTER II

SUMMARY OF EXPERIMENTAL RESULTS

CHAPTER II
TABLE OF CONTENTS

	<u>Page</u>
INTRODUCTION	27
EFFECTS OF SUB-COOLING THE BEARING SURFACE TO CONDENSE LUBRICANT IN THE FILM	29
PERFORMANCE OF AN ORIFICE COMPENSATED STEAM-LUBRICATED JOURNAL BEARING - NO SHAFT ROTATION	30
INVESTIGATION OF INSTABILITIES RELATED TO CONDENSATION, AND PREVENTIVE MEASURES	35
PERFORMANCE OF THE "UNITIZED STEAM BEARING"	37
COMPARISON OF EXPERIMENTAL RESULTS WITH VARIOUS THEORIES	54
REFERENCES	58

INTRODUCTION

If the vapor is maintained dry throughout the bearing, lubrication with steam is no different than gas lubrication. Experimental measurements which will be described have confirmed this. It follows that one approach to designing steam-lubricated bearings is simply to superheat the supply steam and keep the bearing environmental temperature well above the saturation temperature of the supply steam. If these conditions are met, then the available design data for gas lubricated bearings can be used with appropriate values of the physical properties of steam.

In some machines, this is an entirely feasible approach. However, in many others it is not, either because there is no readily available supply of superheated steam, or because some parts of the machine will be at temperature well below the supply steam saturation temperature. For these cases, the effects of condensation within the bearing or of entrained condensate in the steam supply must be considered. Operation with condensation is important also for all steam-bearing applications where the machine may be cold on initial start-up or when "off design" operating conditions may result in lower bearing environmental temperatures.

Steam can be used as the lubricant for either self-acting or externally-pressurized bearings. MHI has concentrated on externally-pressurized bearings for steam lubrication because:

- (a) In nearly all potential applications, steam is available at an elevated pressure.
- (b) Much higher load capacities and bearing stiffnesses are obtainable with external pressurization (unit bearing loads can be about 25 percent of the difference between supply and ambient pressures. This would amount to 100 psi or more in practical designs).
- (c) Pressure generation, and hence load capacity, in hydrodynamic vapor-lubricated bearings is sharply limited by condensation. When the

local film pressure reaches the saturation pressure, the vapor condenses with a large reduction in volume which inhibits any further pressure rise. (Load capacities of self-acting bearings would be of the order of 10 psi or less).

EFFECTS OF SUB-COOLING THE BEARING SURFACE TO CONDENSE LUBRICANT IN THE FILM

Steam-lubrication studies at MTI began with an investigation of the effects of sub-cooled bearing surfaces on the performance of an externally-pressurized thrust bearing model, Ref. II-1. The results showed adverse effects of extensive withdrawal of heat from the film in the form of reduced stiffness and load capacity, and a tendency toward instability characterized by cyclic fluctuations in the film thickness. It should be emphasized that these effects were the results of deliberate, and effective efforts to cool the bearing surfaces. Experiments under more representative conditions and some exploratory tests on a number of special design features were also conducted as reported below.

PERFORMANCE OF AN ORIFICE COMPENSATED STEAM-LUBRICATED JOURNAL BEARING - NO SHAFT ROTATION

In order to investigate the problems of steam lubrication in a more realistic bearing configuration, an externally-pressurized journal bearing apparatus was constructed, Ref. II-2. Figure II-1 illustrates the apparatus. The test bearing was of three inch diameter, $L/D = 1$, with two rows of orifice-restricted feeder holes (12 holes in each row). Provision was included to heat the shaft internally and to heat the bearing externally by radiant heaters. Instrumentation was provided to measure pressures and temperatures at a number of points including the film and supply manifold. Inlet steam could be superheated, if desired. The initial series of experiments with the orifice compensated bearing brought out the following major conclusions:

1. With superheated or dry inlet steam and bearing and shaft surfaces above supply pressure saturation temperature.

The bearing behaved as a gas-lubricated bearing. In Fig. II-2 experimental stiffness and flow data are compared with theoretical results obtained from gas bearing design data (Ref. II-3). The agreement is representative of that obtained with gas-lubricated bearings.

2. With shaft and bearing surface at or slightly below saturation temperature at supply pressure.

The stiffness and flow of the bearing did not agree closely with the theoretical results from the gas-bearing data. Small amplitude motions of the shaft within the bearing clearance occurred at random intervals. The amplitude of the motion was on the order of 0.2 of the radial clearance. The displacement was of short duration with the shaft quickly returning to its equilibrium position. Fig. II-3 shows the outputs of capacitance probes which measure the locus of the shaft center with respect to the bearing center during one of those disturbances. The full bearing clearance is equal to 4.1 large divisions on the vertical scale. An audible hissing sound of brief duration accompanies this effect and for this reason, the phenomenon is referred to as "spitting".

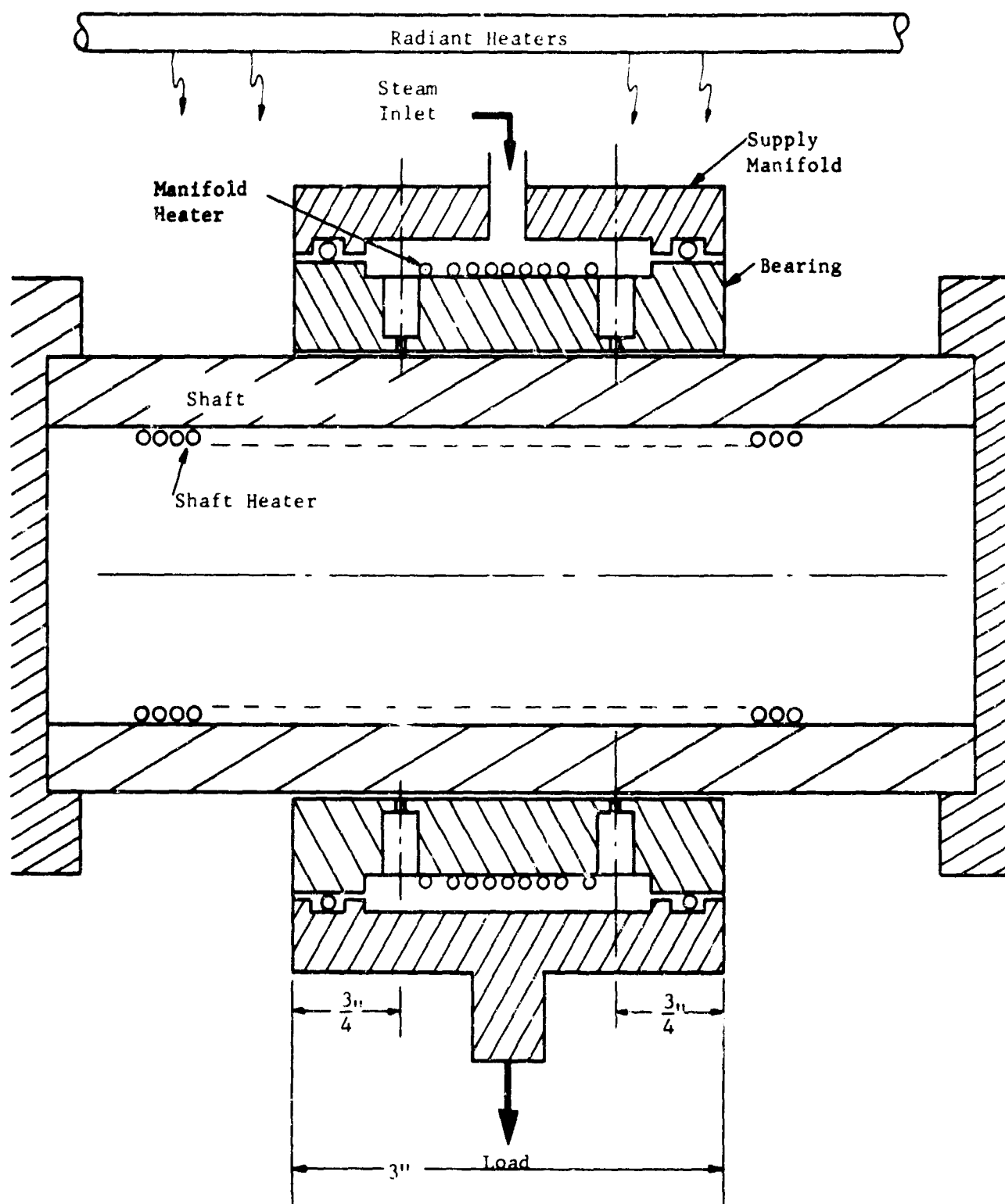


Fig. II-1 Schematic of Non-Rotating Steam Bearing Apparatus

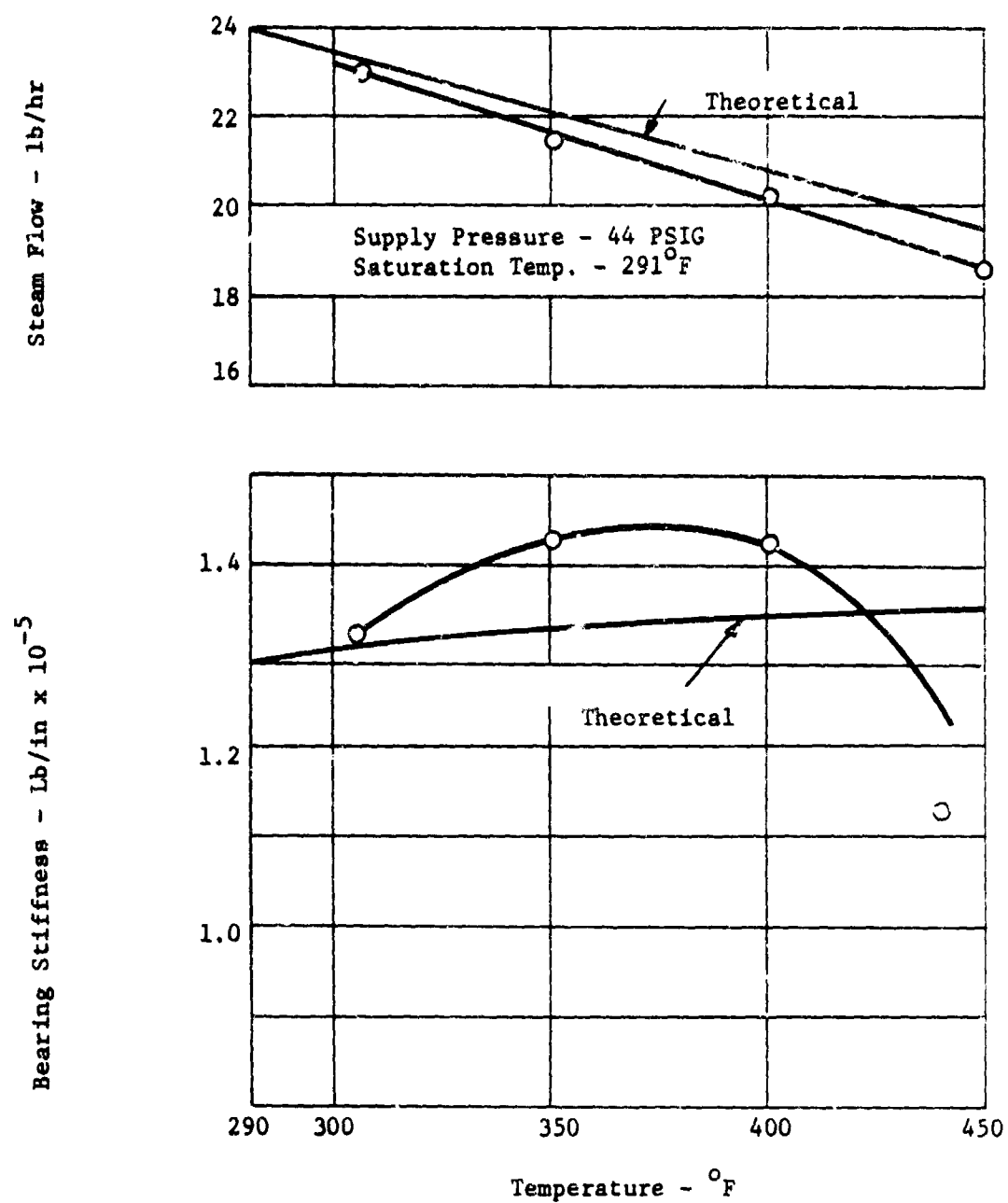
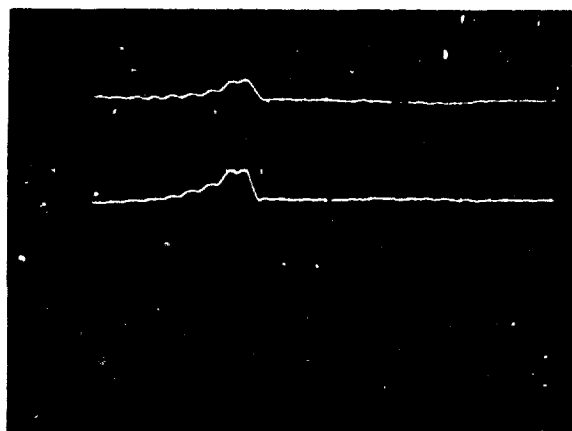


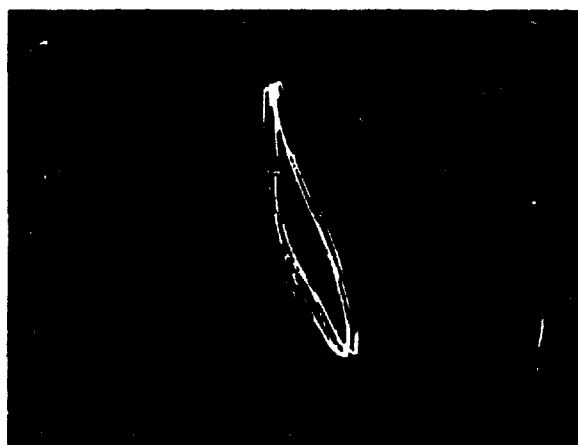
Fig. II-2 Measured and Calculated Stiffness and Flow



MTI-6267

Fig. II-3 Small Amplitude Shaft Motion Associated with "Spitting"

- 1) The traces are the outputs of capacitance probes located 90 degrees apart and 45 degrees from the direction of steady-state load.
- 2) Horizontal time base sweep rate = 20 m sec/large div. (left to right), vertical scale = 0.5 mils/large div., bearing clearance = 4.1 large div.
- 3) $P_s = 65$ psig, $W = 20$ lb.



MTI-6268

Bearing supply manifold pressure ≈ 35 psig
 Bearing temperature - 280°F
 Shaft temperature - 265°F
 Bearing load ≈ 20 lbs
 Inlet steam wet - $T_s - 280$

Fig. II-4 Instability "Orbit" - Wet Steam with Metal Temperature Below T_s

3. With shaft and bearing temperatures more than a few degrees below saturation temperature at supply pressure

Operation under these conditions resulted in violent instability or hammer. Figure 11-4 shows the shaft motion in the bearing clearance when the bearing was hammering. The shaft motion occupied entire bearing clearance and the vibration was so violent that there appeared to be a danger of damage to the bearing surface.

These results were somewhat discouraging since they suggested that reliable, stable operation required dry vapor and bearing and shaft temperatures exceeding the saturation temperature of the supply steam. Unless other means of preventing or attenuating hammer were found, this would mean that the bearing area must be preheated for start-up; and that for operation, additional heat must be supplied from the environment, or from some external source such as electric heaters.

INVESTIGATION OF INSTABILITIES RELATED TO CONDENSATION, AND PREVENTIVE MEASURES

Next, a brief series of experiments were performed for the purpose of investigating the instabilities associated with condensation, Ref. II-4. It was hoped that these instabilities could be avoided without having to rely on external heaters or limiting steam bearing applications to situations with high superheat or high temperature environments. For this purpose, several significant changes in the test bearing were made: (1) inherent compensation* was used in place of the orifices which had been used, and (2) a mechanical moisture separator was installed in the steam line just ahead of the bearing inlet.

Inherent compensation was known to effectively eliminate hammer instability in gas-lubricated bearings. It was clear that steam hammer instability is not the same as air hammer (since steam hammer was clearly associated with condensation and did not occur when operating at temperatures above the saturation temperature). Nevertheless, it seemed reasonable to attempt to avoid steam hammer by applying steps which were known to be effective against air hammer. The moisture separator was added because it was recognized that there was a finite moisture content in the supply steam when the superheater was not in use.

These steps were effective and steam hammer instability was encountered only briefly during temperature transients following starts from room temperature. At the time, this was attributed to the use of inherent compensation. Subsequent experimental observations strongly suggest that the moisture separator was also a critical factor in this improved performance. Moreover, the experiments had all been performed with just one steam supply pressure (65 psig) and it was recognized that the problem could reappear at higher pressures.

*In an inherently compensated bearing the principal restriction to flow from the feeder holes to the film occurs at the annular "curtain" formed by the circumference of the feed hole and the bearing clearance. The feed hole cross section shown in Fig. II-5 is inherently compensated. An orifice compensated feed hole would have an orifice restriction just ahead of the entrance from the feed hole to the film and the principal restriction to flow would occur at the orifice. Inherent compensation reduces the obtainable stiffness of the bearing by about 30 percent but this can be offset by increasing the bearing area or raising the supply pressure.

The inherently compensated bearing continued to be subject to small amplitude, spitting instability. By separately varying the external heat applied by heaters located in the shaft and in the bearing manifold, the relationship between temperatures at various points in the bearing and shaft and the onset of spitting were established. It became clear that spitting is associated with subcooled walls of the bearing supply manifold. Large droplets of water formed by condensation on the manifold walls occasionally become entrained; entered a single feed hole; and momentarily plug the restrictor resulting in a transient asymmetrical film pressure distribution. The shaft responds by moving toward the plugged restrictor then returning as the momentary stoppage clears. Spitting can be avoided by heating or insulating the manifold walls so that steam does not condense on them.

Aside from a momentary reduction in load capacity (assuming the plugged restrictor is on the loaded side of the bearing), spitting does not appear to represent a serious hazard to bearing operation. It is possible that there will be additional consequences related to shaft rotation but there is not apparent reason to expect any significant difference. Nevertheless, it is obviously desirable to prevent spitting and, if possible, to do so without having to resort to external heaters in the bearing manifold.

During the experiments, attempts were made to cool the shaft enough to condense steam within the film. Cold air was blown through the center of the hollow shaft with no detectable effect on performance. The shaft surface temperature was reduced by only 4-6 degrees showing that the shaft surface is closely coupled, thermally, to the steam film. This was encouraging for it indicates that the shaft outside the bearing can be considerably cooler than the steam saturation temperature without serious consequences.

PERFORMANCE OF THE "UNITIZED STEAM BEARING"

The most recent experimental work considered bearing designs which are usable with a saturated or high quality steam supply and without the necessity for external heat sources, Ref. II-5. All of the experiments were performed with the test bearing housing and the shaft, outside the test bearing housing, exposed to a room temperature environment. The available energy of the supply steam is the source of heat to dry or superheat the steam feeding the bearing film and also to control the temperature environment of the bearing. This approach is referred to as the "Unitized Steam Bearing" concept.

Description of Bearings

Three test bearings were used in the experiments, referred to as configurations A, B, and C. The first two were modifications of the same bearing and the same steam supply system was used for both. Bearing C was a new design with different arrangements for steam supply, including some differences in the external piping. All three bearings are externally-pressurized journal bearings of 4 inch diameter and slenderness ratio (L/D) of 1.0. Also, all three have inherently compensated restrictors.

A cross sectional view of bearings A and B is shown in Figure II-5. These bearings have two rows of feeding restrictors, each located at L/4 from the bearing ends. They feature a dual steam header system with inner headers which supply steam to the feed holes and an outer header, covering most of the bearing length. The outer, or jacketing, header is intended to supply the heat load represented by conduction across the flexible mount to the housing, convection to the environment, and by conduction across the clearance space to the shaft with conduction along the shaft. The objective was to supply this heat load by condensation of the steam in the jacketing header with the least possible heat loss from the steam in the inner, supply headers. The reason for this was to avoid condensation in the inner header since this had been related to the "spitting" instability problem in the preliminary journal bearing tests, (Ref. II-4). Steam and condensate were vented from the jacketing header to the housing cavity from a

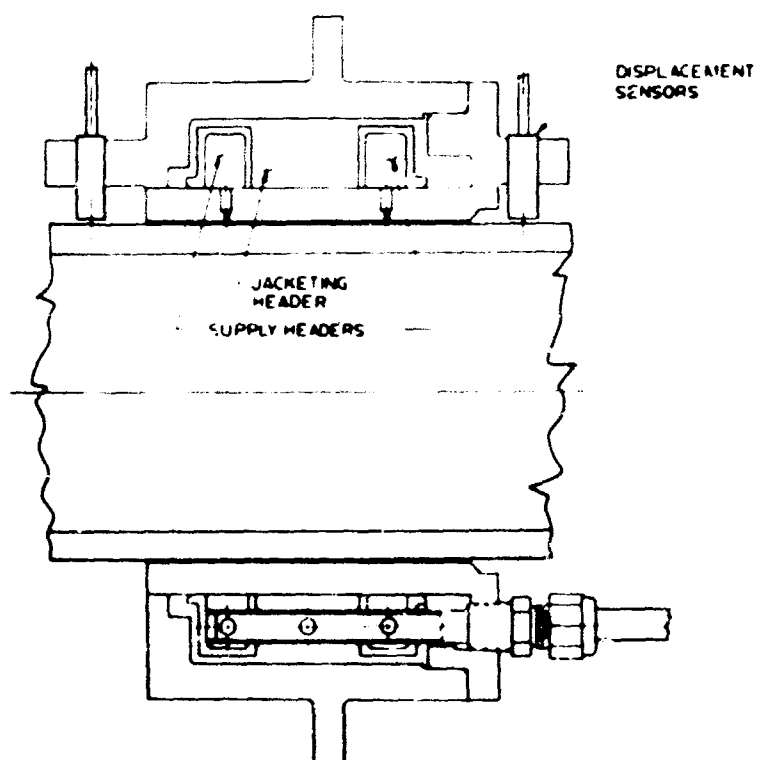


Fig. II-5 Schematic Diagram of a Dual Manifold Double Admission Plane Steam Journal Bearing

HTI-6-304

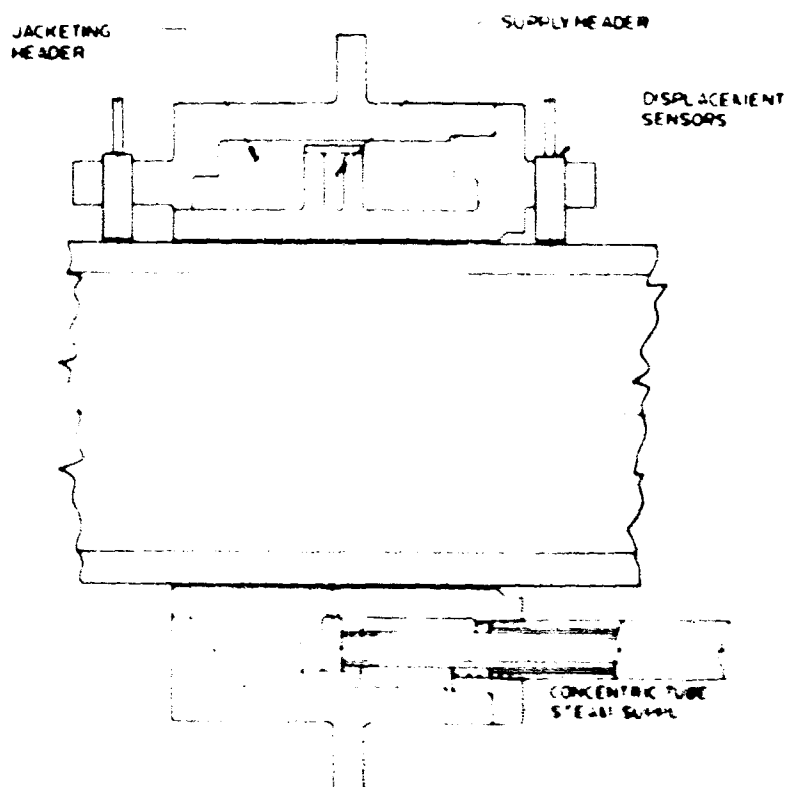


Fig. II-6 Schematic Diagram of a Dual Manifold Single Admission Plane Steam Journal Bearing

HTI-6-305

fixed orifice (0.040 dia.) located on one end of the lowest point on the jacketing header. Inner and outer headers were supplied with steam from the supply line and pressures in both headers were equal.

The significant design parameters of bearings A and B are:

Bearing Clearance (in.) - 1.1×10^{-3} (Bearing A)
 2.0×10^{-3} (Bearing B)

Restrictors - Two rows of 0.055 in. dia.
 holes, 15 holes per row

The only difference between bearings A and B is the clearance.

A cross section of bearing C is shown in Figure II-6. This bearing has a single row of feedholes and, like the others, a dual header arrangement. However, in this bearing the inner, supply, header and the outer, jacketing, header are supplied with steam from separate lines and they are sealed so that it is possible to operate with different, independently controlled, pressures. The bearing design parameters are:

Clearance (C) - 2.0×10^{-3} in.

Restrictors - One row of 16 holes, 0.100 in. dia.

Operation with Unprocessed Steam Supply (Bearings A and B)

Bearings A and B were operated over a range of supply pressures from 90 to 200 psig. In general, steam hammer occurred at the lower end of the pressure range (for Bearing A, less than 150 psig; for Bearing B, less than 120 psig) and operation was stable at higher pressures, up to 200 psig. The conditions of the tests were zero load and with the shaft stationary or rotated slowly (about 400 rpm). The operation was described as unstable if there were any periods of hammer during several separate experiments (other than possibly a brief period of hammer immediately following the transient associated with the change to a higher supply pressure and which stopped of its own accord as temperature equilibrium was approached). Frequently, hammer occurred not as a sustained, continual vibration but instead as intervals separated by periods of stable operation.

There are a large number of effects of changing the supply pressure including those on flow and on the thermal-hydraulic environment of the bearing (that is, the relationships between bearing metal temperature and steam conditions at various points in the bearing). There was an effect of supply pressure on the quality of the supply steam (based on calorimeter measurements). The moisture fraction present in the steam at the bearing inlet was significantly greater at low supply pressures. Probably this was a manifestation of the change in flow rate through the steam lines. This change in steam quality with supply pressure is the most straightforward explanation of the transition from unstable to stable operation with increasing supply pressure. Moreover, the experiments with bearing C showed a similar relationship between calorimeter measurements and stability.

The increased clearance of bearing B which was the only known difference from bearing A had a small favorable effect on stability. There was an appreciable increase in flow as a result of the clearance change. On first consideration, this might appear to result in higher bearing and shaft temperatures, and hence in less tendency toward instability. However, the thermal analysis (Ref. II-5) indicates that this effect is not very significant because of the dominance of conduction from the jacketing header through the bearing wall and across the thin bearing film as the means of supplying the shaft heat load. Unfortunately, calorimeter data were not obtained with bearing A. However, one can hypothesize that the increased flow of bearing B gave better stability characteristics because it resulted in higher supply steam quality.

Operation With Steam Processing (Bearing C)

Bearing configuration C (Figure II-6) was designed with supply and jacketing headers which are supplied from separate steam supply lines and which are sealed so that it is possible to operate with different pressures in the two headers. In addition, a steam processor (identified as processor, X, in Chapter IV of this manual), was installed in the steam supply system with provision for throttling the steam for the supply header followed by reheat using the throttled supply for the jacketing header as the heat source. From the processor to the bearing, the steam flows through concentric supply tubes with the supply header steam in the inner tube and the jacketing header supply outside. These changes were made

to permit experimental determination of the extent to which drying or superheating of the steam supply was necessary to prevent steam hammer. A single row of restrictors was used in the bearing to gain experience with this design and because it simplified the problem of separating and sealing the supply and jacketing headers.

The results of the stability investigation with bearing C and the steam processor are given in Table II-1. The test procedure was to begin with a set jacketing header pressure and with the supply header steam throttled to a lower pressure (usually 10 to 20 psig below the jacketing header pressure). The supply header pressure was then raised in increments until hammer occurred or until the pressures were equal in both headers. If the bearing remained stable with equal header pressures, the jacketing header supply was throttled, reversing the header pressure difference, by small increments (usually 5 psi) until hammer did occur. The most extreme conditions for stability and the conditions at which hammer was first encountered are given in Table II-1.

These results were obtained with zero load and low speed (400 rpm) shaft rotation. The results are consistent with those obtained with bearings A and B in that they show a greater tendency toward hammer when operating with low supply pressures. With higher supply pressures, the bearing remained stable not only with equal pressures in both headers, but even with an inverted pressure difference so that the supply steam in the processor, in the supply line and within the bearing was actually losing heat to the jacketing steam.

There is a good correlation between the stability limits and measured steam quality - at lower pressures the dividing line is about 99 percent and at higher pressures it is about 98.5 percent. This is generally consistent with the results with bearing B. Even allowing for the possibility of error in the quality measured by calorimeter, it is apparent that it is possible to have stable operation with a small (one to two percent) moisture fraction in the supply steam. Certainly some moisture fraction must be present when operating with the supply header pressure equal to, or lower than the jacketing header pressure. Stability under these conditions is probably dependent on a favorable thermal-hydraulic environment within the bearing.

Effects of Steam Supply System Variables

Bearing C was operated also with the spiral-finned heater removed from the inner, bearing supply, section of the steam processor. This was done to establish the effect of the spinning action which it imparted to the flow together with the resulting lengthening of the steam flow path through the processor. With the heater removed, supply steam processing was limited to throttling with separation due to the slow flow up through the inner pipe. Heat transfer calculations indicated that there should be very little reheat with the shortened flow path. Table II-2 shows results for this steam supply arrangement presented in the same manner as the previous results with the complete processing system.

Without the spiraling flow and lengthened flow path, it was necessary to operate with some throttling of the bearing steam supply in order to have stable operation. However, the amount of pressure drop from jacketing to supply headers which was necessary is quite small. Again, there appears to be a correlation between supply steam quality and stability and again the apparent boundary for stability is a small fraction moisture content. In this case, the critical moisture fraction, according to the calorimeter measurements, is lower than it was in the previously described experiments. Hammer occurred with more than 0.5 to 0.8 percent measured wetness.

Effective separation and trapping (drainage) of moisture in the steam supply ahead of the bearing inlet were clearly important to bearing stability. Bearing C could be operated stably with supply pressures equal to or slightly lower than the jacketing header pressure when the spiral-path processor was used. With the straight-path processor, the supply pressure had to be lower than the jacketing header pressure for stability. The difference clearly is not due to reheat with the spiral-path processor since the supply steam should lose, not gain heat when the pressures are inverted. However, the swirling motion imparted to the steam by the spiral path should result in more effective separation of moisture and this is regarded as the probable explanation for the superior performance with the spiral-path processor.

TABLE II-1

STABILITY LIMITS FOR BEARING C USING STEAM
PROCESSOR WITH SPIRALING INNER-TUBE FLOW PATH

Mode of Operation	Supply Header Pressure,psig	Jacketing Header Pressure,psig	Measured Steam Quality,Percent <u>Dry Steam</u>
Stable	55	60	99.1
Unstable	60	60	98.8
Stable	80	80	99.3
Unstable	80	75	99.2
Stable	100	100	99.3
Unstable	100	95	98.3
Stable	125	125	98.7
Unstable	125	120	98.3
Stable	150	145	98.2
Unstable	150	140	97.9
Stable	175	170	98.7
Unstable	175	165	97.8
Stable	225	225	99.5
Unstable	225	220	98.0

TABLE II-2

STABILITY LIMITS FOR BEARING C USING STEAM
PROCESSOR WITH STRAIGHT INNER TUBE FLOW PATH

Mode of Operation	Supply Header Pressure, psig	Jacketing Header Pressure, psig	Measured Steam Quality, Percent Dry Steam
Stable	75	80	99.2
Unstable	78	80	99.0
Stable	115	125	99.6
Unstable	120	125	99.5
Stable	170	175	99.5
Unstable	174	175	99.3
Stable	220	225	99.5
Unstable	225	225	99.3

For moisture separation to be effective, it is necessary to trap or drain the separated liquid from the system in order to prevent reentrainment. Ordinarily, this was done from the drain line at the bottom of the processor inner section by connection to a steam trap (this is a float-controlled valve which opens to discharge water when the accumulation reaches a certain level and then closes to keep steam from escaping). When the drain was closed by a valve in the line, there was a significant and detrimental effect on stability. With the straight-path processor, instability began almost immediately and persisted until the drain was reopened, whereupon stable operation resumed almost immediately. It should be noted that the steam enters the inner processor section very close to the bottom, about 1/4 inch above the drain, so reentrainment would begin very quickly when the drain was closed.

Stability limits were determined experimentally for the spiral-path processor with the drain closed. It was necessary to operate with as much as from 10 to 35 psi throttling of the supply steam in order to avoid hammer when the drain was closed. Supply steam quality measurements do not correlate nearly as well with bearing stability in this case as they did in the other experiments. There is much more variation in the measured quality at the stability boundary, and for several conditions the calorimeter indicated some superheat at the boundary conditions.

The effectiveness of moisture separation in a vertical, rising section of supply line with condensate removal through a trap at the bottom was shown also during experiments with bearing B in which water injection was used to reduce the steam quality. A description of the results of this experiment follows.

Operation With Very Low Steam Quality

The measured quality of the steam as it came from the steam generator, separator without processing was consistently between 97 and 99 percent dry steam. The effects of reduced steam quality were investigated with bearing B. Water was injected into the steam supply under pressure through an oil burner spray nozzle. There was virtually no effect, either on the calorimeter or on bearing stability, even with water injected at a rate of as much as 20 lb/hr with a bearing flow rate of about 80 lb/hr (150 psig supply pressure) with effective draining and

trapping. Evidently the water was being separated from the steam in the vertical section of line below the calorimeter sampling point, and being drained through the trap at the bottom. The vertical line was 3/4 inch pipe so the flow velocity was low, about 2.2 ft/sec. When the drain to the trap was valved off, water injection was quite effective and the bearing became unstable as soon as water injection was started. The minimum rate of water injection resulted in a drop in measured quality from 98.7 to 97.3 percent (200 psig pressure). The bearing hammered continuously and violently with water injection up to a rate which lowered the measured quality to or below 94.2 percent (at this point, the calorimeter temperature reaches 212F and will go no lower).

Bearing C (spiral flow path processor) was also operated with very low quality steam at 150 psig supply pressure. In this case, the quality was lowered by progressively lowering the jacketing pressure, which also effects the bearing temperatures. Again, there was continuous and violent hammer for all conditions of steam quality below the stability limit down to the lower limit of the test, which was 96 percent.

Effects of Steady-State Load

Bearings A, B and C were all operated under widely varying conditions of steady state load during the investigation of steam hammer instability. Consistently, there was very little, if any effect of load, either in the direction of inducing hammer with an otherwise stable bearing, or in the direction of stabilizing a bearing which was hammering.

Effects of Shaft Rotation

When operating at conditions which were marginal for hammer (occasional brief periods of hammer with stable operation most of the time), hammer could frequently be induced by rotating the shaft, or even by turning it a few degrees by hand. However, there was no effect of rotation when operating at conditions which clearly resulted in stability at zero or low speed rotation.

Bearing B was operated with shaft rotation at speeds up to 4000 rpm with supply pressures of 150, 175 and 200 psig, with and without rotating, unbalance load. Bearing C with the spiral flow path processor was operated at speeds up to 3950 RPM with supply pressures of 145 and 115 psig. There was no sign of hammer instability, or any other operating problem during these experiments.

Operation During Periods of Transient Conditions

A change in the supply or jacketing header pressures results in a period of transient change in temperature of the steam supply lines and processor and of the bearing, shaft and housing. There is cause for concern over the possible effects of an upward change in pressures especially, since this results temporarily in subcooled line and bearing wall temperatures. Similarly, there is a possible problem of initial startup of a cold machine.

Initial startup from room temperature of bearings A and B invariably resulted in a transient period of hammer instability while the steam line, bearing and shaft surfaces came up to temperature. Assuming that the supply pressure was in the range for stable operation at equilibrium, the transient hammer period was typically shorter than five minutes. There were no apparent ill effects of such periods of hammer on the bearing or shaft. However, rotation of the shaft is clearly not advisable during this time.

Bearing C was started by first introducing steam to the jacketing header only, to preheat the supply lines, bearing and shaft. This usually took above five minutes and then the supply steam was admitted at a pressure which was 15 to 20 psi below the jacketing pressure. The bearing would lift immediately and there was never any sign of hammer.

Step changes upward in supply pressure sometimes resulted in brief periods of hammer with bearings A and B. The effect was investigated specifically with bearing B by making a series of step changes in supply pressure about an equilibrium operating point. The results indicated that large excursions in supply pressure may cause transient hammer, but small perturbations such as might be expected in a reasonably well regulated supply system do not appear to be a problem.

Operating experience with bearing C was consistent with this. Pressure changes in going from one operating point to another did not cause hammer. Generally these changes were made beginning with a favorable pressure difference between jacketing and supply headers (typically 10-15 psi). The regulated pressure was then increased raising both the jacketing and supply pressures. The change was generally made within a few seconds.

These observations indicate that bearing stability is not sensitive to small perturbations in supply pressure and normal regulation of the steam pressure is adequate. During the thermal transient which follows a change in steam pressures, the supply header and feedhole walls are subcooled. For moderate changes in pressure, this did not result in instability.

Bearing Performance Under Stable Operating Conditions

For obvious reasons, measurements of the performance characteristics of the bearings were made only under stable operating conditions.

Bearing stiffness was measured by applying steady-state load in increments and measuring the change in locus of the journal axis within the bearing clearance. The shaft was rotated at about 400 rpm during these measurements. Results of the stiffness measurements are shown in Fig. II-7 with calculated results. The agreement is reasonably good and is generally typical of agreement between theory and experiment for externally-pressurized, gas-lubricated bearings. The measured stiffnesses are nearly always lower than the calculated values and there is a trend toward increasing disparity at high pressure ratios. This effect is most noticeable with bearing B where the measured results actually indicate a slight reduction in stiffness beyond P_s/P_a of about 13. This trend of the static load/deflection measurements was confirmed by measurements of orbit dimensions when operating bearing B with rotating unbalance load. The orbit diameter for 4000 rpm with 1.4 in. oz. unbalance decreased with increasing P_s/P_a up to a value of 11 and beyond this it remained constant, within the accuracy of measurement.

The load-deflection curves were very nearly linear up to eccentricities of at least 0.6. There was no evidence of a lock-up effect, or a significant reduction

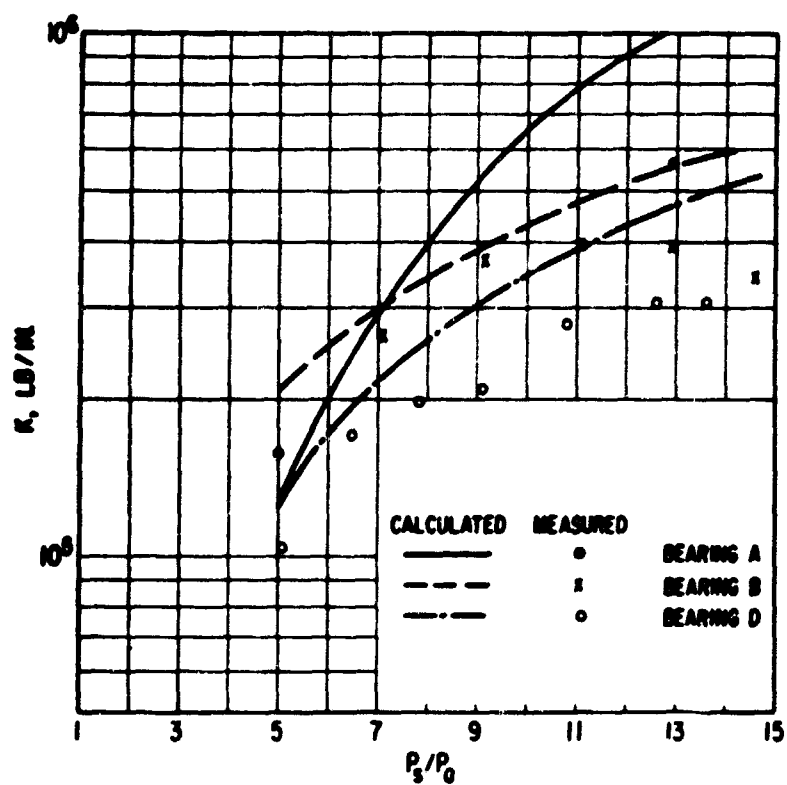
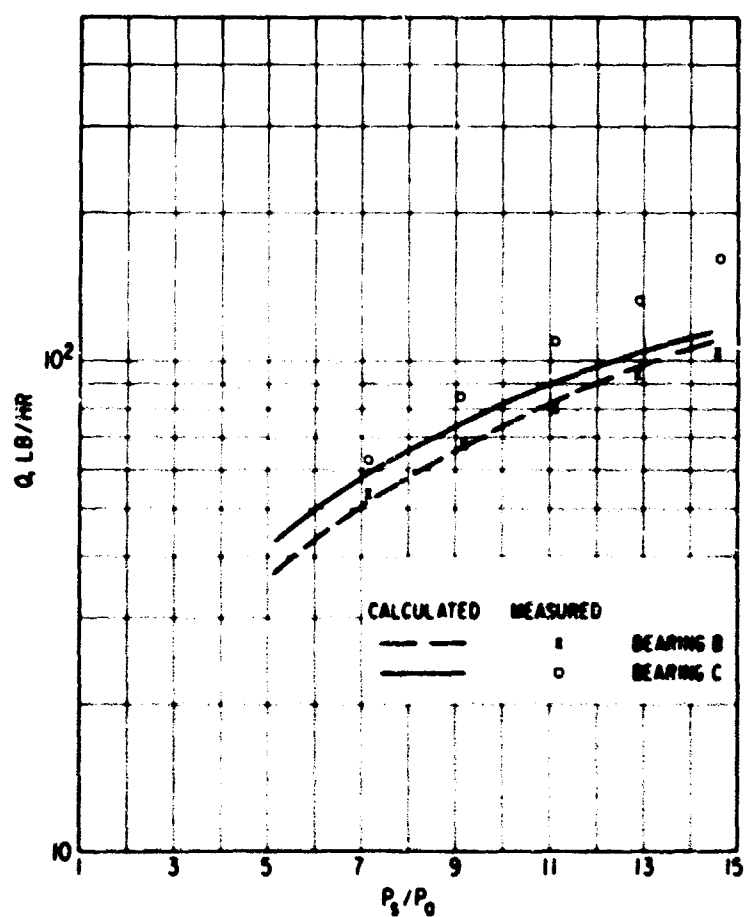


Fig. II-7 Calculated and Measured Bearing Stiffness

NTI-6302

Fig. II-8 Calculated and Measured Bearing Flow, Dual-Header Bearing ($C = 2$ mils)

NTI-6303

in stiffness, even beyond this eccentricity. Normal design practice for externally pressurized bearings is to limit eccentricity ratios to about 0.5 or lower.

Measured and calculated bearing flows were compared. The meaningful flow data were limited by the fact that there were one or more places where steam was vented, in addition to the bearing film itself, and the flow meter measured the total flow. The data for bearing B was obtained by replacing the fixed-orifice vent on the jacketing header with a throttling valve. The valve was closed briefly to obtain a measurement of the bearing flow. The measured and calculated results compared extremely well (Fig. 11-8). Again, this is typical of experience with gas-lubricated bearings — agreement between measured and predicted flow results are better than the agreement for stiffness results.

Flows were measured for bearing C with the jacketing-header vent open and some additional venting from the bottom of the jacketing section of the processor (this would not be necessary if a trap were used), and with the calorimeter in use. Under these conditions, the total flows were roughly 1.5 times the calculated bearing flows. It is probably reasonable to expect total flows of about 1.2 to 1.5 times the calculated bearing flow for the dual header bearing design.

Summary of Results of the Unitized Steam Bearing

The experiments have shown that unitized steam lubricated bearings can be operated stably from a high-quality steam source in a low temperature environment. Stable operation has been demonstrated for supply pressure ratios (P_s/P_a) from 3 to 15 and for a broad range of conditions of steady-state and dynamic load and speed.

To insure stability, it is necessary to maintain a moisture-free supply of steam at the restrictors. The following bearing design and steam supply system features have been found effective for this purpose.

1. Provision for satisfying the environmental and shaft heat loads from a source other than the bearing film supply steam.

A dual header arrangement in which there is an outer, jacketing header and an inner, supply header has been found to be effective for this purpose. The latent heat of steam within the jacketing header satisfies the environmental and shaft heat loads. Temperature measurements and thermal analysis have shown that the shaft is heated by conduction from the jacket through the bearing wall and across the thin bearing film. With the jacketing header, the bearing film is essentially isothermal. Calculated bearing and shaft wall temperatures are consistently above the saturation temperature of the steam at P_c (calculated restrictor exit pressure) indicating that there was no condensation within the bearing film.

A thermal analysis, similar to that described in Ref. II-6 for the test bearings, should be performed as part of steam-lubricated bearing design analysis. Based on current understanding, suitable thermal-hydraulic criteria for bearing design are: (a) maintain bearing wall and shaft temperatures above the saturation temperature of the steam at the restrictor exit, and (b) avoid subcooled wall temperatures in the supply manifold and limit subcooling of the feedhole walls to levels which are no greater than those indicated for the test bearing in Ref. II-6 (typically about 5 F at the mid-point of the bearing wall and 10 to 15 F at the restrictor entrance). Evidently it is not necessary to eliminate any subcooling of the feedholes and it is probably not possible to do so without substantial supply steam superheat. More detail coverage of this subject is covered in Chapter V of this manual entitled "Thermal Design Guide".

2. A steam processing unit to dry the supply steam prior to its entering the bearing supply header.

A number of approaches to supply steam processing were tried and found to be effective. They include: (a) throttling with reheat using unthrottled jacketing steam as the heat source, (b) throttling

with mechanical separation of moisture, (c) mechanical separation alone. With all of these processing techniques, stable operation was obtained when the measured steam supply quality exceeded a value ranging from 98 to 99.5. When the measured steam quality was below this value, the bearing hammered. Chapter IV of this manual covers the tests and results of three steam processing units.

3. Effective trapping and removal of separated condensate from the steam supply.

If separated condensate is not removed from the system, it can become reentrained. There was a considerable difference in the conditions necessary to achieve stability depending on whether separated moisture was drained from the bottom of the supply steam section of the processor. With good drainage, operation was always stable with equal supply and jacketing header pressures (Spiral-path processor), while 15 to 20 psi throttling of the supply steam with reheat by the unthrottled jacketing steam was necessary when the drain was closed.

4. Avoid sudden very large changes in steam supply pressure.

Bearing stability was not sensitive to sudden perturbations in supply pressure of the order of 25 - 30 psi providing there is a reasonable margin of stability at the initial operating point. However, larger pressure changes did result in a transient period of hammer during the thermal transient which follows the pressure change. A brief period of hammer can be expected when starting the bearing cold from room temperature. This can be avoided with the dual-header bearing through preheating by supplying steam to the jacketing header only for a few minutes.

There was very little, if any effect, of steady-state load on conditions for onset or suppression of steam hammer instability.

Most of the investigation of steam hammer instability was performed with very low shaft rotational speeds, 100 rpm or less, in order to minimize the possi-

bility of bearing damage during operation with hammer. However, several of the test bearings were operated at speeds up to 4000 rpm, with and without unbalance loading, under conditions which had been established as being close to the stability limit. Operation was entirely satisfactory and there was no indication of an effect of rotational speed or dynamic load on steam hammer instability.

Spitting instability was not observed during these experiments. The dual header bearing configuration seems to eliminate this problem, at least for conditions which do not result in steam hammer.

Measurements of bearing flow and stiffness are in satisfactory agreement (even with saturated steam), with calculations based on available design data for externally-pressurized gas lubricated bearings modified for the properties of steam. Measured stiffnesses are lower than calculated values and the disparity increases for high ratios of supply pressure to ambient pressure. This observation is consistent with usual experience with gas-lubricated bearings. A comparison of experimental and theoretical results follows.

COMPARISON OF EXPERIMENTAL RESULTS WITH VARIOUS THEORIES

It would be ideal if the bearing design charts developed with saturated steam as the lubricant could include all effects such as moisture content, entrance shocks, turbulence in the film, etc. Unfortunately, an analysis which includes the actual complex physical situation is not presently available. On the other hand, design data obtained from such an extensive analysis would be also much more expensive to develop and complicated to use — thus defeating the advantage of using design charts (simplicity) in selecting a bearing size for a given application. The purpose of this section is to indicate the comparison of saturated, steam lubricated journal bearing stiffness measurements with various theories. Thus an empirical calibration factor can be obtained for the theory which compares more favorably with experiment.

Figures II-9 and II-10 show a comparison of the experimental radial stiffness measurements of bearings C and B described above with the predictions of three theoretical treatments. The three theories differ in the manner in which the restrictor is treated. The first theory (labeled T-1) is that theory used in the development of the presently available gas bearing design charts, Ref. II-3. A theoretical equation for one-dimensional, steady, single phase, isentropic flow for an ideal gas through the restrictor with an orifice, discharge coefficient is used to develop the data, T-1. The second theory (labeled T-2) is similar to T-1 except: (1) the values of the discharge coefficient used are more representative of a sharp-edged orifice, and (2) the value of γ (ratio of specific heats) is 1.3 rather than 1.4 as in T-1. The third theory, T-3, is a more recent development, Ref. II-7, which should be more correct in treating a variable restrictor such as an inherent restrictor. This theory introduces a correction for the dynamic head loss at the entrance to the bearing film. This correction is made in the form of a loss coefficient allowing only a fraction of the total dynamic head to be lost; i.e. if $(p_s - p_i)$ represents the actual total pressure drop at the entrance to the bearing film and $(p_s - p_c)$ represents the total dynamic head at the throat, then $(p_s - p_i)$ may be calculated from the equation

$$(p_s - p_i) = f (R_e) (p_s - p_c)$$

for subsonic flows, where $f (Re_e)$ is a loss coefficient varying from 0.15 to 0.6 as a particular function of the local Reynolds' number.

As indicated by Figs. II-9 and II-10, T-2 seems to provide better agreement with experimental values. This is consistent with the results reported in Ref. II-8, where better agreement for load-carrying capacity between theory and experiment was obtained by using T-2. In Ref. II-8 a single entrance circular thrust bearing was tested.

The data for Bearing C, Fig. II-9 indicates an average value of 0.75 should be used to correct the theoretical predictions for better agreement with theory. Bearing C operates very closely to the optimum value of Λ_s (Restrictor Coefficient, described in next chapter.) over the entire pressure ratio, p_s/p_a , range.

The data for Bearing B, Fig. II-10 indicates a variable correction factor should be applied to the theoretical predictions. This correction factor varies from approximately 0.9 at low supply pressure ($p_s/p_a \sim 5$) to 0.65 at high supply pressures. This bearing operates very closely to optimum Λ_s at $p_s/p_a \sim 5$ and moves to the left of the optimum Λ_s at $p_s/p_a \sim 15$ ($\Lambda_s \sim 0.3$).

The performance curves developed for steam lubricated externally-pressurized journal bearings are presented in the next chapter. Theory-two, T-2, described above was used in their development. Therefore, in light of the above discussion it is suggested to operate near the optimum values of Λ_s whenever possible and to derate the theoretical predictions for stiffness and damping by 10 to 25 percent. If it is necessary to operate far from the optimum values of Λ_s then the theoretical predictions for stiffness and damping should be devated by 35%.

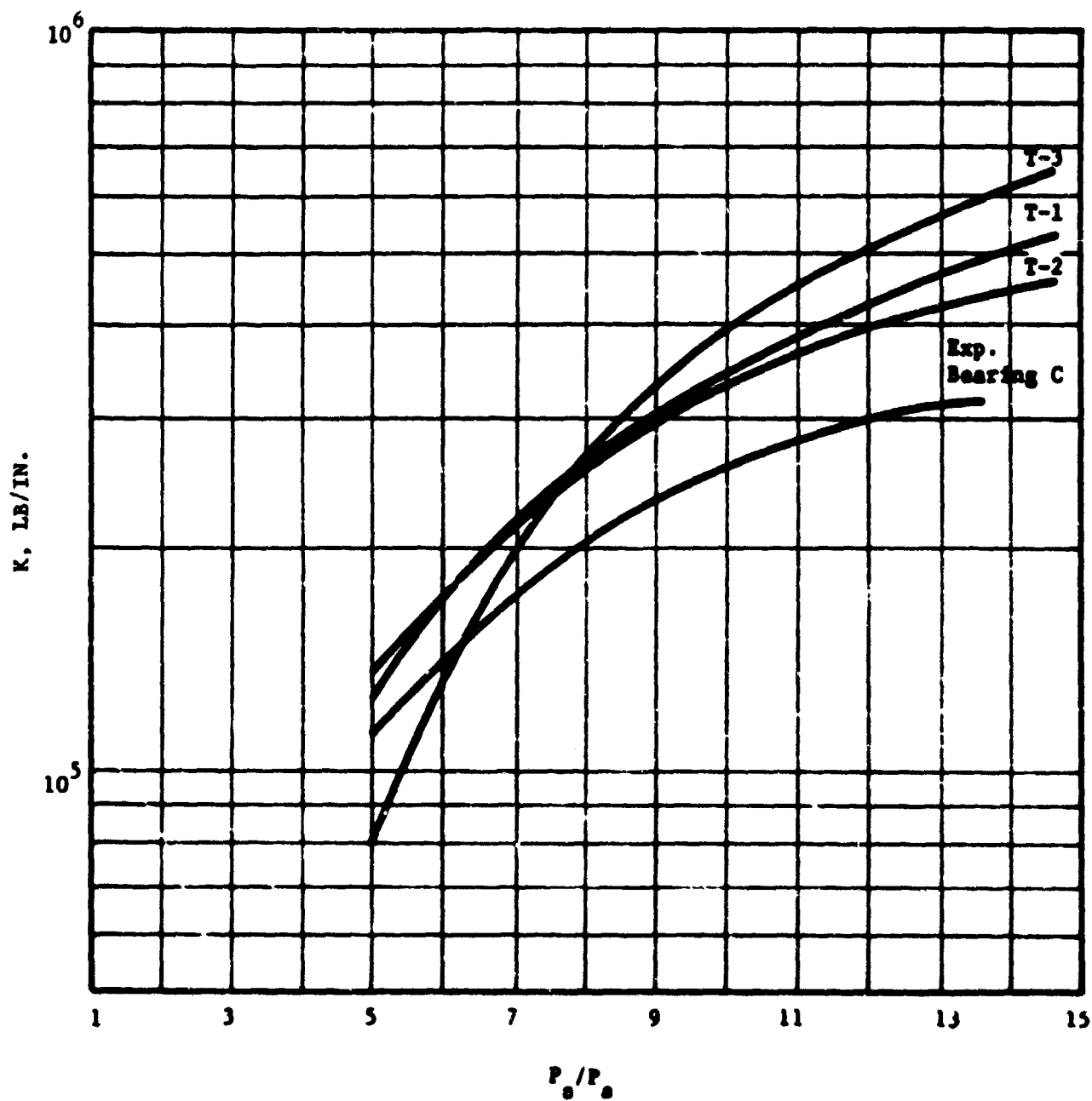


Fig. II-9 Comparison of Experimental Radial Stiffness Measurements with Theory (Bearing C)

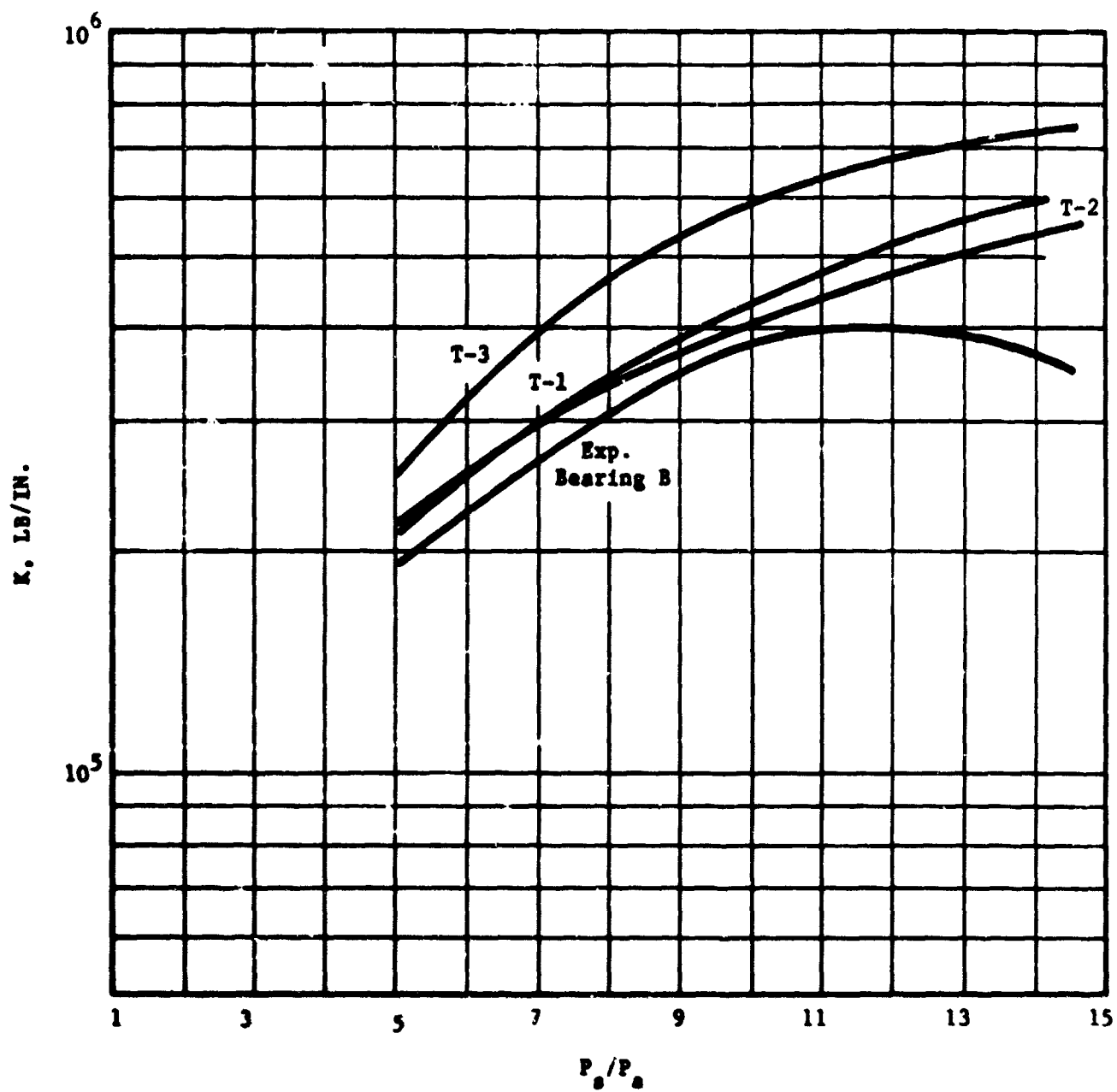


Fig. II-10 Comparison of Experimental Radial Stiffness Measurements with Theory (Bearing B)

REFERENCES

- II-1 Orcutt, F. K., "Experimental Investigation of Condensing Vapor Lubricated Thrust Bearing," ASLE Trans. Vol. 7, No. 2, p. 168 (April 1964).
- II-2 Meacher, J. S., "Experimental Investigation of a Steam-Lubricated Journal Bearing," MTI-64TR20, Contract NONr-3731(00)FBM, (1964).
- II-3 "Design of Gas Bearings," Vol. 1, Design Notes, Section 5, Hydrostatic Bearing Design, Design Manual for RPI-MTI Gas Bearing Design Course, (1966).
- II-4 Dougherty, D. E., and Orcutt, F. K., "Exploratory Investigation of Externally-Pressurized Steam-Lubricated Journal Bearing Instabilities," MTI-66TR37, Contract NONr-3731(00)FBM, (1966).
- II-5 Orcutt, F. K., Dougherty, D. E., and Malanoski, S. B., "Steam Lubrication Studies, Part I - Experimental Investigation of a Steam Lubricated Journal Bearing" prepared under Contract N00014-66-C0214 for the Office of Naval Research, MTI 67TR76, Nov. 1967. A similar manuscript, by the same authors written above and also Pan, C.H.T., entitled "Investigation of Externally-Pressurized Steam-Lubricated Journal Bearings" was presented at the ASME Lubrication Symposium, Las Vegas, Nevada, June 17-20, 1968. Paper No. 68-LUBS-24.
- II-6 Hsing, F., and Dougherty, D. E., "Steam Lubrication Studies, Part II, Thermal Environmental Analysis of an Externally-Pressurized Steam Bearing," MTI-67TR77, Contract N00014-66-C0214, (1967).
- II-7 Private Communication with J. Vohr on Investigation of Inherent Restrictor Losses currently in progress on Contract NONR-3730(00)FBM.
- II-8 Orcutt, F. K., and Malanoski, S. B., "Experimental Study of an Externally-Pressurized Steam Lubricated, Single-Restrictor. Circular Thrust Bearing." Topical Report No. 3, prepared under Contract AT(30-1)3839, Steam Lubrication of Turbo Machinery, for the U. S. Atomic Energy Commission, MTI-68TR35, August, 1968.

CHAPTER III**BEARING DESIGN METHODS AND DATA**

CHAPTER III
TABLE OF CONTENTS

	<u>Page</u>
INTRODUCTION	61
DISCUSSION ON THE PRINCIPLE OF HYDROSTATIC LUBRICATION	62
DIMENSIONLESS DESIGN PARAMETERS	68
SELECTION OF THE BEARING DIMENSIONS AND USE OF THE DESIGN CHARTS	74
REFERENCES	91
NOMENCLATURE	92
ADDENDUM (DESIGN CHARTS AND TABLES)	94

INTRODUCTION

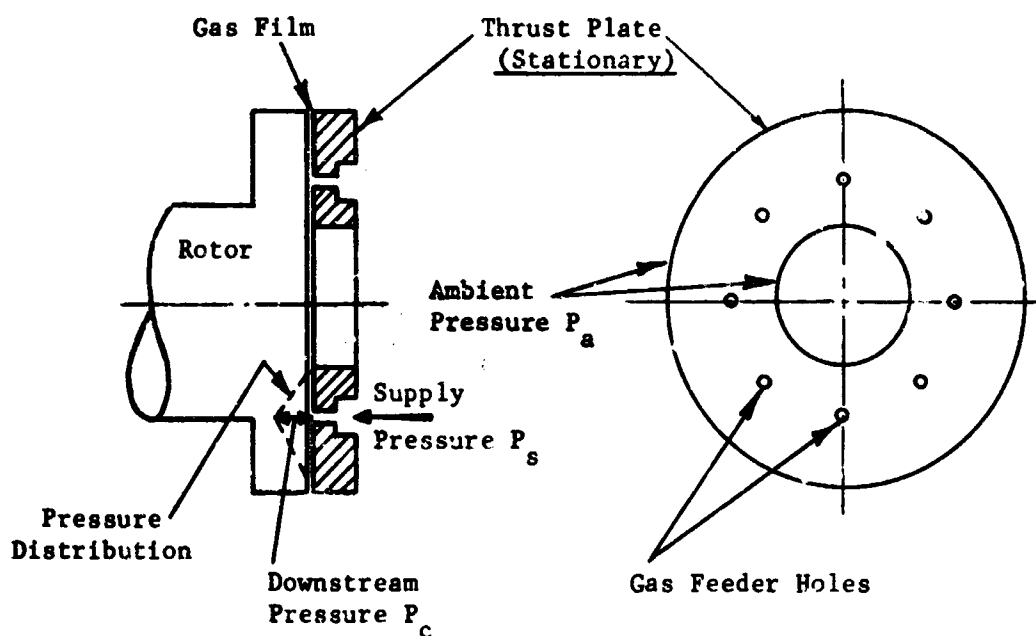
The purpose of this chapter of the manual is to enable a designer to select the dimensions and operating conditions for an externally-pressurized steam bearing which must meet a given set of specifications such as load, bearing stiffness, etc. The report gives design methods and numerous design charts from which the actual bearing performance can be evaluated. The design charts are in dimensionless form whereby a wide range of journal bearing geometries and operating conditions are covered.

The pressurized steam is supplied to the bearings through inherently compensated feeding holes. Other methods of restriction in normal gas bearing design have been applied at times (fixed orifice, porous walls, thin tubes, membranes, etc.), but most of the experience and data thus far obtained are concerned with the inherently compensated feed holes. Hence, the present section is devoted solely to inherently compensated bearings.

The data for the design charts have been obtained by computer programs. The basic analyses can be found in Refs. III-1 to III-5 and have not been included in the present text. The fundamental equations derive from the theory of gas lubrication and embody the conventional set of assumptions such as: the steam film is very thin compared to the other bearing dimensions, the film is isothermal, inertia effects are small (laminar flow) and the steam is single-phased (i.e., wet steam is excluded). Probably the most serious limitation on the analysis, and thus on the numerical results, is the neglect of shock effects and turbulence effects in the film. These effects may dominate in the film around the feeder hole entrances and can have a profound influence on the overall bearing performance. At present there is no method by which these effects can be included in the analysis but the designer should be aware of this shortcoming. Presently this design data does predict actual performance quite adequately as is indicated in the chapter on experimental results.

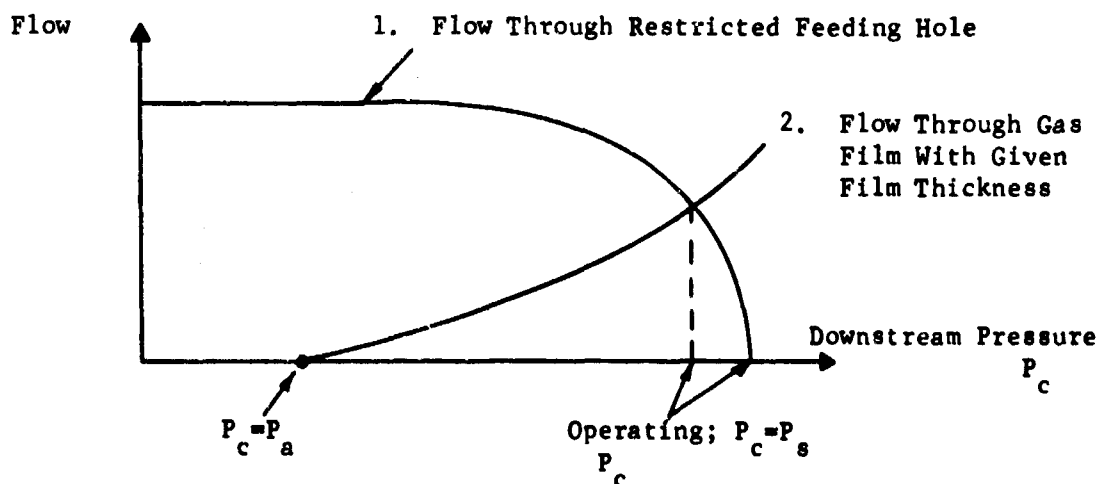
DISCUSSION ON THE PRINCIPLE OF HYDROSTATIC LUBRICATION

The function of a bearing is to separate two members which move relatively to each other. The gap between the members, called the "film", is filled with a lubricant which in the present case is high quality, or superheated steam. The thickness of the film is generally of the order of .5 to 3 mils. In order to maintain separation the film must be under pressure. In the externally pressurized bearing this pressure is produced directly by supplying pressurized gas to the bearing through feed holes in the bearing wall. To illustrate the principle of hydrostatic or externally pressurized bearing lubrication consider first a thrust bearing:



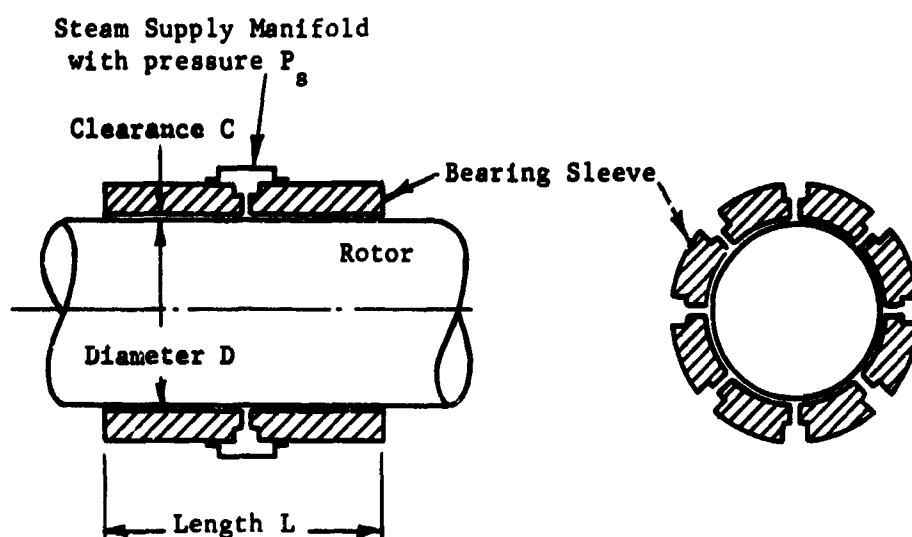
The gas is supplied at a pressure of P_s psia and exhausts to ambient pressure P_a psia at the inner and outer circumference of the annular bearing. The pressure immediately downstream of the feeding holes is denoted as P_c such that P_c is smaller or equal to the supply pressure P_s , depending on the amount of restriction present at the feeder hole. The pressure distribution radially is then "triangular" with its apex at the feeder hole and the load carrying capacity can be calculated simply by integrating the pressure over the area of the bearing. The maximum load for a given supply

pressure is obtained if the feeder holes afford no restriction in which case the pressure downstream of the holes equals the supply pressure ($P_c = P_s$). The load becomes simply the product of the supply pressure and an "area factor," determined solely by the dimensions of the bearing. Thus, it is evident that the bearing is "unstable" since the film force does not vary with the film thickness. If the actual thrust load is greater than this fixed value, the two bearing members would be in solid contact, and if the thrust load is smaller the separation of the members would, theoretically, become infinite, in other words, the stiffness of the bearing is zero. Therefore, the feeding holes must be designed such that they restrict the flow and produce a pressure drop (i.e., $P_c < P_s$). The restriction takes place in the small, annular "curtain" area between the rim of the feeding hole and the surface of the thrust collar. This type of restriction is called "inherent compensation." When the feeding holes are restricted, the bearing possesses stiffness and is "stable" from the point of view of load carrying capacity, (it may still be "dynamically" unstable as discussed later). To illustrate, assume the bearing to operate with a certain load and a downstream pressure P_c where $P_c < P_s$. P_c is determined from the requirement of flow equilibrium, i.e., the mass flow into the bearing through the feeding holes must equal the mass flow exhausted to ambient through the gas film. The higher the downstream pressure is, the smaller becomes the flow into the bearing (curve "1" below) and the larger becomes the gas film flow (curve "2" below), and vice versa. This can be shown graphically:



Next, increase the external thrust load. Then the gas film thickness diminishes, consequently the flow resistance of the film becomes larger and the downstream pressure P_c must increase in order to reduce the inflow (i.e. curve "2" above moves down). The net result is an increase in load carrying capacity to balance the added external load, i.e., the bearing possesses stiffness. Thus, it can be concluded that only with restricted feeding holes does the bearing have stiffness. However, if the restriction is so large that the pressure drop through the feeding holes absorb all the available supply pressure, the downstream pressure P_c becomes essentially equal to ambient in which case both the load carrying capacity and the stiffness are zero. Therefore, it is evident that there is an optimum amount of restriction at which the stiffness is a maximum or to be more specific, there is an optimum ratio between the flow resistance of the gas film and the flow resistance of the feeding holes. This "resistance ratio" is dimensionless and is called the restrictor coefficient, identified by the symbol Λ_s . It is one of the dimensionless parameters governing the performance of an externally pressurized bearing and is used in all the design charts given in this section. Another dimensionless parameter is the pressure ratio: P_s/P_a , i.e. the ratio between supply pressure and ambient pressure. A third parameter is used to describe the bearing geometry; namely, L/D (L = bearing length, D = bearing diameter). Once the values of these three parameters are known, the bearing load carrying capacity, flow, stiffness, etc., can be calculated from design charts as demonstrated later. The design charts and tables are presented separately, as an Addendum, at the end of this chapter.

In the externally pressurized journal bearing the feeding holes are arranged around the circumference of the bearing and there may be one or two planes of holes, identified by "Single Plane Admission" or "Double Plane Admission":



Externally Pressurized Journal Bearing, Single Plane Admission

The load carrying capacity of the externally pressurized bearing derives from a variation of pressure around the circumference. Thus, if the journal is concentric with the bearing sleeve the pressure is uniform circumferentially and the net load becomes zero. If the journal is displaced downwards so that it is eccentric with respect to the sleeve, the thickness of the gas film at the bottom becomes smaller, the flow resistance increases and forces the pressure at the bottom feeder holes to increase. At the same time the pressure in the top half of the bearing decreases due to the increase there of the film thickness. Thereby a net force is produced, directed upwards, which resists the displacement of the journal center, i.e., the bearing is able to carry a load. This method of carrying the load is completely analogous to the way the externally pressurized thrust bearing generates its stiffness. As a matter of fact, the externally pressurized journal bearing can in principle be looked upon as consisting of a number of axial strips, each

strip fed by one feeding hole and each strip acting as a thrust bearing. Projecting the stiffness of each strip upon the direction of load and summing up over all the strips would yield the total stiffness and, hence, the load carrying capacity of the journal bearing. Therefore, the restrictor coefficient Λ_s is a very important design parameter for the journal bearing and it has an optimum value at which the load carrying capacity is a maximum.

To calculate the performance of an externally pressurized bearing it is necessary to establish the pressure and the flow throughout the steam film. This is done by setting up a flow balance for a very small film element expressed in terms of a partial differential equation, and then integrate throughout the film. At each feeding hole the pressure (called P_c) must be adjusted such that the flow into the steam film equals the flow through the hole. This latter flow is a function of the downstream pressure P_c as shown by curve "1" in the figure on page 3. Note that when $P_c/P_s \leq .546$ the feeder hole is choked such that the feeder hole flow is fixed and independent of P_c .

The greatest difficulty arising in the solution of the externally pressurized bearing is to establish the downstream pressure P_c . Thus, the restrictor flow curve discussed above is really only valid when the restrictor area is much smaller than any other area in the flow passage and when the gas velocity can be neglected both before and after the restrictor. However, in an externally pressurized bearing the flow enters the bearing as a jet, impinging on the journal surface and thereby recovering some of the pressure drop. Furthermore, as the flow enters the gas film proper there occurs entrance losses which frequently are of a substantial magnitude. If the flow is large, there may even exist a region of shock with corresponding subambient pressures. It is evident that an analysis which represents this complex physical situation by means of a single value for the downstream pressure can only be approximate. On the other hand, to include a more exact analysis would make the calculation of the bearing much more complicated and expensive and would also introduce a large number of additional design parameters. Thereby the advantage of using design charts

for designing would be greatly reduced with the corresponding loss in simplicity, so important when selecting the dimensions and the operating conditions for the bearing. Fortunately, experience has shown the general validity of the simplified analysis but in using the design charts one must realize their inherent limitations and safety margins must be imposed on the calculated results. See for example the previous chapter of this manual on experimental results.

DIMENSIONLESS DESIGN PARAMETERS

The performance of the externally pressurized journal bearing is given by design charts and tabulations of data. In order for the charts and data to have general validity and thereby cover as wide a range of bearing dimensions and operating conditions as possible, it is most economical to plot the charts and tabulate the data in dimensionless form. In the following the definition of the dimensionless parameters will be given. The use of the design data is discussed later.

Externally Pressurized Journal Bearing

For the journal bearing there are 5 governing dimensionless parameters, namely:

1. The Length-to-Diameter Ratio: L/D

Referring to Fig. III-1, it is seen that L is the overall bearing length. For a double plane admission bearing it is necessary to also specify the length L_1 between the admission planes.

Hence, an additional parameter enters, namely, L_1/D . Setting the combined length outside the feeding planes equal to L_2 such that $L = L_1 + L_2$, it proves to be convenient to use L_2/D as a separate parameter, denoted as ξ . Therefore:

$$\begin{aligned} \text{Outside Length-to-Diameter Ratio: } \xi &= \begin{cases} \frac{L_2}{D} & \text{for single plane admission} \\ \frac{L_2}{D} & \text{for double plane admission} \end{cases} \\ \text{Inside Length-to-Diameter Ratio} &= \begin{cases} 0 & \text{for single plane admission} \\ \frac{L_1}{D} & \text{for double plane admission} \end{cases} \end{aligned}$$

2. The Supply Pressure Ratio: P_s/P_s

3. The Restrictor Coefficient: $\Lambda_s = \frac{6\mu qd\sqrt{RT}}{P_s C^2}$

(i.e. the ratio between the flow resistance of the gas film to the resistance of the feeder hole restrictor).

4. The Eccentricity Ratio: e

5. Squeeze Number: $\sigma = \frac{12\mu v}{p_a} \left(\frac{R}{C}\right)^2$

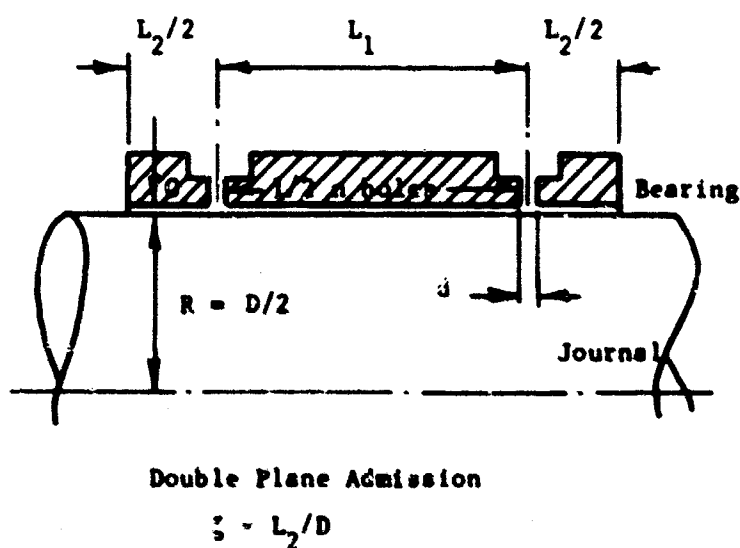
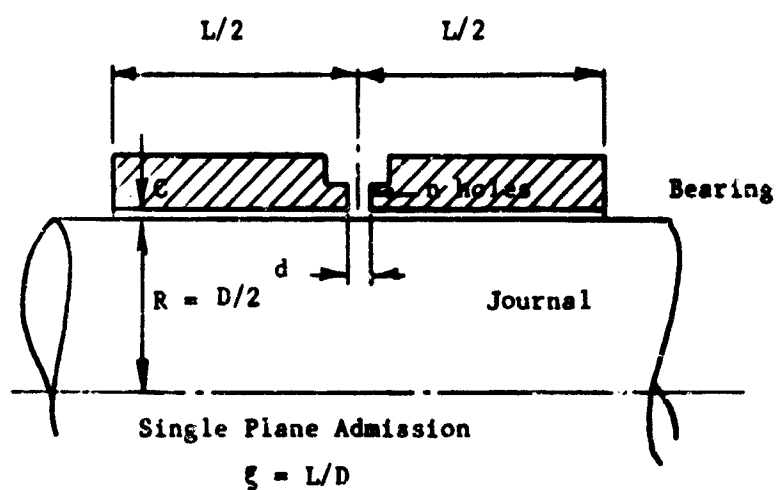


Figure III-1 Externally Pressurized Journal Bearing

The Nomenclature is (refer also to Fig. III-1)

C	Radial clearance, inch
D	Bearing diameter, inch
d	Feeder hole diameter, inch
e	Eccentricity between bearing and journal centers, inch
n	Total number of feeding holes, (i.e. total of all admission planes)
L	= $L_1 + L_2$, total bearing length, inch
L_1	Distance between admission planes, inch
L_2	Combined length outside admission planes, inch
P_a	Ambient pressure, psia
P_s	Supply pressure, psia
Q	Gas Constant, $\text{in}^2/\text{sec}^2/^\circ\text{R}$
T	Total temperature, $^\circ\text{R}$
γ	Ratio of specific heats, average value for steam = 1.3
δ	= $\frac{nd}{C}$, Inherent compensation factor
Δp	= $P_s - P_a$, Pressure difference, psi
μ	Gas viscosity, $\text{lbs. sec}/\text{in}^2$ (unit also called reyn)
ν	Squeeze frequency, rad/sec

Notes: In most published data the gas constant Q is not given in the above specified units. Two conversion factors shall be given:

$$Q, \frac{\text{in}^2}{\text{sec}^2/^\circ\text{R}} = \begin{cases} 4632.8 \left[Q, \frac{\text{ft. lbs}}{\text{lbs. } ^\circ\text{R}} \right] \\ 3.6051 \times 10^6 \left[Q, \frac{\text{Btu}}{\text{lbs. } ^\circ\text{R}} \right] \end{cases}$$

The figure which follows, (Fig. III-2), gives values of Q for saturated and superheated steam.

The total temperature is given by:

$$T, ^\circ R = T, ^\circ F + 460$$

For saturated steam at $250^\circ F$, $RT = 710 \times 83.5 \times 4632.8 = 2.8 \times 10^8 \frac{\text{in}^2}{\text{sec}^2}$

$$\text{and } \sqrt{RT} = 1.68 \times 10^4 \frac{\text{in}}{\text{sec}}$$

The viscosity μ is given in reyns where $1 \text{ reyn} = 1 \text{ lb. sec/in}^2$. Frequently, published data give the viscosity in centipoise (cps). The conversion factor is:

$$\mu, \text{ reyn} = 1.45046 \times 10^{-7} \left[\mu, \text{ centipoise} \right]$$

Figure III-3 gives the viscosity for saturated & superheated steam as a function of temperature and pressure. Saturated steam at 100 psi has $\mu = 2.5 \times 10^{-9} \text{ reyn}$.

The above 5 parameters are the input parameters necessary to enter the design charts and tabulation of data. The output parameters are:

$$\text{Dimensionless stiffness: } \frac{CK}{\Delta p LD}$$

$$\text{Dimensionless mass flow: } \frac{6\sqrt{RT}}{\pi C^3 P_s^2} \xi G$$

$$\text{Dimensionless angular stiffness: } \frac{CK_{\text{ang}}}{\Delta p L^3 D}$$

$$\text{Dimensionless damping coefficient: } \frac{B}{\mu L \left(\frac{R}{C}\right)^3}$$

$$\text{Dimensionless angular damping: } \frac{B_{\text{ang}}}{\mu L^3 \left(\frac{R}{C}\right)^3}$$

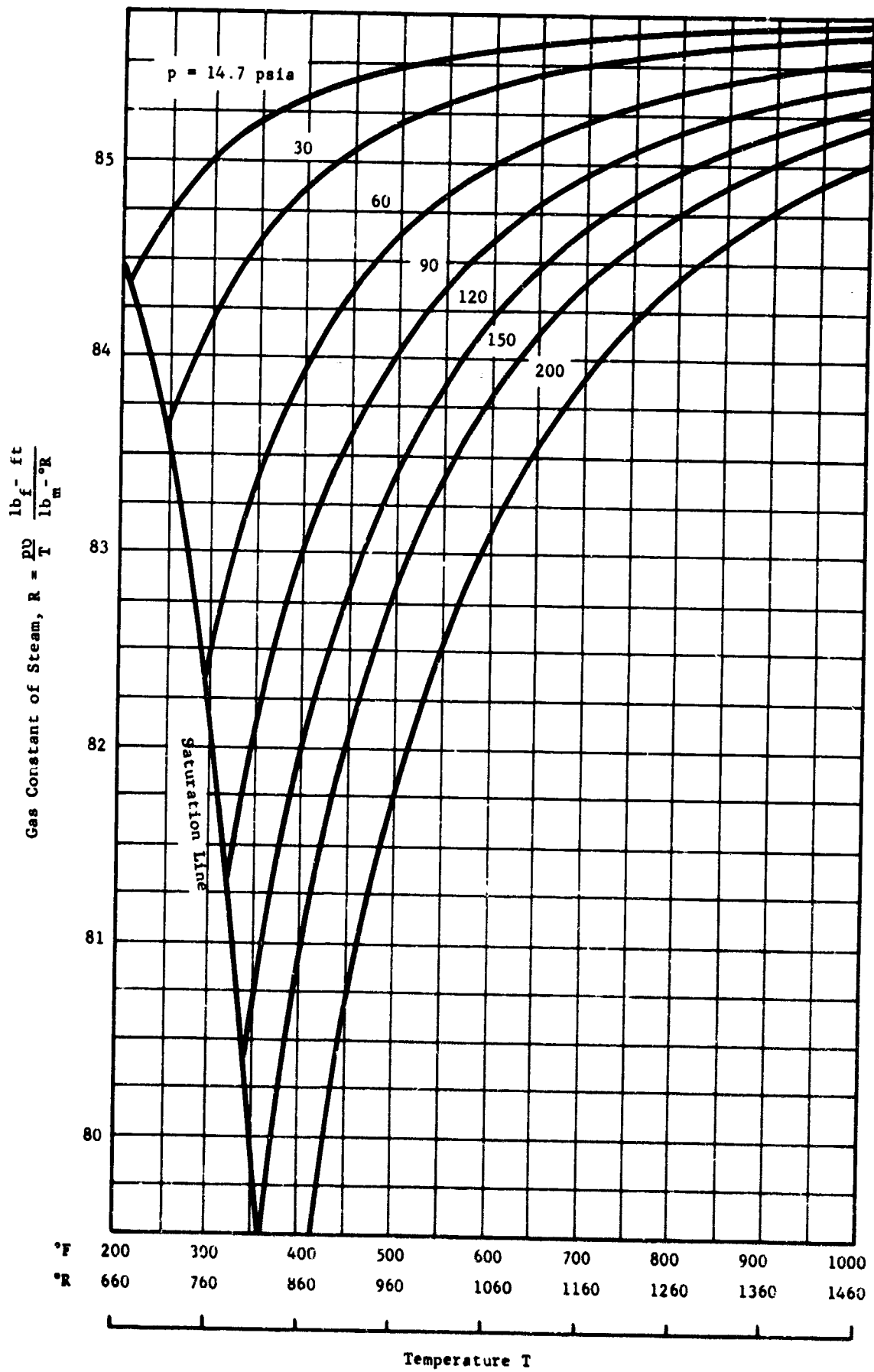


Fig. III-2 Gas Constant of Steam vs Temperature (calculated from properties given in Ref. 7)

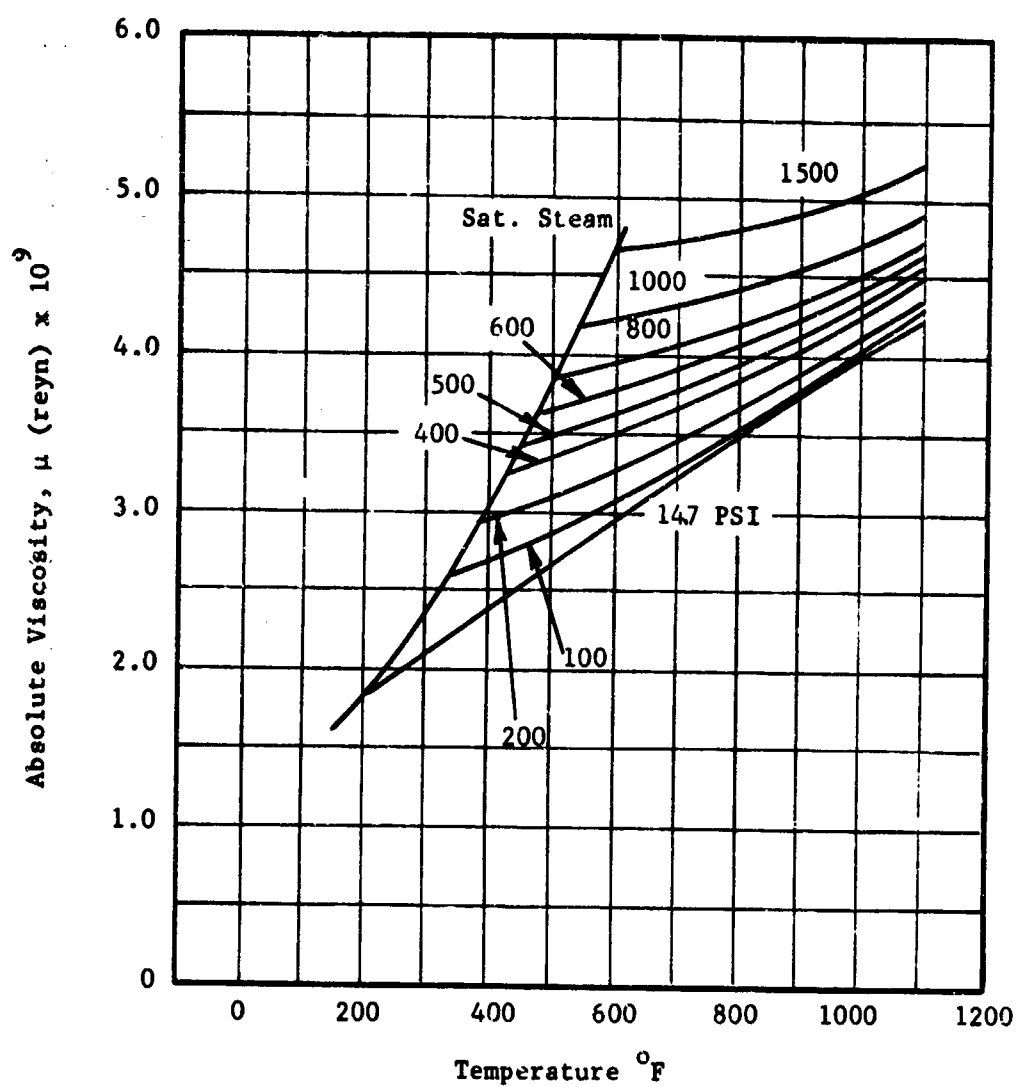


Fig. III-3 Experimental Values of Absolute Viscosity of Steam
(Refs. III-6 and III-7)

SELECTION OF THE BEARING DIMENSIONS AND USE OF THE DESIGN CHARTS

Externally Pressurized Journal Bearing

The role of the externally pressurized journal bearing is to support a given rotor. The rotor dimensions are selected from such considerations as the function the rotor must perform, the strength of the rotor and its stiffness. Once a rotor layout is available the bearing reactions and the journal diameters are known. These values may of course be subject to later change, depending upon the outcome of the bearing calculations, but as a first step towards sizing the bearing it is necessary to have this information.

Supply Pressure and Bearing Length

Let the given bearing reaction be W lbs. and the specified journal diameter be D inch. The first objective is to select the bearing length L and the required supply pressure P_s psia. To this end use the rule-of-thumb:

$$\frac{W}{(P_s - P_a)LD} \approx \begin{cases} .15 & \text{for single plane admission} \\ .20 & \text{for double plane admission} \end{cases}$$

where P_a is the ambient pressure in psia. Said in other words, the externally pressurized journal bearing can turn approximately 15 to 20 per cent of the available pressure drop into useful load carrying capacity. Within the limits normally imposed on the available supply pressure and the available space for the bearing, this relationship allows selecting P_s and L . The question of single plane versus double plane admission is largely a question of how critical it is to obtain the highest possible load and stiffness. Note, that in the design charts for double plane admission the planes are located halfway between the center of the bearing and the ends. This arrangement seems to be most practical, being a compromise between the maximum obtainable load carrying capacity and the corresponding increase in the flow requirements.

Radial Clearance

Once the supply pressure, the bearing length and the number of admission planes have been chosen the next step is to select the radial clearance, C , inch.

The clearance is the most critical dimension and should be set as small as possible since the flow is proportional to the cube of the clearance and the stiffness is inversely proportional to the clearance. Normal practice tends to give the clearance such a value that:

$$\frac{C}{R} \approx 0.5 \times 10^{-3} \text{ to } 1.5 \times 10^{-3}$$

where R is the journal radius in inch (i.e. $R = 0.5 \times D$). There are no firm rules for determining the exact value, rather the choice is based on the size of foreign particles which may enter the steam film, the magnitude of any possible heat expansion, the growth of the shaft due to rotation and the accuracy with which the journal and the bearing can be manufactured. The centrifugal growth of a hollow shaft due to rotation can be calculated from the equation:

$$\text{radial centrifugal growth, inch} = 0.025564 \frac{\Gamma N^2 R^3}{E} \left[\frac{1-2\nu}{1-\nu} + \left(\frac{R_i}{R} \right)^2 \frac{3-2\nu}{1-\nu} \right]$$

where ν is Poisson's ratio ($\nu = .3$ for steel), E is Young's modulus of elasticity ($E = 3 \times 10^7$ lbs/in² for steel), Γ is the weight density in lbs/in³ ($\Gamma = 0.283$ lbs/in³ for steel), N is the speed in RPS and $\frac{R_i}{R}$ is the ratio of shaft inner to outer radii.

The manufacturing tolerances on the journal diameter and the bearing diameter should be specified such that the machined clearance does not deviate by more than 10 to 20 per cent from its nominal value.

Radial Stiffness

It is now possible to turn to the design charts. Use first Design Charts 1-6 which give the dimensionless radial stiffness $CK/(\Delta p LD)$ (defined on page 71) as a function of the restrictor coefficient $\Lambda_s \xi$ for several values of the length-to-diameter ratio $\frac{L}{D}$, for several values of the supply pressure ratio P_s/P_a and for both single and double plane admission. It is seen that the stiffness has a maximum value occurring at:

$$\Lambda_s \xi \approx 0.7 \text{ to } 1.0$$

where $\xi = L/D$ for single plane admission and $\xi = L_2/D$ for double plane admission. As a first estimate, choose the optimum value of $\Lambda_s \xi$. It is unnecessary at this stage to know the value of each quantity making up Λ_s .

Read off the corresponding value of the dimensionless stiffness $\bar{K} = CK/(\Delta p LD)$ using interpolation between the charts if necessary. Calculate the actual radial stiffness:

$$K = \Delta p LD \bar{K} / C \text{ lbs/in}$$

Critical Speeds of the Rotor

To decide if the obtained value of K is acceptable it is necessary to investigate the critical speeds of the rotor as influenced by K . In most applications employing externally pressurized gas bearings the rotor is very stiff compared to the bearing stiffness and the two lowest critical speeds may be calculated from:

$$[N, \text{RPS}]_{\text{critical}} = \frac{1}{2\pi} \sqrt{\frac{1}{2}(n_2 + n_1) \pm \sqrt{\frac{1}{4}(n_2 - n_1)^2 + n_3^2}}$$

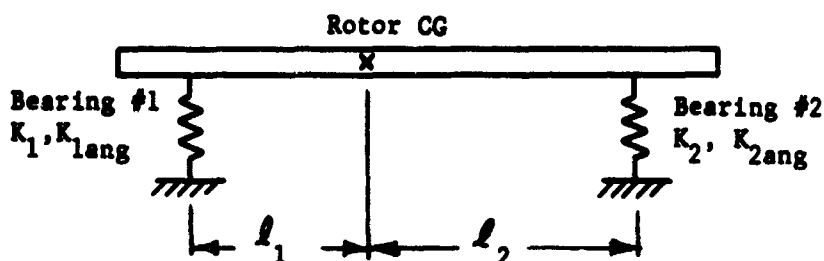
where:

$$n_1 = \frac{K_1 + K_2}{M} \left(\frac{\text{rad}}{\text{sec}} \right)^2$$

$$n_2 = \frac{K_1 l_1^2 + K_2 l_2^2 + K_{1\text{ang}} + K_{2\text{ang}}}{I_T - I_p} \left(\frac{\text{rad}}{\text{sec}} \right)^2$$

$$n_3 = \frac{(-K_1 l_1 + K_2 l_2)^2}{M(I_T - I_p)} \left(\frac{\text{rad}}{\text{sec}} \right)^4$$

and:



K_1, K_2 Radial stiffness of bearing 1 and 2, respectively, lbs/in

$K_{1\text{ang}}, K_{2\text{ang}}$ Angular stiffness of bearing 1 and 2, respectively, lbs.in/radian

l_1, l_2 Distance from CG of rotor to bearing 1 and 2, respectively, inch

M Total rotor mass = (rotor weight, lbs)/386.07, lbs.sec²/in

I_T Transverse mass moment of inertia around CG, lbs.in.sec.²

I_p Polar mass moment of inertia, lbs.in.sec.²

The angular stiffness K_{ang} is discussed later and may at this stage be set equal to zero in the above equation. Thus, the two lowest critical speeds may be determined and if one of them coincides with the operating speed or is close to the operating speed (within approximately 25 percent) the design must be modified, in general by changing the bearing stiffness.

Hydrodynamic Instability

A further consideration is important in this connection. The bearing stiffness must be sufficiently high that the lowest critical speed is greater than half of the operating speed. This requirement is necessary in order to avoid hydrodynamic instability (fractional frequency whirl). Adding a safety margin the requirement can be expressed as:

$$\text{lowest critical speed} > 0.6 \text{ (operating speed)}$$

Experience indicates that this is not a conservative rule.

Bearing Flow

At this point the final design value of the restrictor coefficient Λ_s should be known. Knowing Λ_s , and the supply ratio P_s/P_a enter Design Chart-7 to read off the dimensionless flow $\bar{G} = 6\mu RT_5 G / (\pi p_s^2 C^3)$. Calculate the actual total mass flow to the bearing:

$$G, \text{ lbs. sec./in} = \frac{\pi C^3 P_s^2}{6\mu RT_5} \bar{G}$$

To get the flow in another, more convenient unit:

$$G, \text{ lbs/ hr} = 1.39 \times 10^6 \left[G, \text{ lbs. sec/in} \right]$$

If this flow exceeds the maximum available capacity of the supply source or is excessive from other considerations usually the only possibility is to reduce the radial clearance C (the supply pressure can of course be reduced if the calculated stiffness and load is greater than required). Note, that by decreasing the clearance the stiffness is increased (the stiffness is inversely proportional to C) so that a reduction in supply pressure may be possible, thereby further reducing the flow. Hence, from the flow calculation in combination with the previously mentioned considerations the final design value of the radial clearance can be established.

Restrictor Downstream Pressure

Occasionally, it is desired to know the pressure P_c downstream of the restrictor (for an inherently compensated bearing P_c is the pressure just outside the rim of the feeder hole). P_c can be calculated as follows: from the already determined dimensionless flow \bar{G} and the corresponding value of $\Lambda_g \xi$ compute: $\bar{G}_0 = \frac{\bar{G}}{\Lambda_g \xi}$. Enter Fig. III-4 and read off the value for P_c/P_s from which P_c is found directly. \bar{G}_0 is the dimensionless restrictor mass flow:

$$\bar{G}_0 = \frac{G_0 \sqrt{RT}}{\pi d h P_s} = \begin{cases} C_d \sqrt{\frac{2k}{k-1}} \left(\frac{P_c}{P_s}\right)^{1/k} \sqrt{1 - \left(\frac{P_c}{P_s}\right)^{\frac{k-1}{k}}} & \text{for } \left(\frac{2}{k+1}\right)^{\frac{k}{k-1}} \leq \frac{P_c}{P_s} \leq 1 \\ C_d \sqrt{\frac{2k}{k+1}} \left(\frac{2}{k+1}\right)^{\frac{1}{k-1}} & \text{for } \frac{P_c}{P_s} \leq \left(\frac{2}{k+1}\right)^{\frac{k}{k-1}} \text{ (choked orifice)} \end{cases}$$

where:

G_0 Mass flow per feeder hole, lbs. sec/in

k The ratio of specific heats

C_d Discharge coefficient

and the other symbols have been defined previously. The present design curves are based on $k = 1.3$ (valid over a wide range of steam conditions) such that the feeder hole is choked for $P_c/P_s \leq .546$ where $\bar{G}_c = 0.67 C_d$. The discharge coefficient C_d is representative of a sharp-edged orifice and decreases "quadratically" as the orifice becomes unchoked, assuming a value of approximately 0.6 for $P_c/P_s = 1$. Under choked conditions $C_d \approx 0.72$.

It should be noted that the feeder holes are choked for small values of $\Lambda_g \xi$ (approximately for $\Lambda_g \xi < .3$), becoming unchoked as $\Lambda_g \xi$ increases.

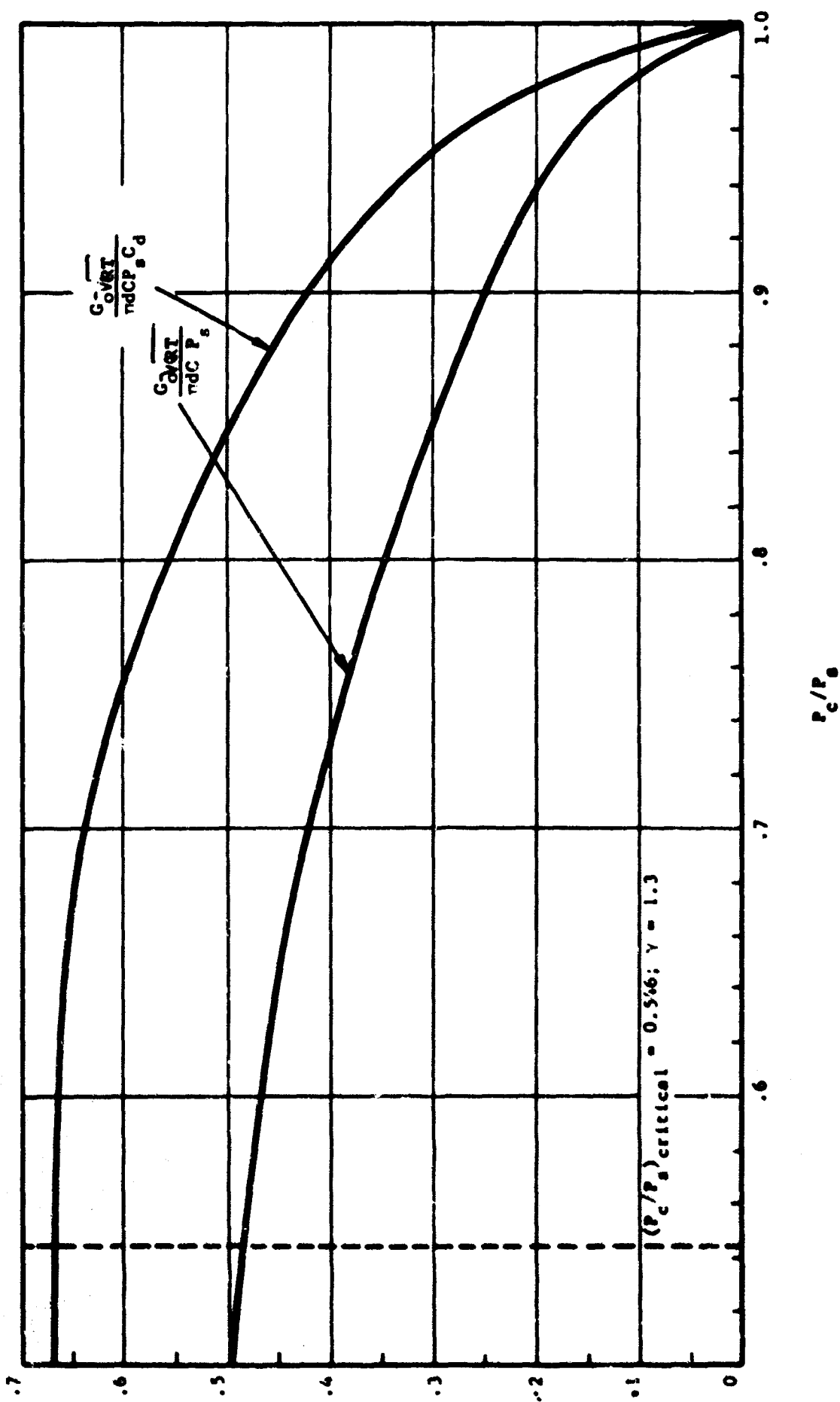
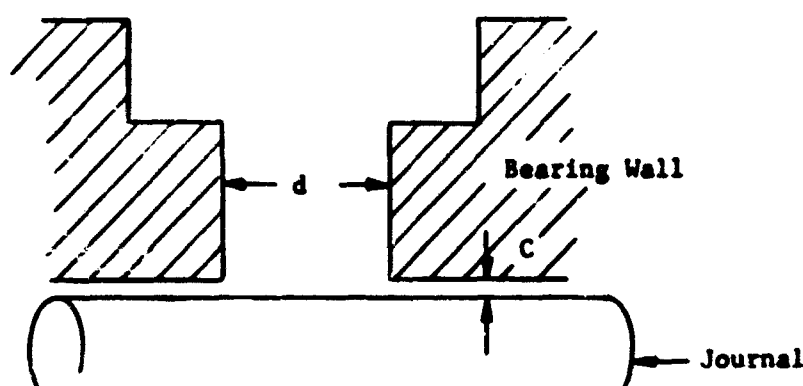


FIG. III-4 Dimensionless Flow Through Restrictor (Steam, $\gamma = 1.3$)

Number and Diameter of Feeder Holes

The next step is to determine the number of feeder holes, n , and the diameter, d , of the feeder hole:



Feeder Hole Geometry

According to the definition of Λ_s :

$$nd = \frac{P_s C^2}{6\eta \sqrt{RT}} \Lambda_s \text{ for inherently compensated restrictor.}$$

The values of all the quantities on the right hand side of the equation are known: the supply pressure P_s psia, the radial clearance C inch, the restrictor coefficient Λ_s , the gas viscosity η , reyns (see page 71 and Fig. III-3), the gas constant R , $\frac{\text{in}^2}{\text{sec}^2 \text{ } ^\circ\text{R}}$ (see page 70 and Fig. III-2) and the total temperature T , $^\circ\text{R}$. Hence, the value of the right hand side can be computed. A rule of thumb that can be used is to set $n > 4\pi \frac{D}{L}$ for single plane feeding and $n > 8\pi \frac{D}{L_2}$ for double plane feeding. Normally one does not design with double plane feeding unless absolute maximum stiffness is desired. Then, $\frac{L}{D}$ is usually greater than one. A minimum required number is obtained from Fig. III-5 which established the validity of the design charts. Use Fig. III-5, the rule of thumb, and the definition of Λ_s to establish n and d . Calculate $\frac{1}{\xi} \frac{d}{D}$ ($\xi = \frac{L}{D}$ for single plane admission and $\xi = L_2/D$ for double plane admission), enter Fig. III-5 and read off the minimum allowable value for $n \xi$. From this the minimum required number of holes is established.

and the actual number should be greater, at least such that n should never be less than 6 to 8 (to prevent lock-up, see later).

Having followed the outlined procedure and satisfied all the specified requirements the number of holes, n , and the feeder hole diameter, d , have been established. Hence, the exact value of the restrictor ratio Λ_s can be computed:

$$\Lambda_s = \frac{6\mu n d \sqrt{RT}}{P_s C^2}$$

From Design Charts 1 through 7, the dimensionless stiffness and flow can be obtained, thus allowing the computation of the actual stiffness and flow. It should be checked if this final stiffness value satisfied the requirements imposed by considerations of critical speeds and hydrodynamic instability as discussed earlier. Secondly, the load carrying capacity must be determined.

Load-Carrying Capacity and Lock-Up

For the normal range of operating conditions (say $0.1 \lesssim \Lambda_s \lesssim 2$) the load-carrying capacity is nearly linear with displacement up to an eccentricity ratio of $e \approx 0.4$ to 0.5 . Hence, if the specified bearing load is W lbs. and the calculated stiffness is K lbs/in., the operating eccentricity ratio becomes:

$$e = \frac{W}{CK}$$

(C = radial clearance, inch)

This value of e should be less than 0.4 (or maximum 0.5) in order to avoid the danger of lock-up. Lock-up is a phenomenon which is not too well understood. It manifests itself as a sudden forcing of the journal against the bearing wall when the journal eccentricity reaches a certain value. Thus, lock-up is equivalent to a negative spring rate beyond a critical load:

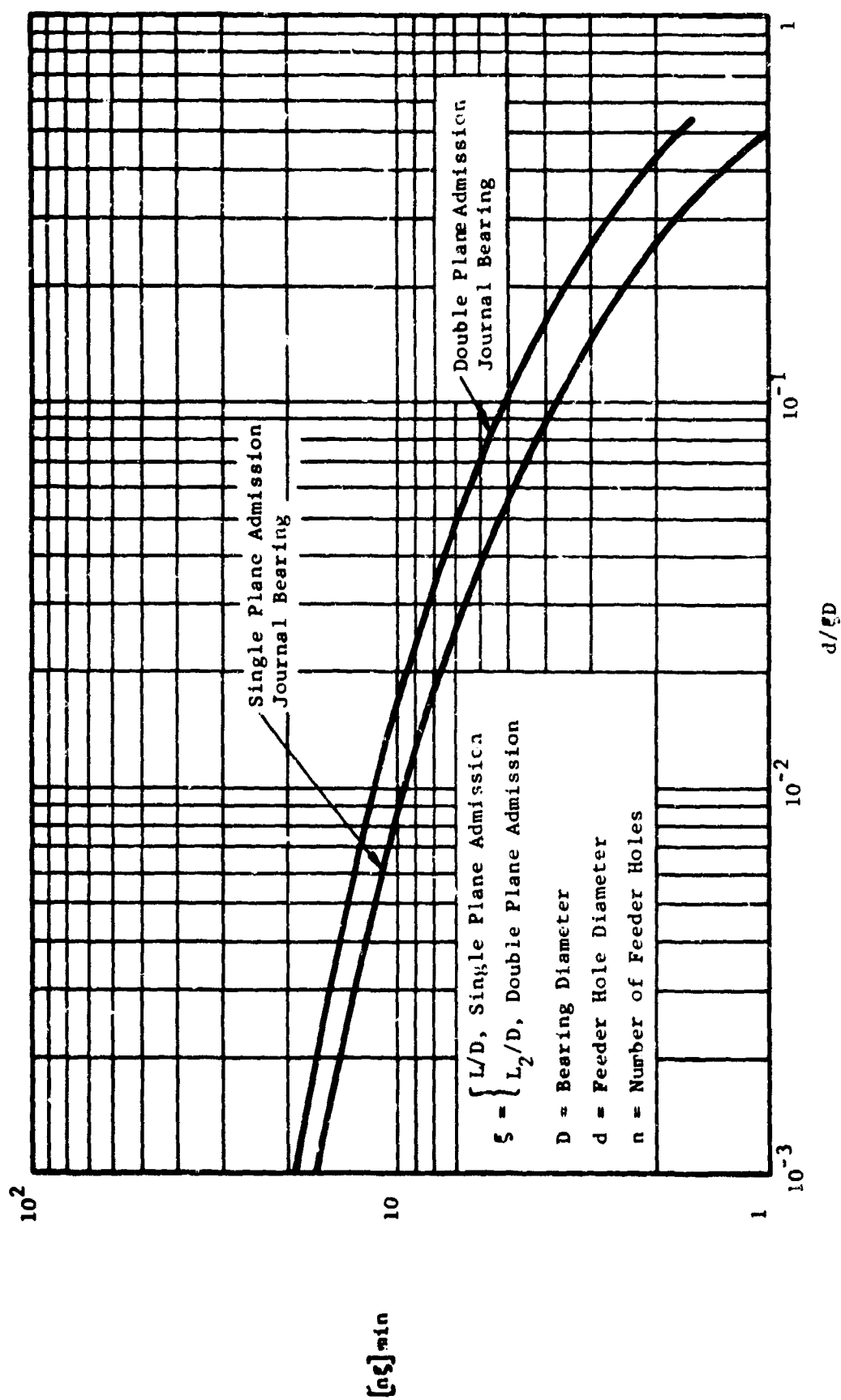
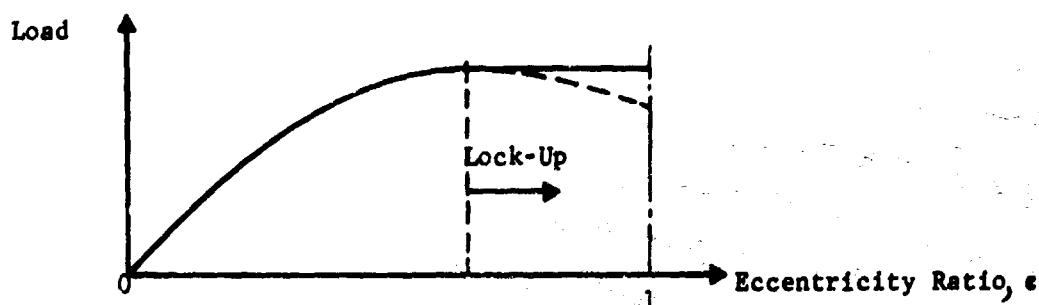


Fig. III-5 Minimum Number of Feeder Holes



Experience seems to indicate that lock-up is largely governed by the number of feeder holes and the feeder hole geometry. Too few feeder holes enhances the possibility of getting lock-up. Furthermore, unevenness in the flow distribution among the feeder holes due to manufacturing inaccuracies or faulty design may lead to lock-up. The localized pressure drop around the feeder hole rim as the flow enters the gas film may also contribute to lock-up. Too small a feeder hole diameter could cause large local pressure drops and should be avoided.

Power Requirements

The externally pressurized steam bearing uses power in two ways: the power needed to pump the steam through the bearing and the power extracted from the rotating shaft due to friction.

The power required to pump the steam through the bearing is given by:

$$\left[\text{Pumping power} \right]_{\text{steam through bearing}} = \frac{G \cdot R T}{6600} \log_e \left(\frac{P}{P_a} \right), \text{ HP}$$

Even though the viscosity of gases is very small compared to more conventional lubricants like oil, the friction power loss in a gas bearing cannot be neglected. Rotors supported in gas bearings are normally running at high speeds and the radial clearance is smaller than in conventional bearings. Furthermore, in an oil bearing the oil helps to cool the bearing whereas

in a gas bearing the generated heat must be carried away by the bearing and the shaft. Hence, for high speed rotors it is necessary to know the bearings power loss in order to ensure that the dissipated heat does not cause high temperature gradients and thereby make it impossible to operate the bearing. In addition, the overall input or output power for the machine may be sufficiently small that the friction loss in the bearing can be a substantial amount of the total losses, thus impairing the efficiency of the unit.

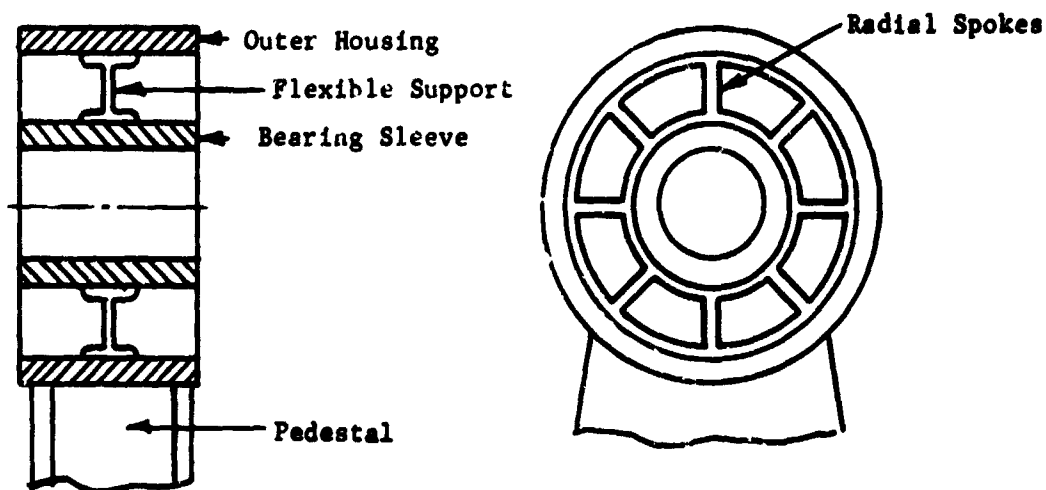
The friction power loss of an externally pressurized journal bearing is closely given by:

$$\text{Friction Power Loss} = \frac{\pi \mu L D^3 N^2}{6600 C \sqrt{1-e^2}} \text{ , HP.}$$

Rotor and Bearing Alignment, Angular Stiffness

Since the externally pressurized journal bearing normally has a small radial clearance and the bearing frequently is relatively long in order to carry the required load it becomes difficult to ensure a sufficiently accurate alignment between the bearings without taking special precautions. It takes only a small amount of misalignment to effectively lock the rotor in its bearings and prevent operating the rotor. In most cases, therefore, the bearings should not be mounted rigidly in their pedestals but instead they should be provided with supports that will allow self-alignment of the bearings. Among the methods employed to obtain self-alignment the most common are: a) mounting the bearing in ball bearings, b) providing a spherical seat between the bearing housing and the pedestal, and c) mounting the bearing in a flexible diaphragm. The two first methods suffer from the requirement of lubricating the members in contact thereby losing some of the advantages of the gas bearing. Thus, if grease lubrication is employed, the bearing must be sealed from the high temperature steam environment. It is possible to design the spherical seat as an externally bearing in itself, but too little experience is available to serve as a guide for a design. However, the third method i.e. mounting the bearing in a flexible support, has been tried with success. Schematically, this method

can be illustrated by a sketch:



The shown flexible support consists of a number of radial spokes which are stiff in the radial direction but flexible in accommodating misalignment. Let the two corresponding stiffnesses be denoted as: the radial stiffness k_R and the angular stiffness k_A . For given dimensions of the spokes these stiffnesses are easily calculated from the standard beam formulas in strength of materials handbook. Note, that in calculating the angular stiffness the spokes both bend and twist.

The stiffnesses of the flexible support must satisfy two requirements:

- a) the radial stiffness k_R must be sufficiently high that the critical speeds of the rotor are not drastically lowered (usually greater than twice the bearing stiffness),
- b) the angular stiffness k_A must be sufficiently low that the bearing is able to follow the misalignment of the rotor (usually less than one-half the bearing angular stiffness).

To check the first requirement let the mass of the bearing housing be denoted as m_B lbs.sec²/in. Then the overall radial stiffness of the gas film plus the flexible support is:

$$\text{overall stiffness: } \frac{K(k_R - m_B \omega^2)}{K + k_R - m_B \omega^2}$$

where ω is the vibratory frequency in radians/sec and K is the previously determined bearing stiffness. ω should be set equal to $2\pi N$ where N is the rotor speed in RPS. This overall stiffness replaces the K value as used in the earlier equation for determining the critical speeds of the rotor. Thus, the system becomes more complex (it actually becomes a two-mass system with a corresponding increase in the number of natural frequencies). For practical purposes it is sufficient to require:

$$m_B < \frac{k_R}{16\pi^2 N^2} \quad \frac{\text{lbs. sec}^2}{\text{in}}$$

where N is the operating speed in RPS. This relationship assures that the natural frequency of the support by itself is twice the operating speed. If this imposes too severe a restriction, a more detailed analysis is necessary. When the inequality is satisfied, the overall stiffness is closely given by:

$$\text{overall stiffness} \approx \frac{K(k_B)}{K+k_R}$$

The value should be computed and the critical speeds of the rotor should be recalculated to ensure that they have not been seriously affected by the flexible support. It is seen that even if the radial stiffness of the support is double the bearing stiffness the critical speeds are still lowered by 20 per cent.

Turning to the alignment capability of the supports it is necessary first to obtain the angular stiffness of the gas film. This stiffness is given as a dimensionless quantity $\bar{K}_{ang} = CK_{ang} / (\Delta P L^3 D)$ in Design Charts 8-13. Enter the graphs with the already determined value of $\Lambda_g \xi$ using interpolation where necessary and calculate the actual angular stiffness of the bearing as:

$$K_{ang} = \frac{1}{C} \Delta P L^3 D \bar{K}_{ang}$$

where all symbols have been previously defined.

Next, denote the mass moment of inertia of the bearing housing around a transverse axis through CG as I_B lbs. in. sec². Call the "misalignment" angle of the rotor θ , and that of the bearing housing, θ_B . Then:

$$\frac{\theta_B}{\theta} = \frac{K_{ang}}{K_{ang} + k_A - (2\pi N)^2 I_B}$$

The bearing housing will follow the misaligned rotor as long as this ratio is close to unity. From a practical point of view, this is satisfied if the properties of the bearing housing and the flexible support satisfies the relationships:

$$I_B < \frac{k_A}{(2\pi N)^2} \quad \text{lbs. in. sec.}^2$$

$$k_A < \frac{1}{2} K_{ang}$$

where N is the operating speed in RPS. Hence, the first inequality simply requires the angular natural frequency to be above the running speed. If this requirement cannot be satisfied, then this angular natural frequency must be kept low within the normal operating speed range.

Dynamic Operations and Bearing Damping

Occasionally the operating requirements are so severe or the available supply pressure and the space allowed to the bearing are so limited that the design of the bearing and its supports become marginal. Under such circumstances, it is frequently necessary to perform a detailed dynamic analysis of the rotor-bearing-support system to ensure satisfactory performance throughout the speed range. It is outside the scope of the present manual to set up such an analysis, but if the rotor is rigid for all operating speeds it is relatively simple to analyze the system by elementary methods as a two or three-mass system, each mass having two

degrees of freedom. If the rotor is flexible, it is almost a necessity to have access to a computer program which can handle the calculations. In either case, it is necessary to know the damping of the gas film in addition to the stiffnesses.

The steam film dynamic stiffness is expressed as two coefficients: K and K_{ang} as discussed previously. However, the dynamic coefficients are frequency dependent; but for inherent compensation and $P_s/P_a > 5$, only mildly so. The variation of dynamic radial and angular stiffnesses with squeeze number is given in Design Tables 1 through 6.

The steam film damping is expressed by two damping coefficients: B (lbs.sec/in), the radial damping coefficient, and B_{ang} (lbs.in.sec/radian), the damping coefficient for angular motion. The latter coefficient is primarily of importance in investigating the angular vibrations of the flexibly supported bearing housing. Unfortunately, the damping coefficients depend strongly on the frequency of the vibration (i.e. the rotor speed) and reduce to zero for high frequencies. However, for rotor speeds less than:

$$N < 0.05 \frac{P_s C^2}{\mu R^2}$$

all four coefficients are reasonably unaffected by frequency. Under those circumstances the static value of these coefficients can be given in form of design charts. Design Charts 14-19 give the dimensionless radial damping coefficient $\bar{B} = B/[\mu L(R/C)^3]$ and Design Charts 20-25 give the dimensionless angular damping coefficient $\bar{B}_{ang} = B_{ang}/[\mu L^3(R/C)^3]$. The actual coefficients are then computed as:

$$B = \mu L \left(\frac{R}{C}\right)^3 \bar{B} \quad \text{lbs. sec/in.}$$

$$B_{ang} = \mu L^3 \left(\frac{R}{C}\right)^3 \bar{B}_{ang} \quad \text{lbs. in. sec/radian}$$

The effects of vibration frequency on these quantities are given with the related dynamic stiffness quantities in tabular form in Design Tables 1 through 6. In order to use the charts and tables, it is necessary to know the values of $\frac{L}{D}$, $\Lambda_s \xi$, $\frac{s}{P}$ and σ . It should be noted that the angular damping coefficient may become negative. If the radial coefficient B was negative, which it is not for an inherently compensated bearing, the bearing would experience pneumatic hammer instability. However, a negative value of B_A only implies pneumatic hammer in exceptional cases which it would take a detailed analysis to investigate, Ref. III-8.

REFERENCES

- III-1. J. W. Lund, "The Hydrostatic Gas Journal Bearing with Journal Rotation and Vibration," JOURNAL OF BASIC ENGINEERING, TRANS. ASME, Series D, Vol. 86, 1964.
- III-2. J. W. Lund, "Hybrid Gas Journal Bearing Instability," Mechanical Technology Incorporated Report No. MTI-63TR60, issued for ONR, December 1963.
- III-3. J. W. Lund, "A Theoretical Analysis of Whirl Instability and Pneumatic Hammer for a Rigid Rotor in Pressurized Gas Journal Bearings," Mechanical Technology Incorporated Report, submitted for approval as a paper for ASME.
- III-4. J. W. Lund, R. J. Wernick and S. B. Malanoski, "Analysis of the Hydrostatic Journal and Thrust Gas Bearing for the NASA AB-5 Gyro Gimbal Bearing," Mechanical Technology Incorporated Report No. MTI-62TR26, issued for NASA, Huntsville, Alabama, October 1962.
- III-5. J. W. Lund, "Static Stiffness and Dynamic Angular Stiffness of the Combined Hydrostatic Journal-Thrust Bearing," Mechanical Technology Incorporated Report No. MTI-63TR45, issued for NASA, Huntsville, Alabama, October 1963.
- III-6. Hawkins, Solberg and Potter, "Super Heated Steam": TRANS. ASME 62, pp. 677-688, 1940.
- III-7. Keenan and Keyes, Thermodynamic Properties of Steam, John Wiley and Sons, Twenty-Third Printing, September 1951, p. 76.
- III-8. "Design of Gas Bearings," Vol. 1, Design Notes, Section 5.8, Hydrostatic Bearing Design, Dynamic Performance and Stability, and Section 6.1, Self-Acting Bearings, Fixed Self-Acting Journal Bearings. Design Manual for RPI-MTI Gas Bearing Design Course, (1966).

NOMENCLATURE

B	Radial damping coefficient, lbs.sec./in.
\bar{B}	$= B / \left[\mu L \left(\frac{R}{C} \right)^3 \right]$ for journal bearing, dimensionless damping coefficient
B_{ang}	Angular damping coefficient, lbs.in.sec./radian
\bar{B}_{ang}	$= B_{ang} / \left[\mu L^3 \left(\frac{R}{C} \right)^3 \right]$ for journal bearing, dimensionless angular damping coefficient
C	Journal bearing radial clearance, in.
C_d	Discharge coefficient
D	Journal bearing diameter, in.
d	Feeder hole diameter, in.
E	Modulus of Elasticity, psi
e	Journal eccentricity with respect to bearing center, in.
I_T	Transverse mass moment of inertia of rotor around CG, lbs.in.sec. ²
I_p	Polar mass moment of inertia of rotor, lbs.in.sec. ²
I_B	Transverse mass moment of inertia of bearing sleeve, lbs.in.sec. ²
K	Radial stiffness, lbs./in.
\bar{K}	$= CK / \left[(P_s - P_a) L D \right]$ for journal bearing, dimensionless stiffness
K_{ang}	Angular stiffness, lbs.in./radian
\bar{K}_{ang}	$= CK_{ang} / \left[(P_s - P_a) L^3 D \right]$ for journal bearing, dimensionless angular stiffness
k_R	Radial stiffness of flexible support, lbs./in.
k_A	Angular stiffness of flexible support, lbs. in./radian
k	Ratio of specific heats for steam ($\gamma = 1.3$)
L	Total length of journal bearing, in.
L_1	Distance between admission planes in journal bearing, in. ($L_1 = 0$ for single plane admission)
L_2	$= L - L_1$, combined journal bearing length outside admission planes, in. ($L_2 = L$ for single plane admission)
l_1, l_2	Distance of CG of rotor to the supporting journal bearings, in.
M	Rotor mass, lbs.sec. ² /in.
m_B	Mass of bearing sleeve, lbs.sec. ² /in.
n	Total number of feeding holes
N	Rotor speed, RPS
n_1, n_2, n_3	See Page 77
P_a	Ambient pressure, psia

P_s	Supply pressure, psia
P_c	Pressure downstream of feed g hole, psia
G	Mass flow, lbs.sec./in.
\bar{G}	$= G / \frac{\pi C^3 P_s^2}{6\mu \pi T \xi}$ for journal bearing, dimensionless flow
G_o	$= G/n$, mass flow per feeder hole, lbs.sec/in.
\bar{G}_o	$= \bar{G} / \Lambda_g \xi$ for journal bearing, dimensionless feeder hole flow (See Page 79)
R	$= 1/2 D$, journal bearing radius, in.
R_2	Inner radius of shaft, in.
R	Gas constant, in. ² /sec. ² /°R
T	Total temperature, °R
W	Bearing Load, lbs.
\bar{W}	$= W / [(P_s - P_a) LD]$ for journal bearing, dimensionless load
Γ	Weight density, lbs/in ³
ΔP	$P_s - P_a$, psi
δ	$= nd/C$, inherent compensation factor
e	$= e/C$, journal bearing eccentricity ratio
Λ_g	$= 6\mu nd \sqrt{RT/(p_s C^2)}$, restrictor coefficient
μ	Gas viscosity, lbs.sec./in ²
ν	Poisson's ratio ($\nu = .3$ for steel); Frequency, rad/sec.
ξ	$= L/D$, journal bearing, single plane admission $= L_2/D$, journal bearing, double plane admission
σ	Squeeze Number
ω	Frequency, radians/sec.

ADDENDUM (DESIGN CHARTS AND TABLES)**Fig. No.****Dimensionless Radial Stiffness vs Restrictor Coefficient
for:**

L/D = 1/2,	Single Row	1
L/D = 1,	Single Row	2
L/D = 1-1/2,	Single Row	3
L/D = 2,	Single Row	4
L/D = 1,	Double Row	5
L/D = 2,	Double Row	6

**Dimensionless Flow vs Restrictor Coefficient
for:**

All L/D	7
---------	---

**Dimensionless Angular Stiffness vs Restrictor Coefficient
for:**

L/D = 1/2,	Single Row	8
L/D = 1,	Single Row	9
L/D = 1-1/2,	Single Row	10
L/D = 2,	Single Row	11
L/D = 1,	Double Row	12
L/D = 2,	Double Row	13

**Dimensionless Radial Damping vs Restrictor Coefficient
for:**

L/D = 1/2,	Single Row	14
L/D = 1,	Single Row	15
L/D = 1-1/2,	Single Row	16
L/D = 2,	Single Row	17
L/D = 1,	Double Row	18
L/D = 2,	Double Row	19

ADDENDUM (DESIGN CHARTS AND TABLES) Cont'dFig. No.

Dimensionless Angular Damping vs Restrictor Coefficient
for:

L/D = 1/2,	Single Row	20
L/D = 1,	Single Row	21
L/D = 1-1/2,	Single Row	22
L/D = 2,	Single Row	23
L/D = 1,	Double Row	24
L/D = 2,	Double Row	25

Table No.

Dynamic Data, L/D = 1/2,	Single Row	1
Dynamic Data, L/D = 1,	Single Row	2
Dynamic Data, L/D = 1-1/2,	Single Row	3
Dynamic Data, L/D = 2,	Single Row	4
Dynamic Data, L/D = 1,	Double Row	5
Dynamic Data, L/D = 2,	Double Row	6

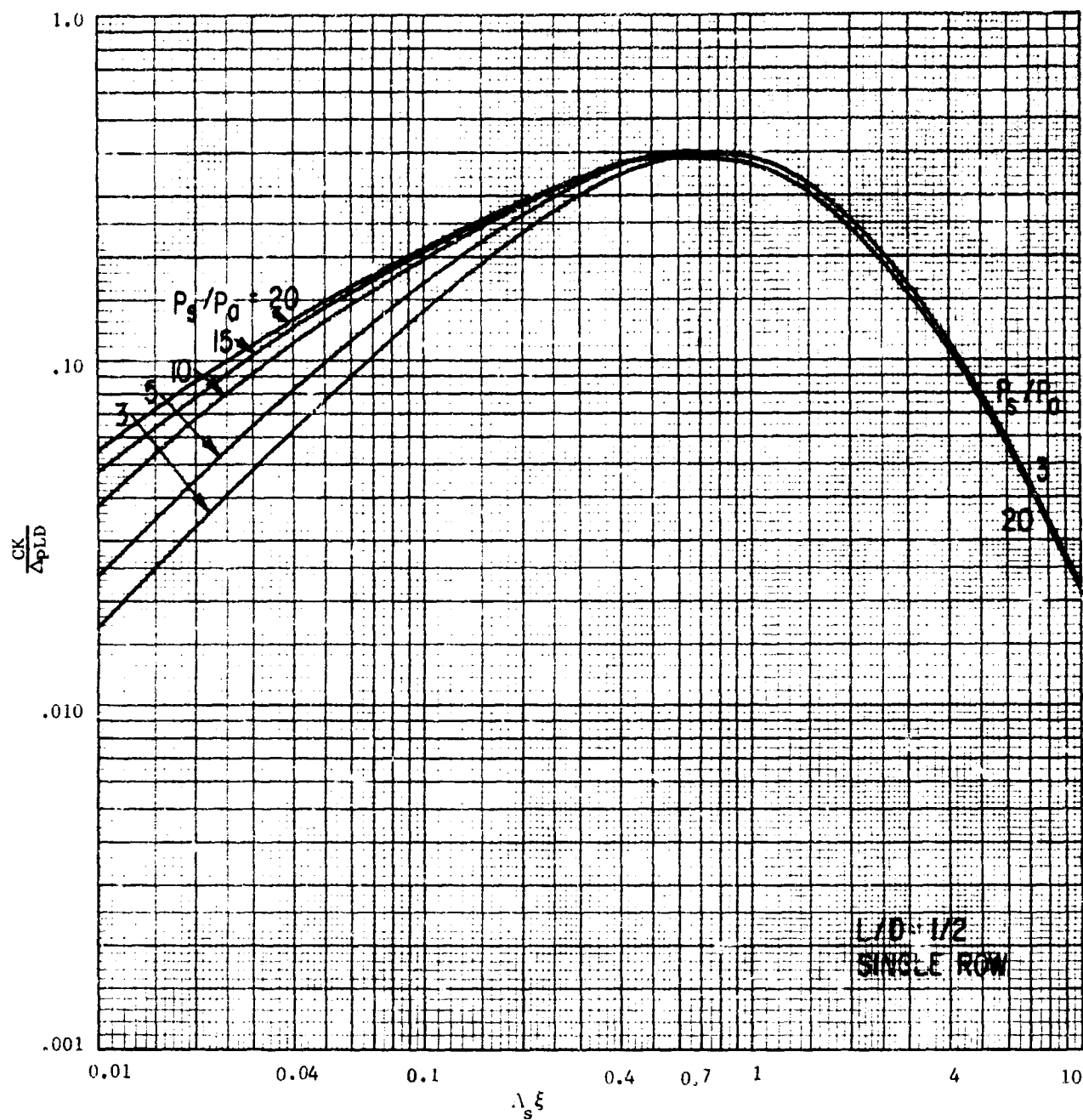


Fig. 1 Dimensionless Radial Stiffness Versus Restrictor Coefficient,
 $L/D = 1/2$, Single Row

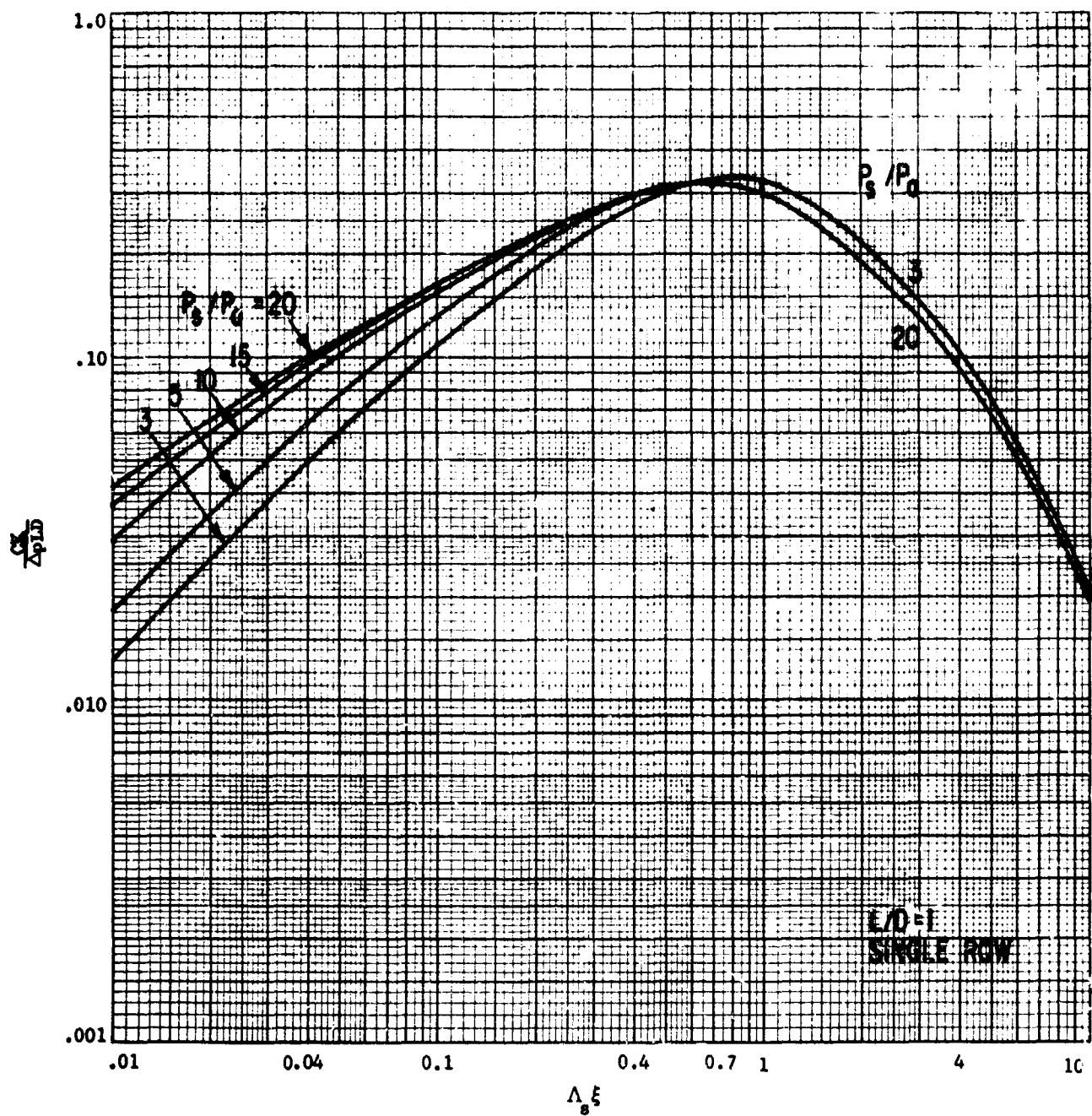


Fig. 2 Dimensionless Radial Stiffness Versus Restrictor Coefficient, $L/D = 1$, Single Row

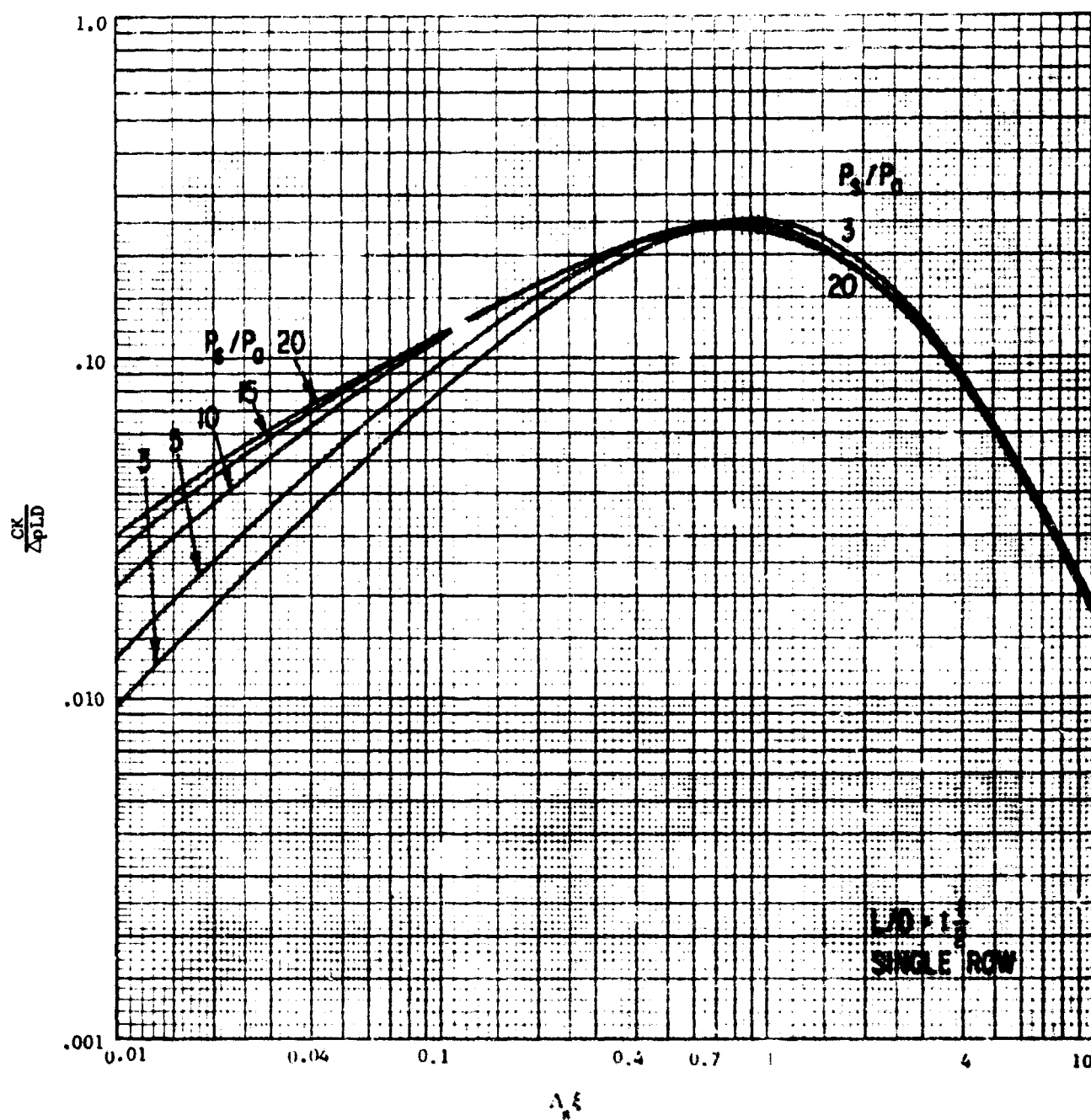


Fig. 3 Dimensionless Radial Stiffness Versus Restrictor Coefficient, $L/D = 1\frac{1}{2}$, Single Row

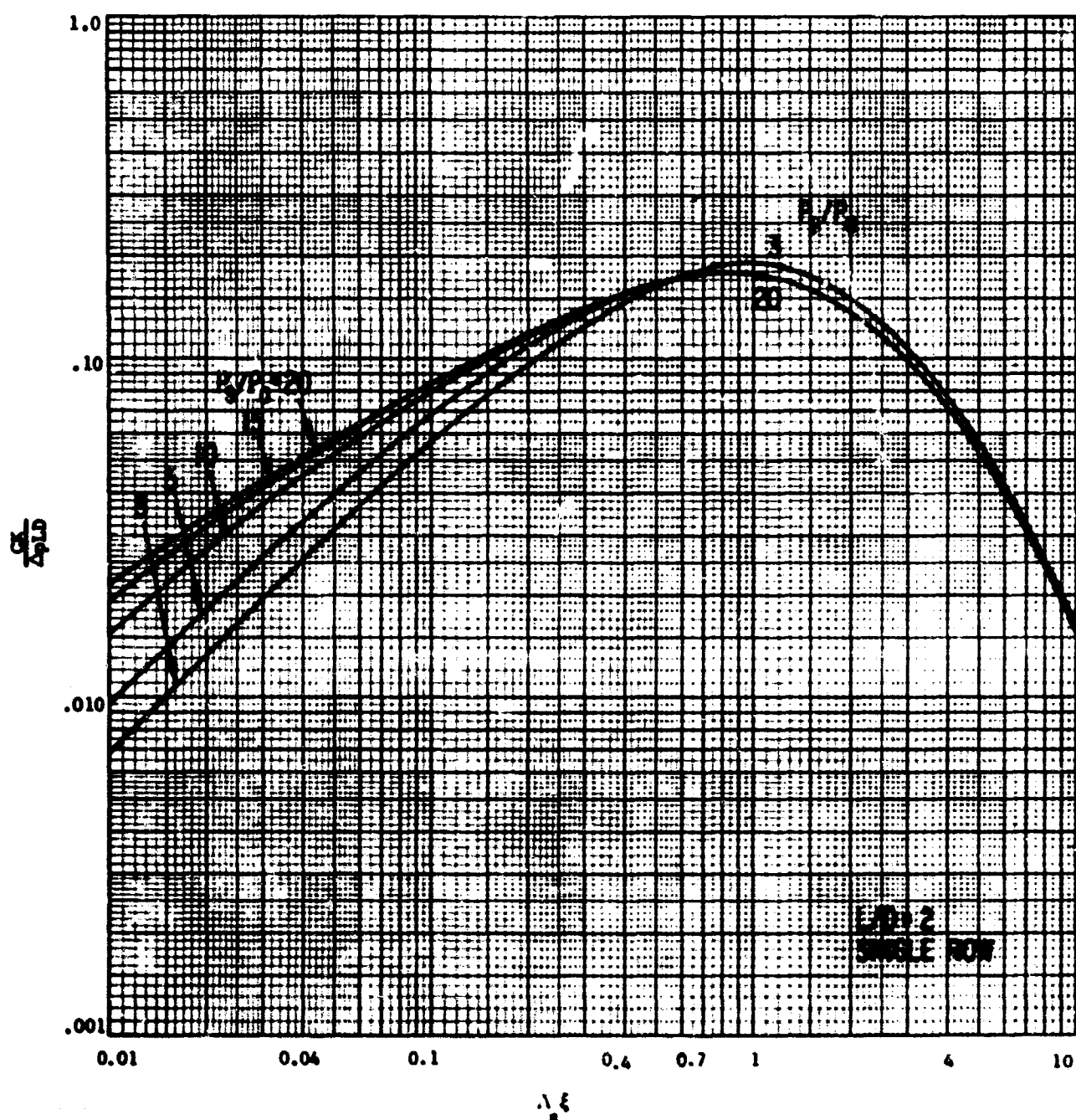


Fig. 4 Dimensionless Radial Stiffness Versus Restrictor Coefficient,
 $L/D = 2$, Single Row

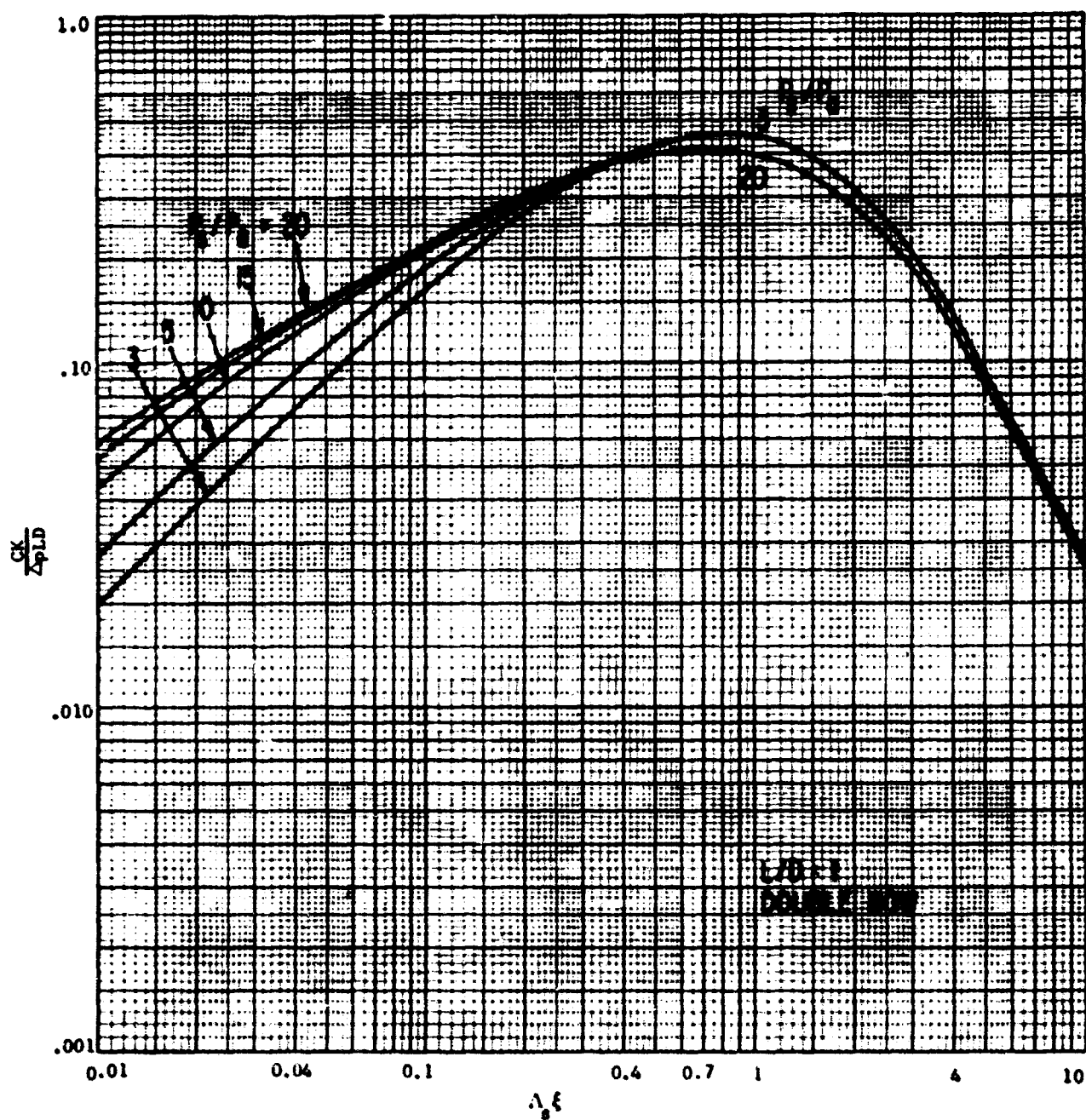


Fig. 5 Dimensionless Radial Stiffness Versus Restrictor Coefficient,
 $L/D = 1$, Double Row

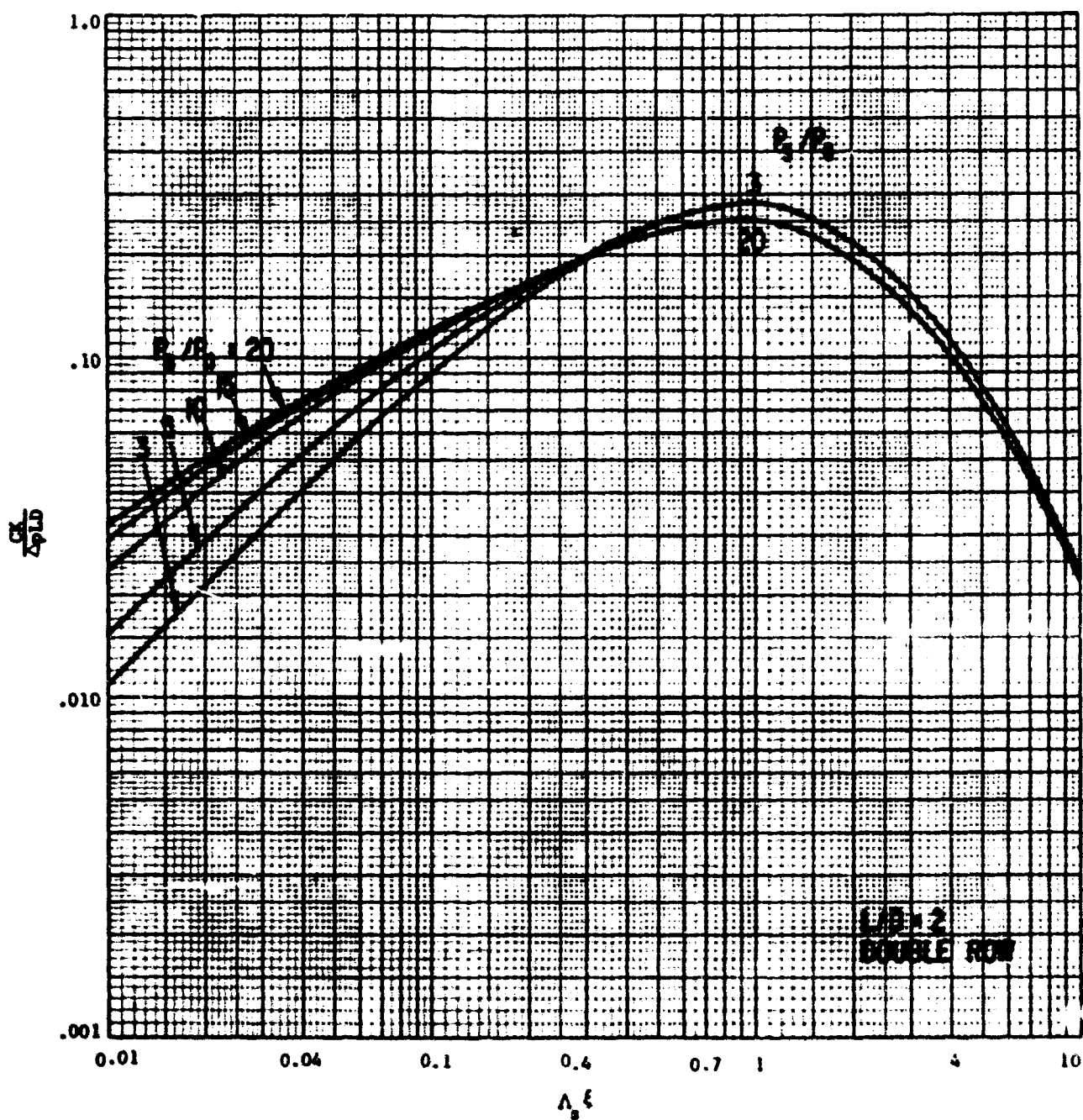


Fig. 6 Dimensionless Radial Stiffness Versus Restrictor Coefficient,
 $L/D = 2$, Double Row

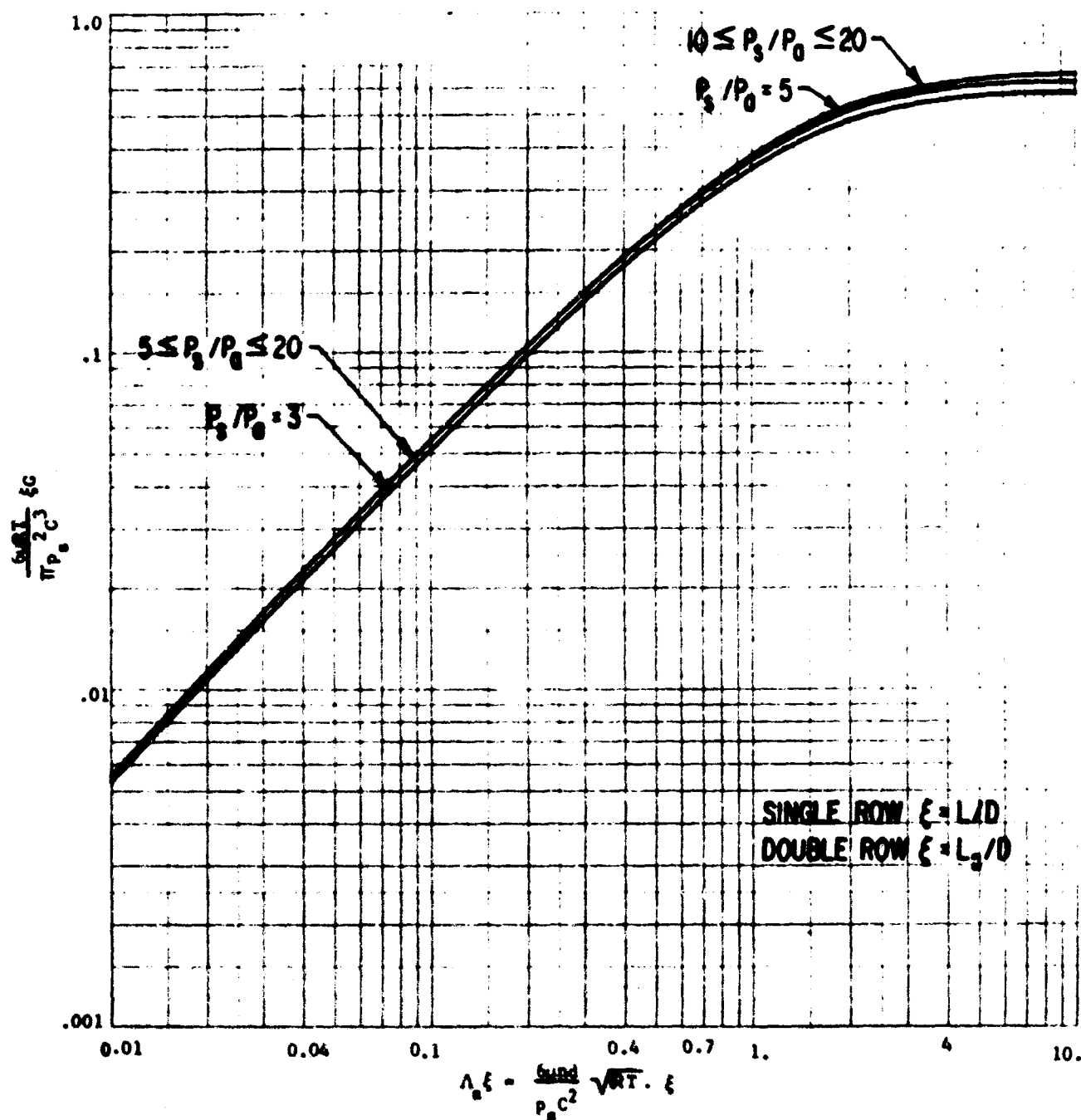


Fig. 7 Dimensionless Flow Versus Restrictor Coefficient for all L/D

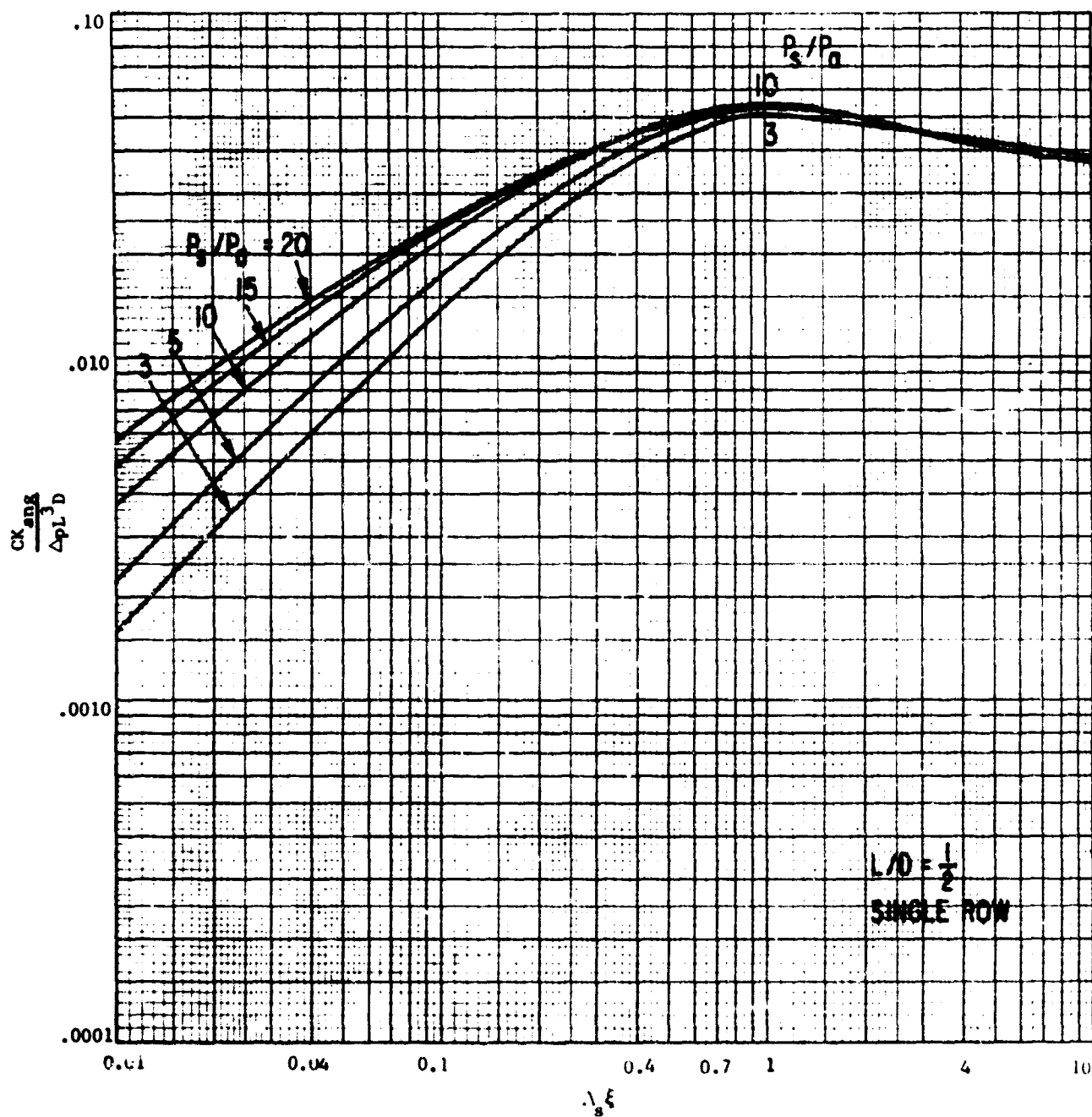


Fig. 8 Dimensionless Angular Stiffness Versus Restrictor Coefficient,
 $L/D = 1/2$, Single Row

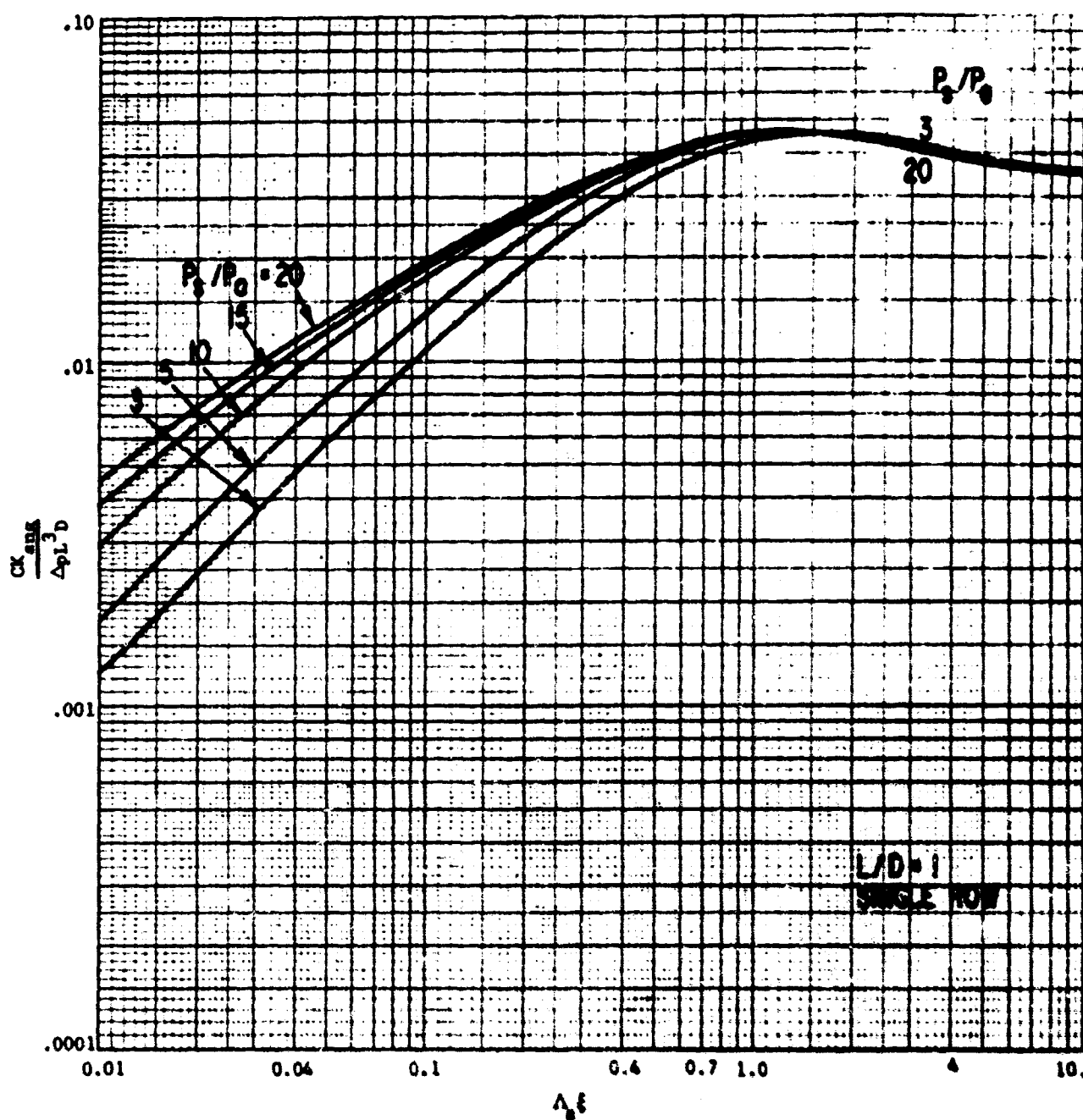


Fig. 9 Dimensionless Angular Stiffness Versus Restrictor Coefficient, $L/D = 1$, Single Row

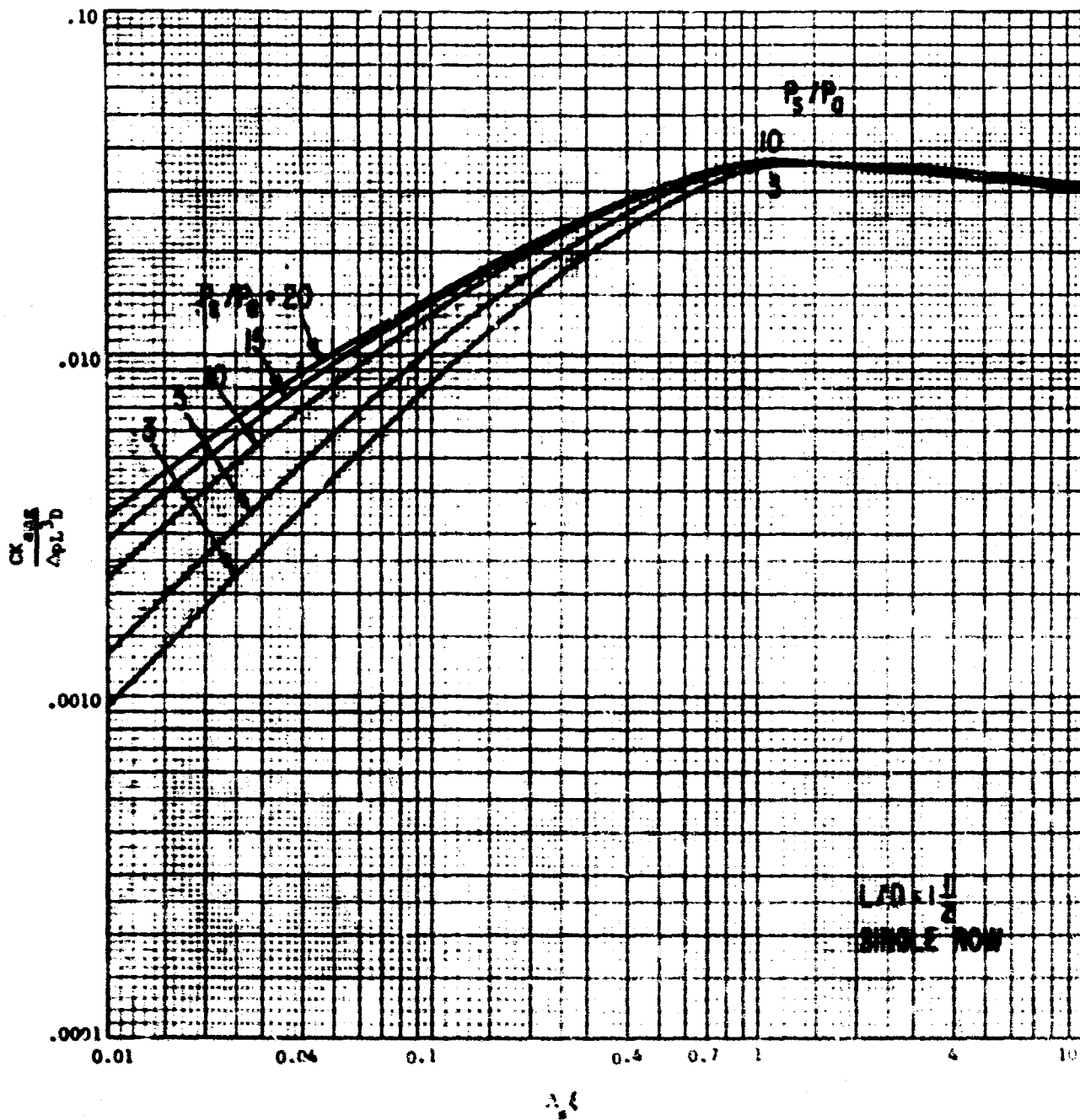


Fig. 10 Dimensionless Angular Stiffness Versus Restrictor Coefficient,
 $L/D = 1\frac{1}{2}$, Single Row

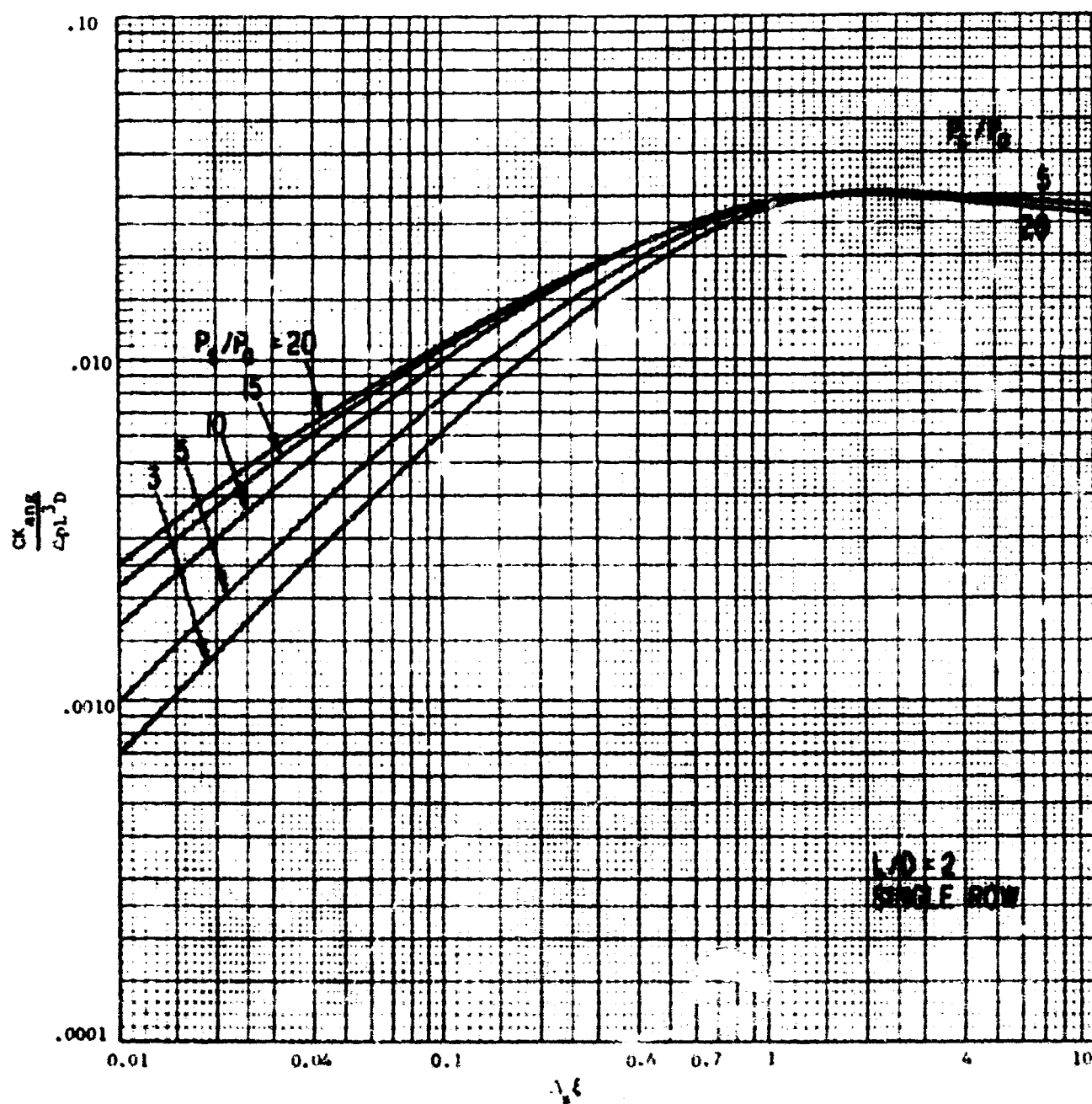


Fig. 11 Dimensionless Angular Stiffness Versus Restrictor Coefficient,
 $L/D = 2$, Single Row

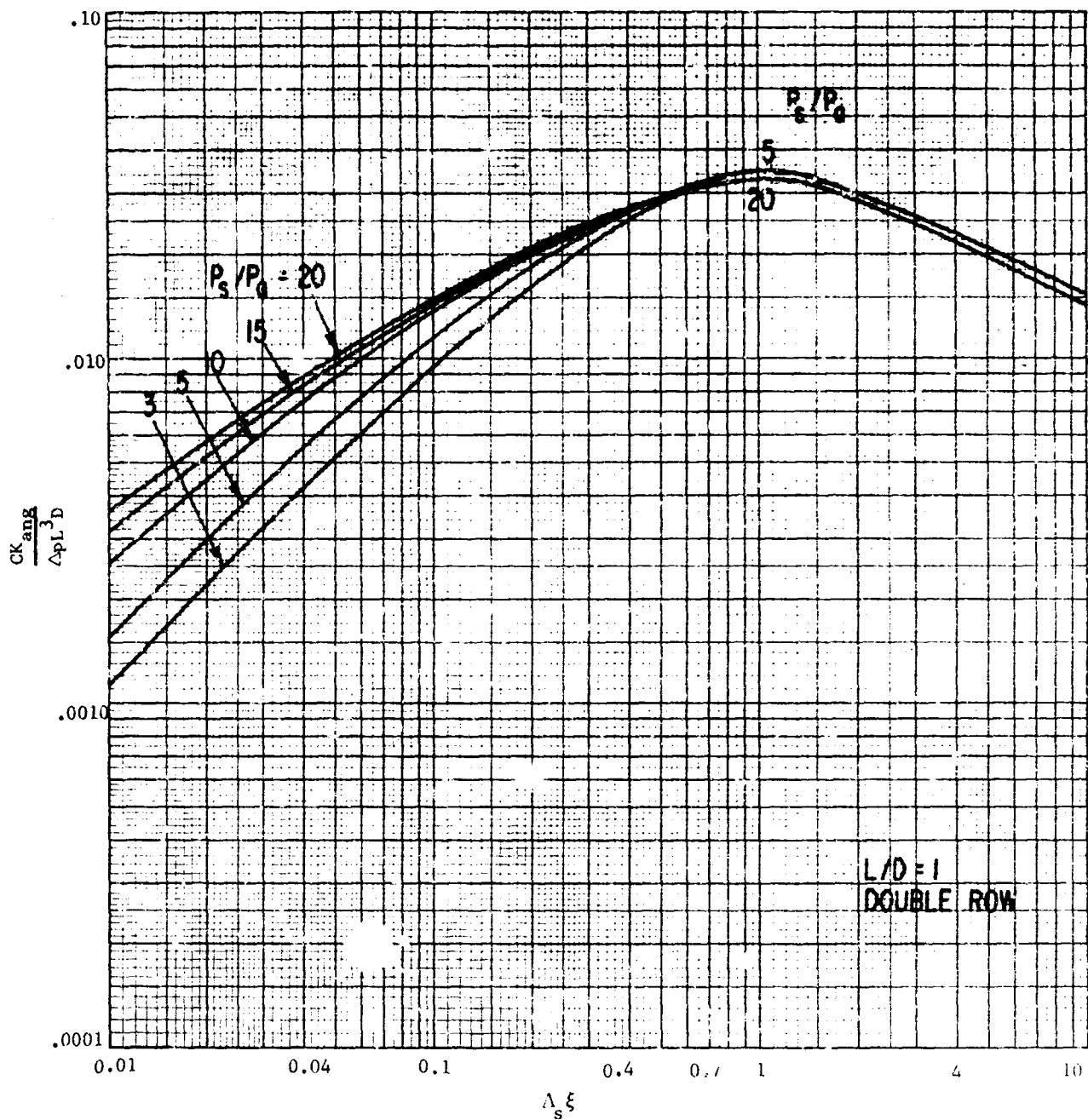


Fig. 12 Dimensionless Angular Stiffness Versus Restrictor Coefficient, $L/D = 1$, Double Row

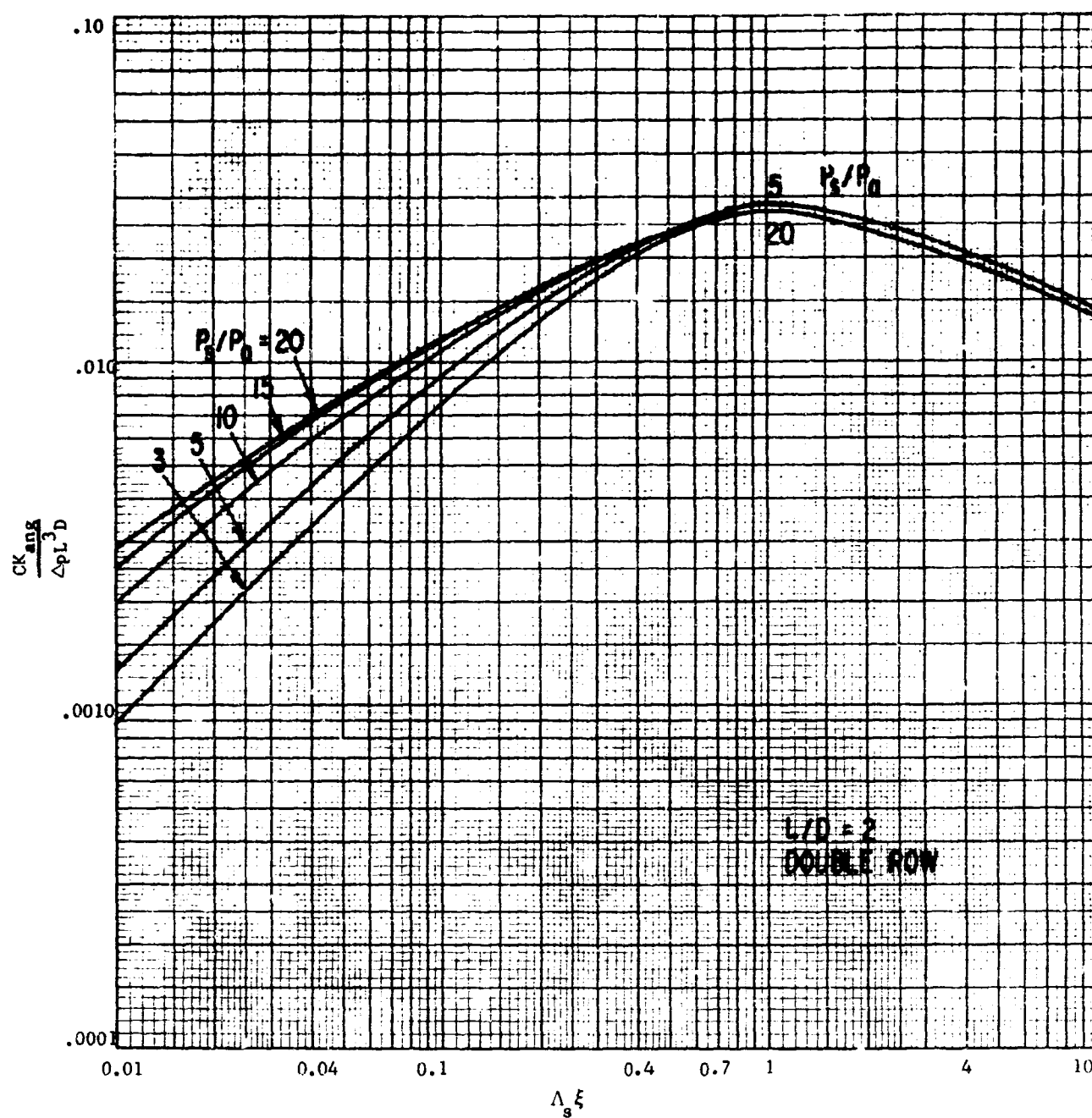


Fig. 13 Dimensionless Angular Stiffness Versus Restrictor Coefficient,
 $L/D = 2$, Double Row

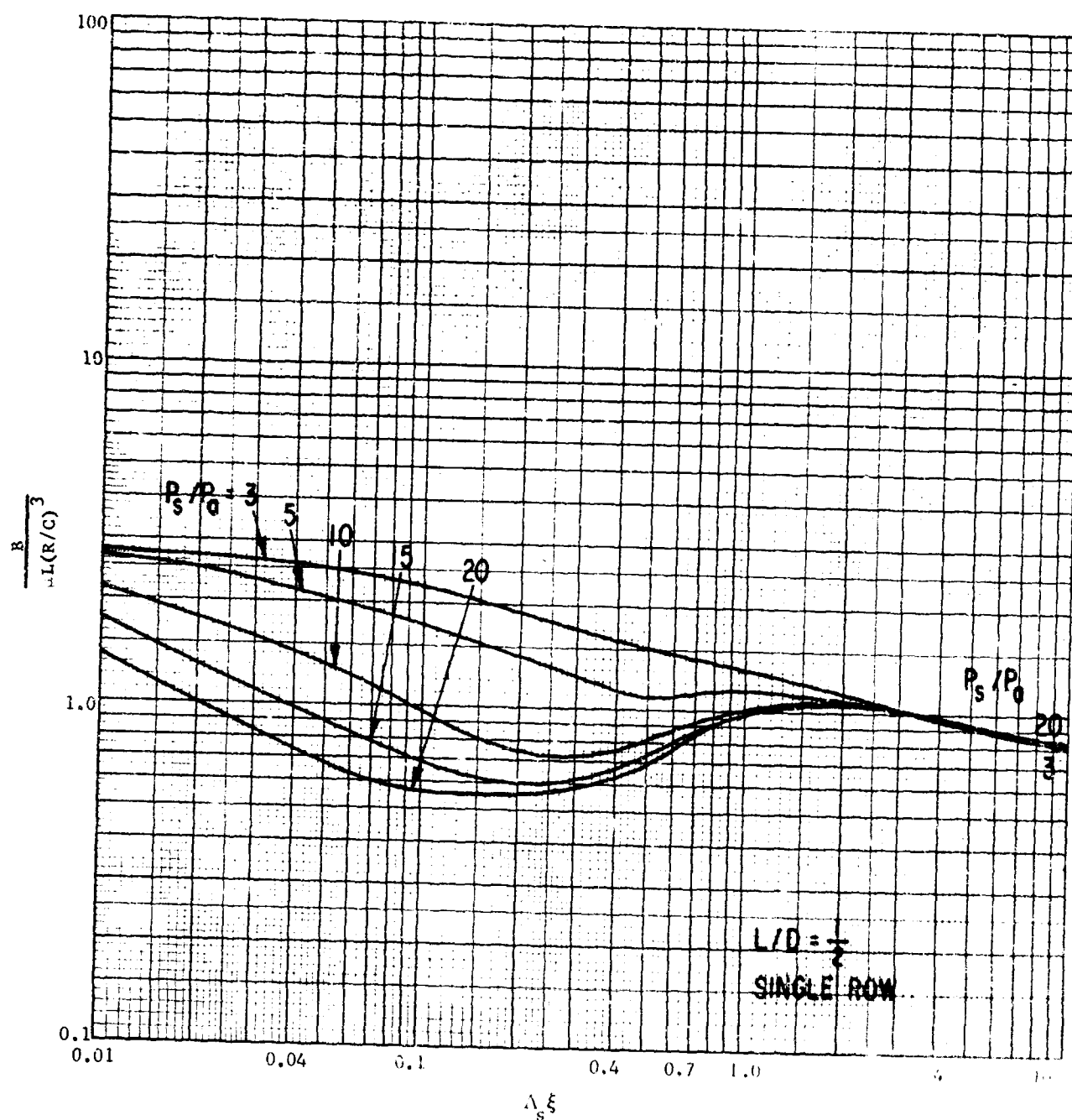


Fig. 14 Dimensionless Radial Damping Versus Restrictor Coefficient, $L/D = 1/2$, Single Row

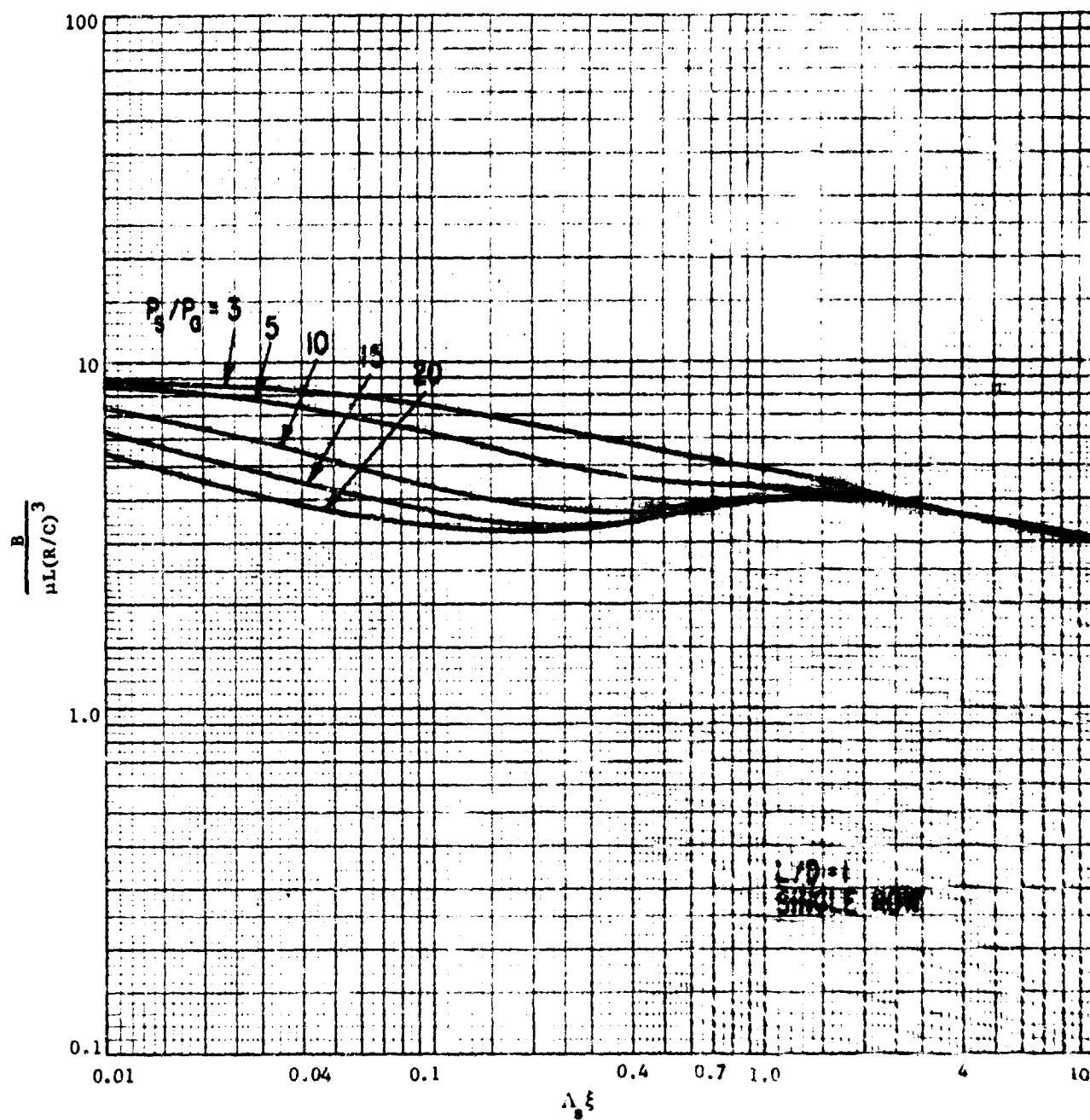


Fig. 15 Dimensionless Radial Damping Versus Restrictor Coefficient,
 $L/D = 1$, Single Row

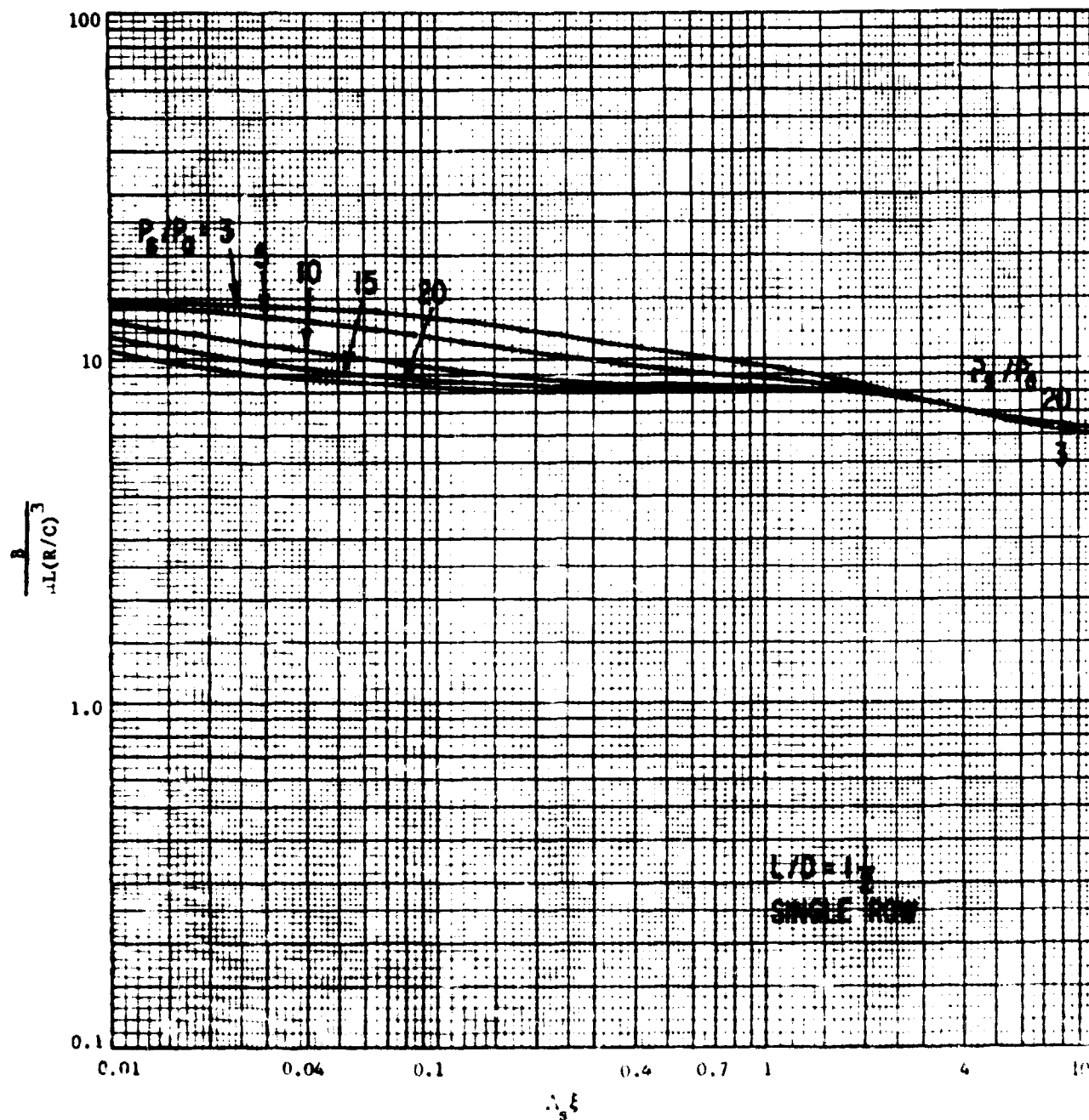


Fig. 16 Dimensionless Radial Damping Versus Restrictor Coefficient,
 $L/D = 1\frac{1}{2}$, Single Row

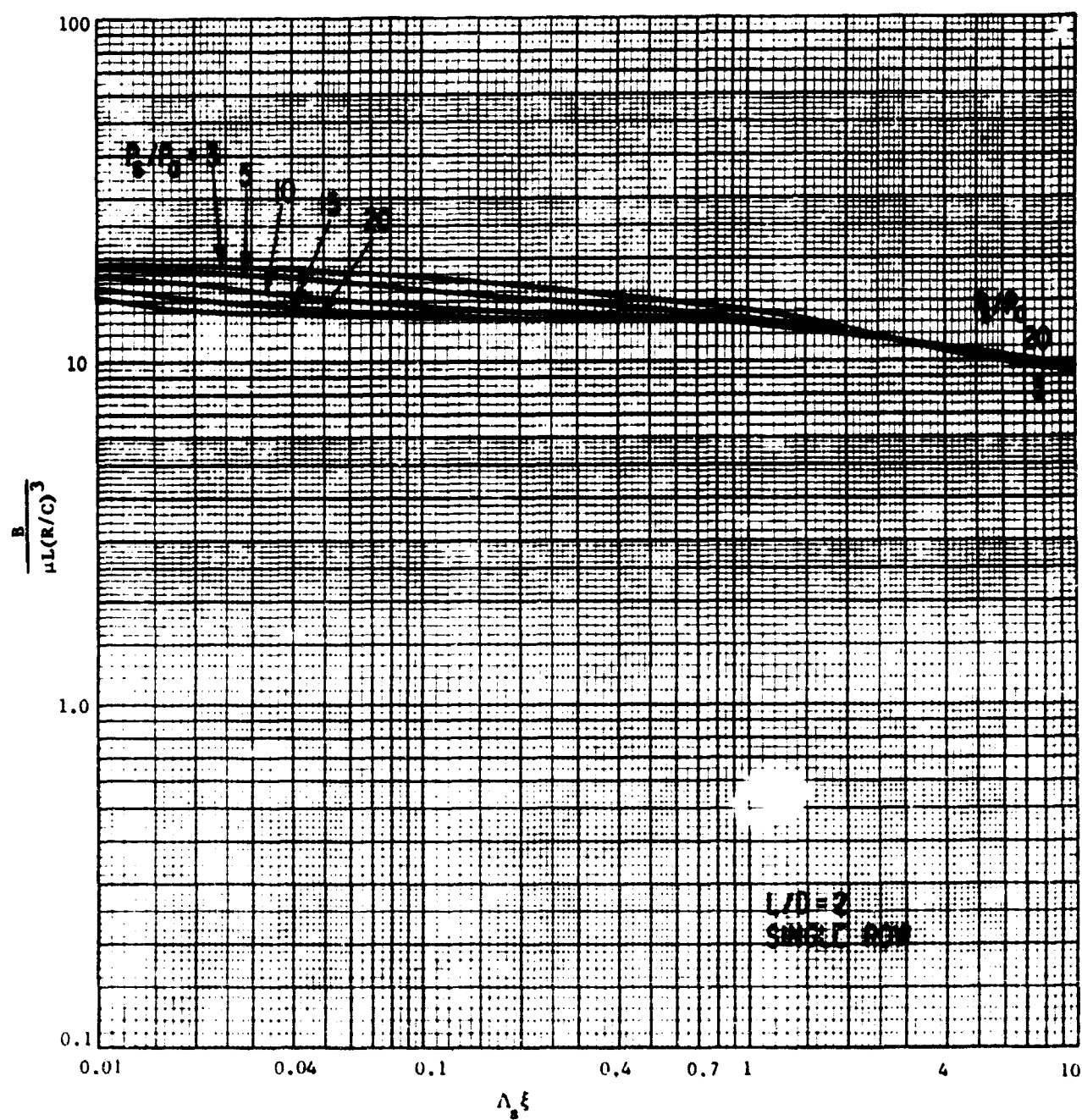


Fig. 17 Dimensionless Radial Damping Versus Restrictor Coefficient,
 $L/D = 2$, Single Row

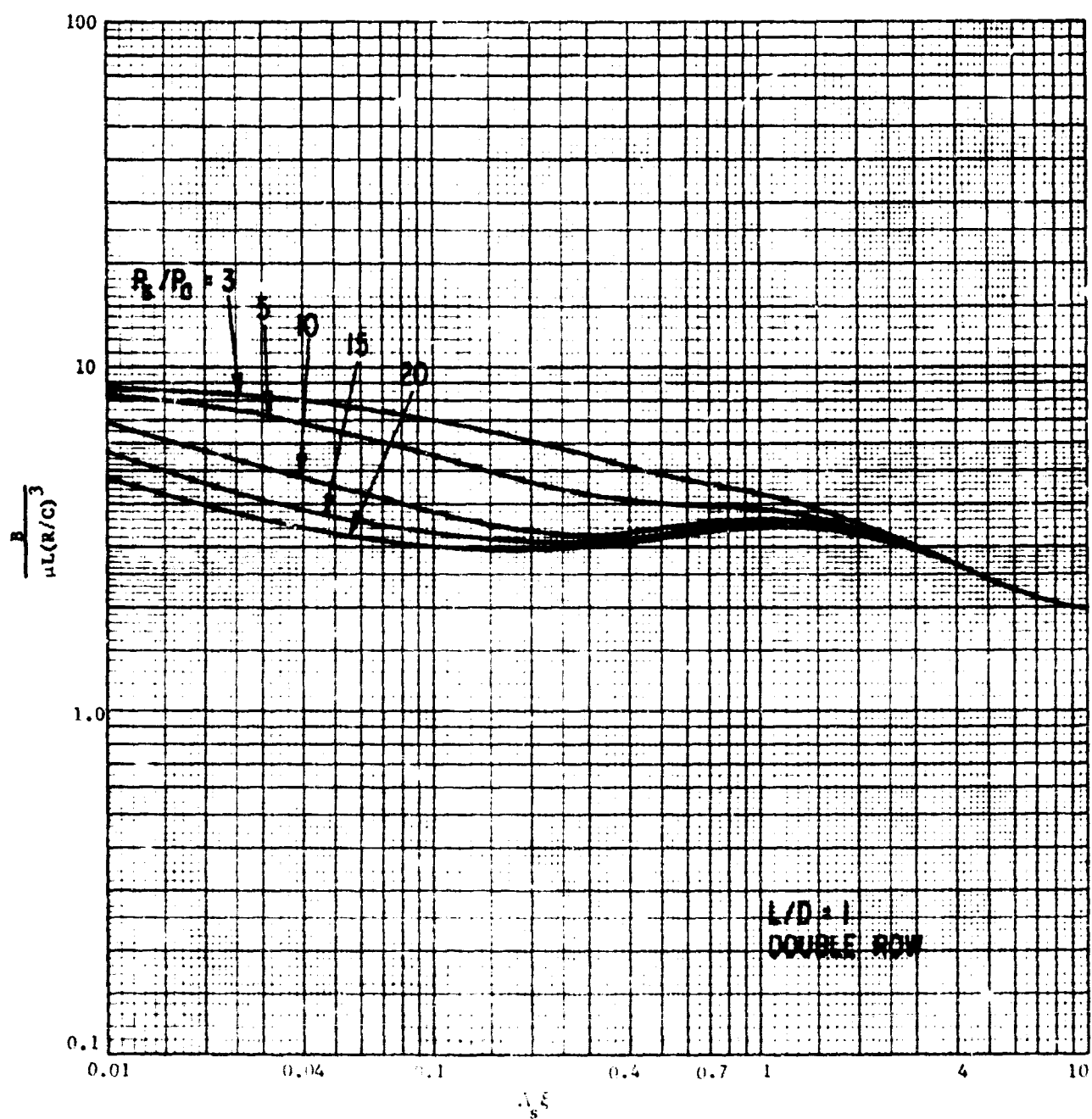


Fig. 18 Dimensionless Radial Damping Versus Restrictor Coefficient,
 $L/D = 1$, Double Row

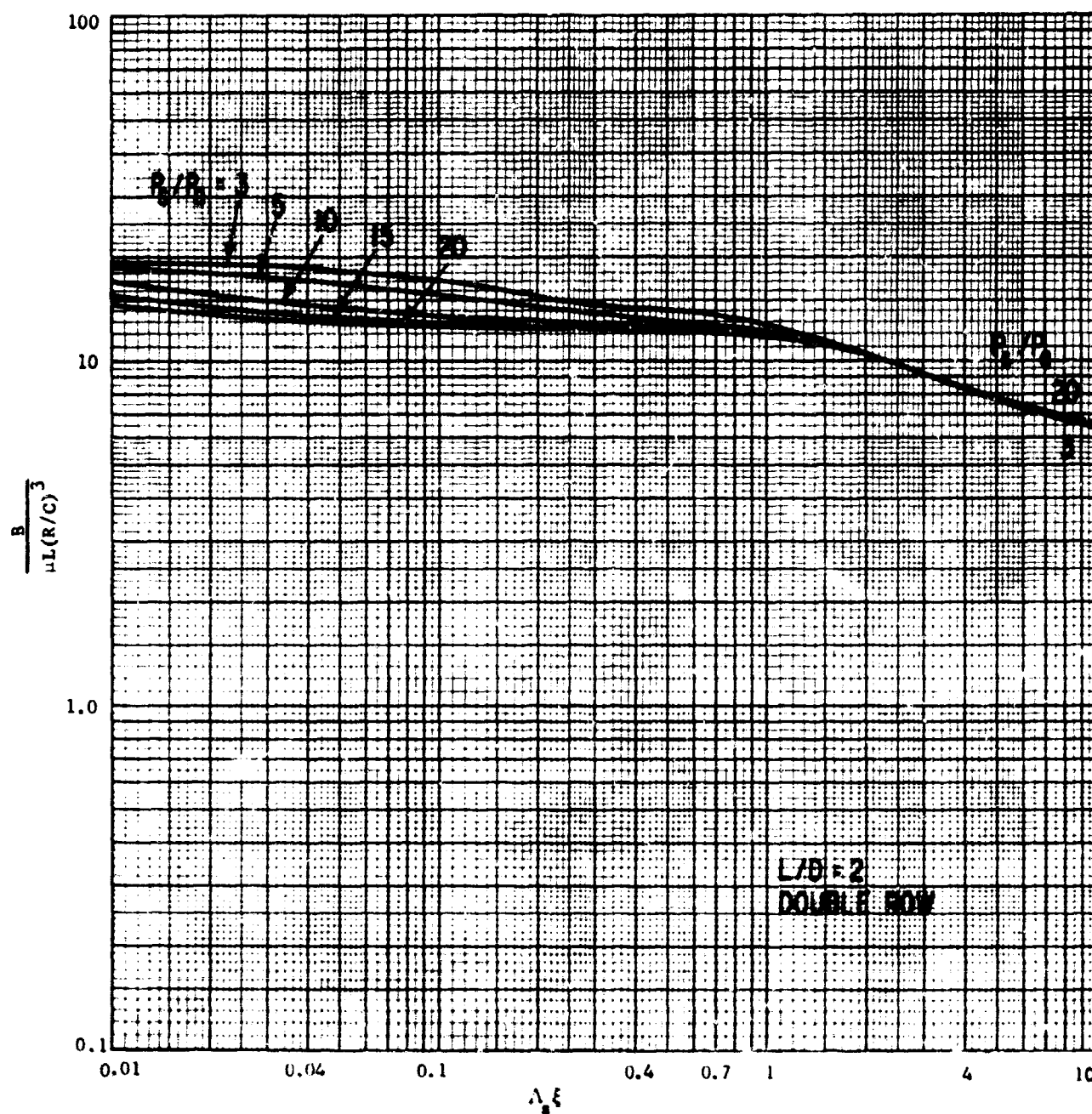


Fig. 19 Dimensionless Radial Damping Versus Restrictor Coefficient,
 $L/D = 2$, Double Row

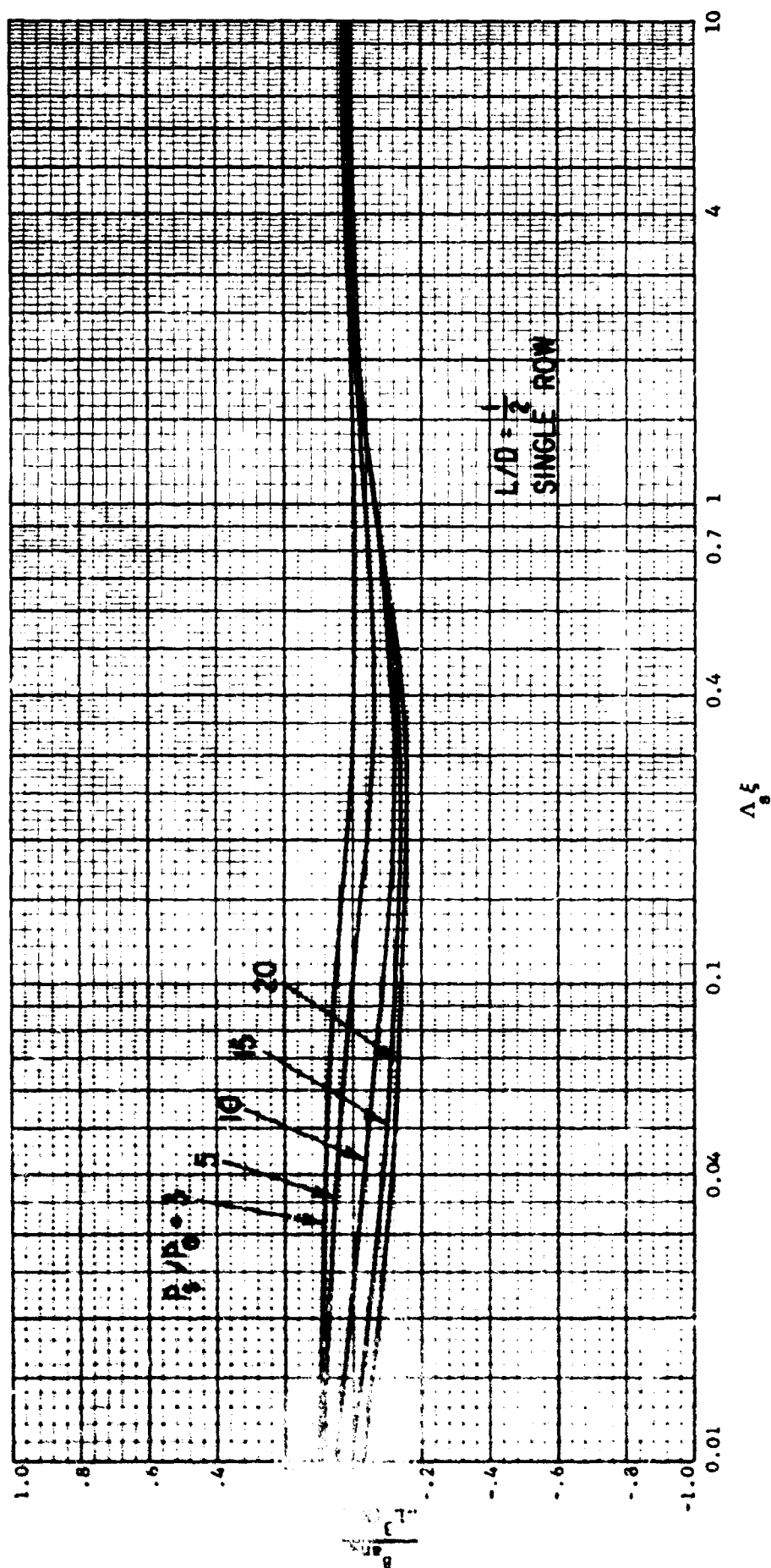


Fig. 20 Dimensionless Angular Damping Versus Restrictor Coefficient,
 $L/D = 1/2$, Single Row

MTI-6294

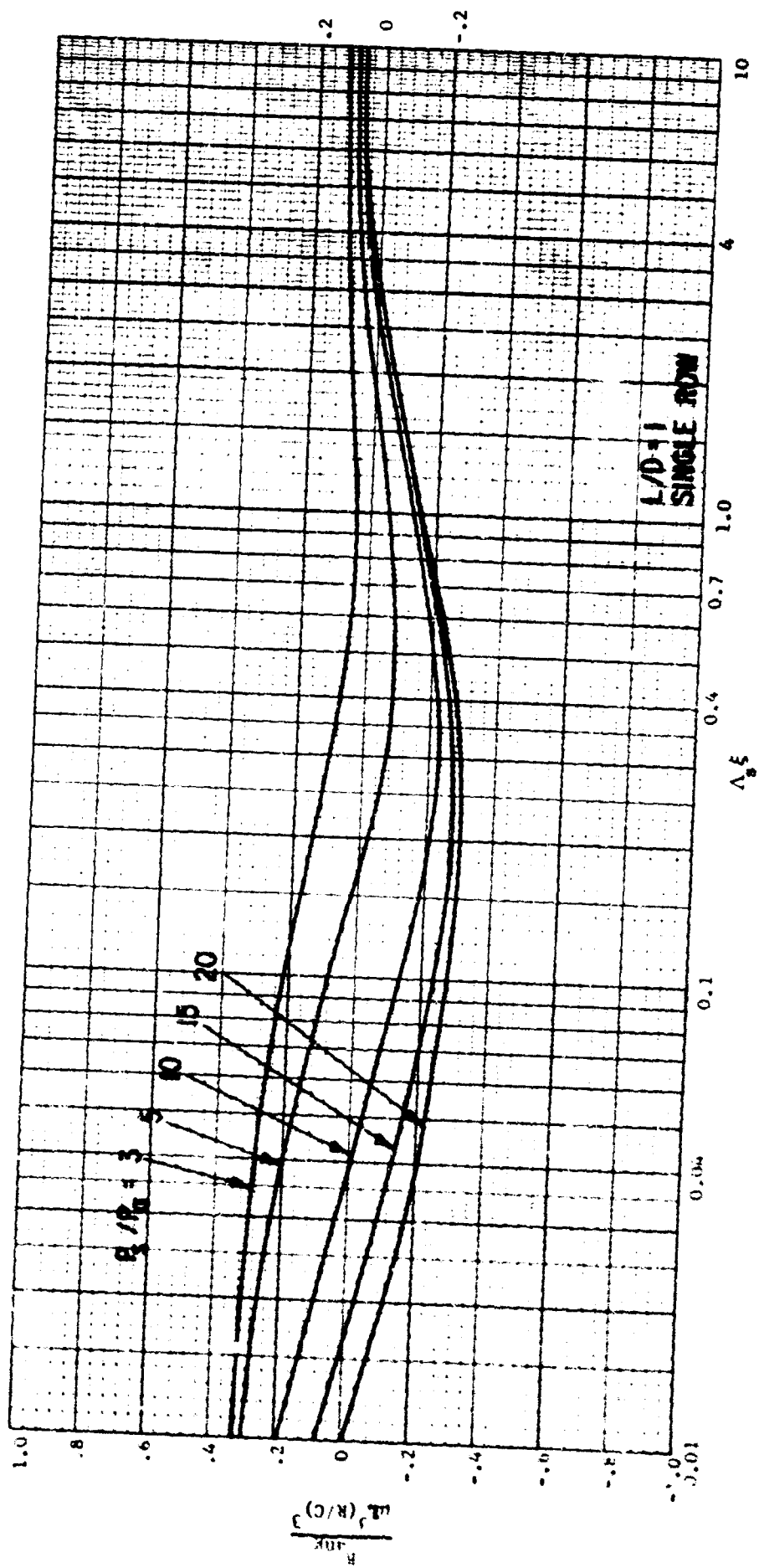


Fig. 21 Dimensionless Angular Damping Versus Restrictor Coefficient.
L/D = 1, Single Row

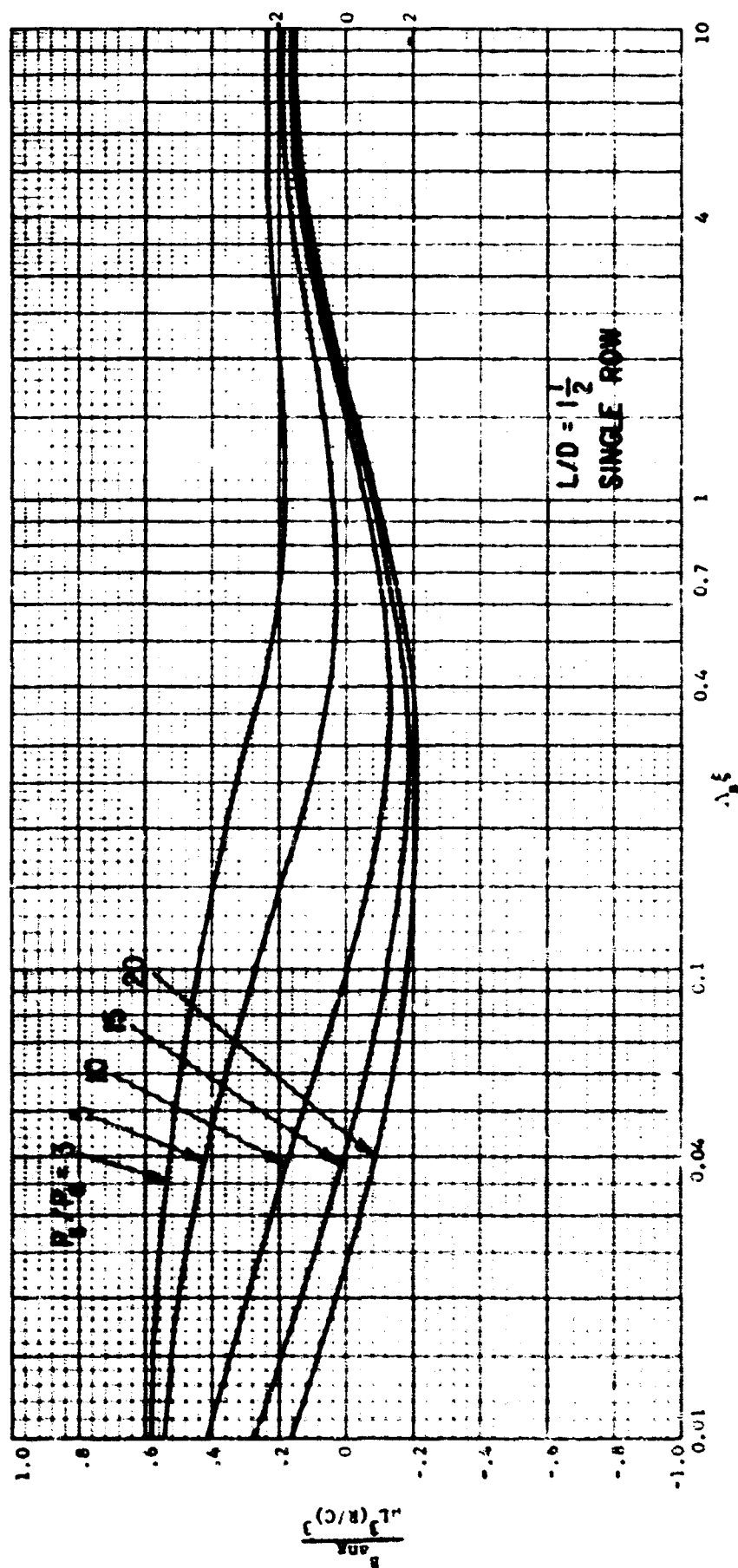


Fig. 22 Dimensionless Angular Damping Versus Restrictor Coefficient,
 $L/D = 1\frac{1}{2}$, Single Row

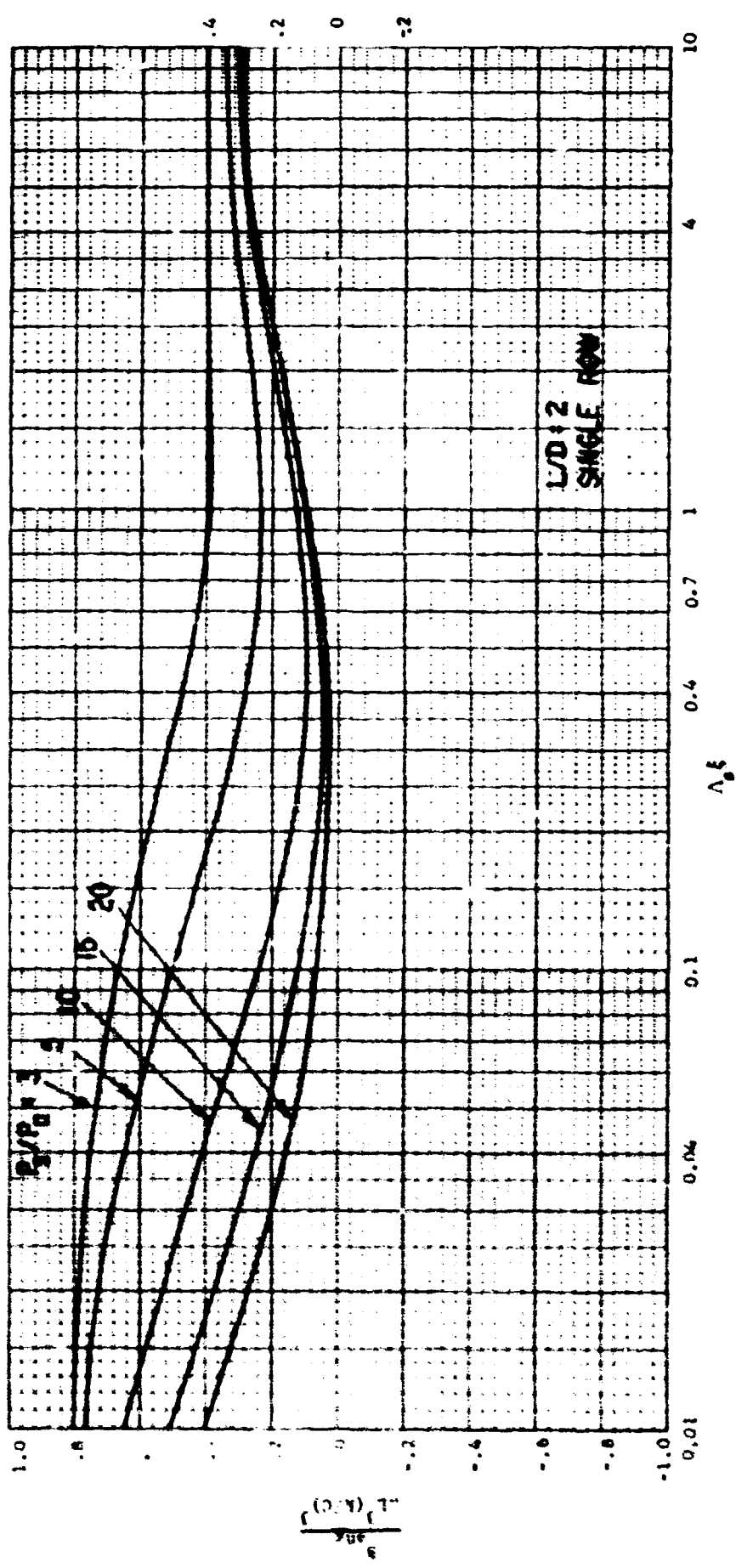


Fig. 23 Dimensionless Angular Damping Versus Restrictor Coefficient,
L/D = 2, Single Row

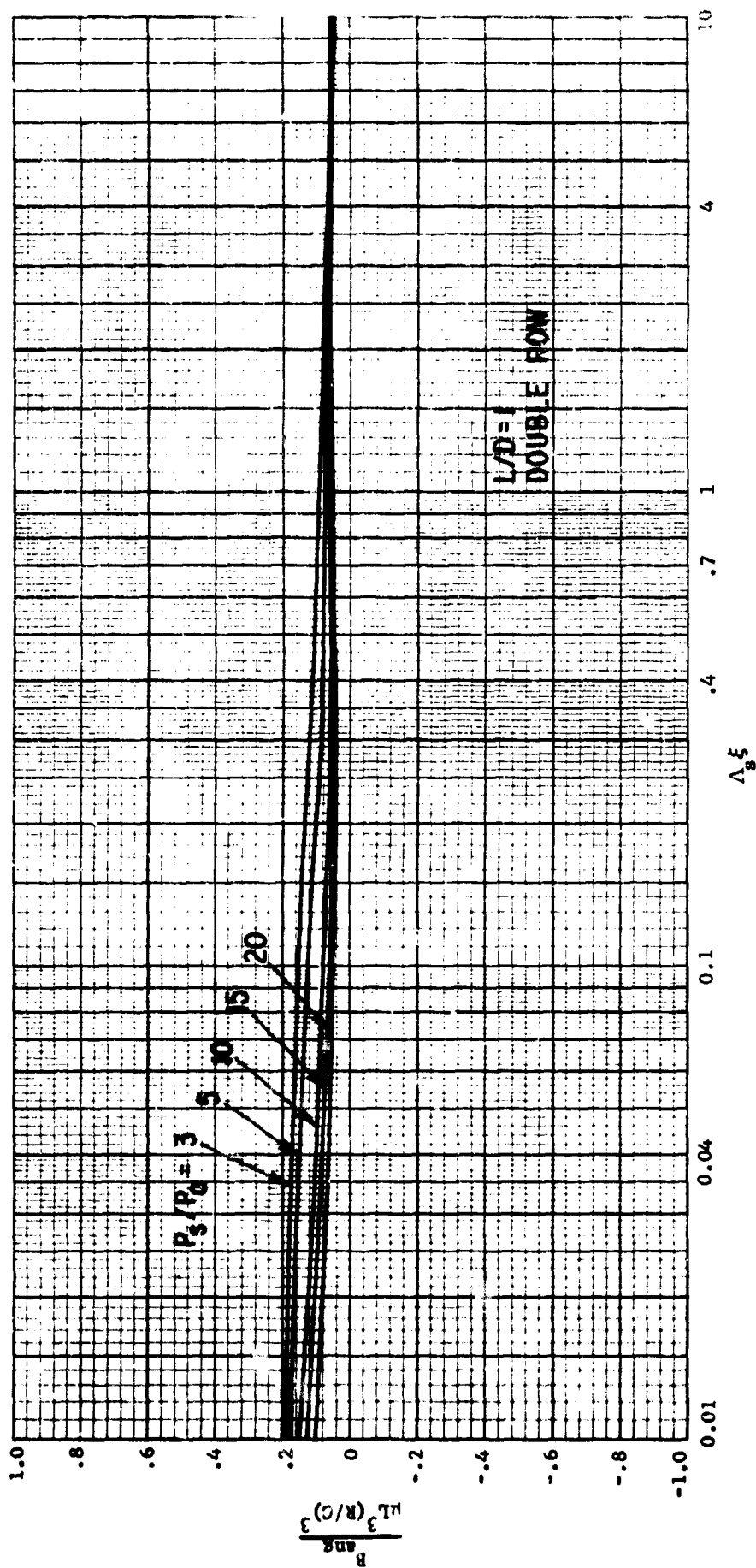


Fig. 24 Dimensionless Angular Damping Versus Restrictor Coefficient,
 $L/D = 1$, Double Row

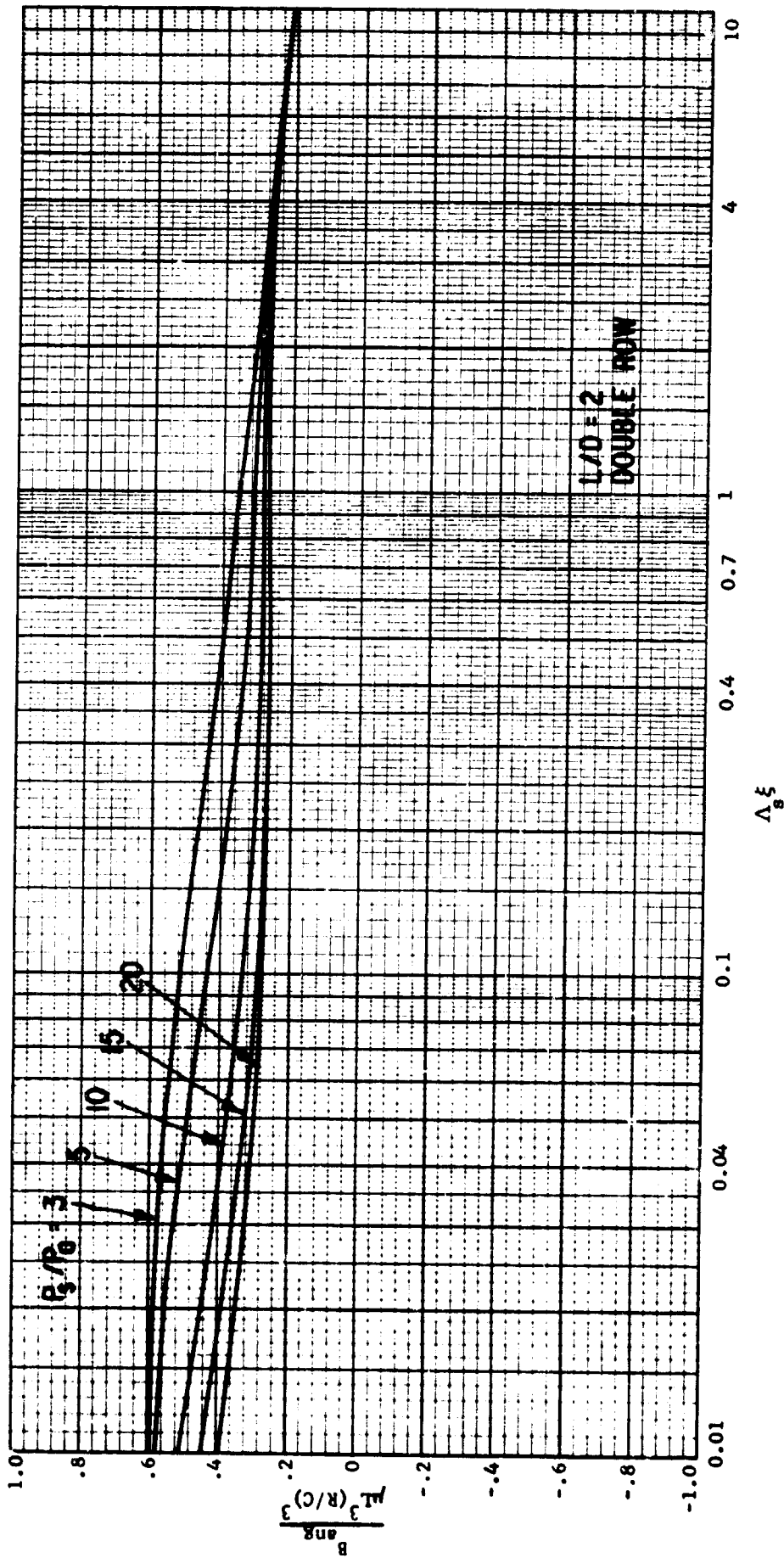


Fig. 25 Dimensionless Angular Damping Versus Restrictor Coefficient,
 $L/D = 2$, Double Row

Table 1 Dynamic Data, L/D = 1/2, Single Row

Parameter	P_s / P_a	$\Lambda \frac{g}{s}$	σ	0.01	1.0	10.	100.
CK/ ($\Delta p L D$)	3	0.1		0.139	0.142	0.362	0.754
		0.7		0.393	0.395	0.500	1.04
		4.0		0.112	0.112	0.145	0.988
	10	0.1		0.199	0.199	0.215	0.301
		0.7		0.395	0.395	0.402	0.585
		4.0		0.112	0.112	0.114	0.307
	20	0.1		0.211	0.211	0.214	0.256
		0.7		0.386	0.386	0.388	0.479
		4.0		0.108	0.108	0.109	0.166
CK _{ang} / ($\Delta p L^3 D$)	3	0.1		0.0136	0.0137	0.0181	0.0384
		0.7		0.0463	0.0473	0.0463	0.0500
		4.0		0.0428	0.0428	0.0435	0.0643
	10	0.1		0.0218	0.0218	0.0203	0.0138
		0.7		0.0518	0.0518	0.0511	0.0339
		4.0		0.0431	0.0431	0.0431	0.0442
	20	0.1		0.0243	0.0243	0.0236	0.0129
		0.7		0.0513	0.0513	0.0511	0.0404
		4.0		0.0420	0.0420	0.0420	0.0422
B/ ($\mu L (\frac{R}{C})^3$)	3	0.1		2.24	2.22	1.41	0.0556
		0.7		1.41	1.41	1.19	0.0798
		4.0		0.963	0.962	0.936	0.254
	10	0.1		0.968	0.966	0.825	0.0623
		0.7		0.917	0.916	0.893	0.248
		4.0		0.969	0.969	0.966	0.722
	20	0.1		0.566	0.566	0.538	0.0923
		0.7		0.855	0.854	0.849	0.502
		4.0		0.970	0.970	0.969	0.892
B _{ang} / ($\mu L^3 (\frac{R}{C})^3$)	3	0.1		0.0554	0.0551	0.0395	0.00786
		0.7		-0.00542	-0.00539	-0.00299	0.00589
		4.0		0.0242	0.0242	0.0236	0.00802
	10	0.1		-0.0858	-0.0856	-0.0715	0.00220
		0.7		-0.0840	-0.0840	-0.0816	-0.0183
		4.0		0.00646	0.00646	0.00644	0.00515
	20	0.1		-0.142	-0.142	-0.134	-0.0160
		0.7		-0.0959	-0.0959	-0.0952	-0.0540
		4.0		0.00441	0.00441	0.00440	0.00415

Table 2 Dynamic Data, $L/D = 1$, Single Row

Parameter	P/P_a	$\Lambda \xi$	σ	0.01	1.0	10.	100.
$CK/(\Delta pLD)$	3	0.1		0.108	0.144	0.650	0.806
		0.7		0.321	0.336	0.824	1.10
		4.0		0.102	0.107	0.431	1.28
	10	0.1		0.155	0.157	0.251	0.313
		0.7		0.321	0.322	0.396	0.643
		4.0		0.102	0.102	0.136	0.735
	20	0.1		0.164	0.164	0.199	0.264
		0.7		0.313	0.313	0.334	0.577
		4.0		0.0986	0.0987	0.107	0.490
$CK_{ang}/(\Delta pL^3D)$	3	0.1		0.0109	0.0117	0.0264	0.0532
		0.7		0.0394	0.0394	0.0420	0.0659
		4.0		0.0392	0.0393	0.0478	0.0786
	10	0.1		0.0174	0.0173	0.0139	0.0178
		0.7		0.0431	0.0431	0.0394	0.0330
		4.0		0.0394	0.0394	0.0398	0.0470
	20	0.1		0.0194	0.0194	0.0163	0.0137
		0.7		0.0427	0.0427	0.0415	0.0292
		4.0		0.0384	0.0384	0.0385	0.0420
$B/(\mu L(\frac{R}{C})^3)$	3	0.1		7.45	7.04	1.16	0.0278
		0.7		5.18	5.08	1.71	0.0362
		4.0		3.55	3.54	2.58	0.108
	10	0.1		4.36	4.28	1.61	0.0362
		0.7		3.91	3.90	3.03	0.124
		4.0		3.58	3.58	3.42	0.646
	20	0.1		3.40	3.38	2.22	0.0669
		0.7		3.75	3.75	3.49	0.418
		4.0		3.59	3.59	3.54	1.65
$B_{ang}/(\mu L^3(\frac{R}{C})^3)$	3	0.1		0.218	0.208	0.0698	0.00514
		0.7		0.0438	0.0437	0.0375	0.00529
		4.0		0.100	0.100	0.0756	0.00563
	10	0.1		-0.136	-0.133	-0.0271	0.00547
		0.7		-0.170	-0.170	-0.126	0.00506
		4.0		0.0418	0.0418	0.0402	0.0104
	20	0.1		-0.278	-0.276	-0.170	0.00545
		0.7		-0.203	-0.203	-0.187	-0.00784
		4.0		0.0350	0.0350	0.0346	0.0182

Table 3 Dynamic Data, $L/D = 1-1/2$ Single Row

Parameter	P/P	$\Delta \xi$	σ	0.01	1.0	10.	100.
$CK/(\Delta pLD)$	3	0.1		0.0790	0.172	0.721	0.821
		0.7		0.244	0.293	0.961	1.11
		4.0		0.0895	0.107	0.807	1.34
	10	0.1		0.112	0.121	0.275	0.317
		0.7		0.242	0.246	0.438	0.649
		4.0		0.0883	0.0897	0.206	0.830
	20	0.1		0.118	0.121	0.208	0.266
		0.7		0.236	0.237	0.307	0.593
		4.0		0.0855	0.0859	0.118	0.686
$CK_{ang}/(\Delta pL^3D)$	3	0.1		0.00820	0.0108	0.0351	0.0570
		0.7		0.0310	0.0317	0.0466	0.0702
		4.0		0.0344	0.0349	0.0570	0.0829
	10	0.1		0.0132	0.0131	0.0132	0.0189
		0.7		0.0339	0.0339	0.0311	0.0356
		4.0		0.0345	0.0346	0.0366	0.0493
	20	0.1		0.0147	0.0146	0.0124	0.0148
		0.7		0.0336	0.0336	0.0321	0.0309
		4.0		0.0336	0.0337	0.0342	0.0439
$B/(\mu L(\frac{R}{C})^3)$	3	0.1		13.0	11.2	0.908	0.0180
		0.7		10.0	9.42	1.43	0.0240
		4.0		7.06	6.96	2.88	0.0675
	10	0.1		9.38	8.95	1.66	0.0270
		0.7		8.44	8.36	4.47	0.0911
		4.0		7.15	7.13	6.07	0.409
	20	0.1		8.29	8.17	3.32	0.0577
		0.7		8.26	8.24	6.70	0.316
		4.0		7.16	7.16	6.85	1.30
$B_{ang}/\mu L^3(\frac{R}{C})^3$	3	0.1		0.442	0.394	0.0882	0.00326
		0.7		0.197	0.190	0.0763	0.00347
		4.0		0.230	0.227	0.104	0.00374
	10	0.1		-0.000388	0.00317	0.0509	0.00376
		0.7		-0.0934	-0.0922	-0.0265	0.00612
		4.0		0.130	0.130	0.112	0.00998
	20	0.1		-0.179	-0.175	-0.0367	0.00536
		0.7		-0.138	-0.137	-0.103	0.0113
		4.0		0.119	0.119	0.114	0.0256

Table 4 Dynamic Data, $L/D = 2$, Single Row

Parameter	$\frac{L}{P}$	$\frac{A}{g}$	σ	0.01	1.0	10.	100.
CK/ ($\Delta p L D$)	3	0.1		0.0569	0.207	0.754	0.827
		0.7		0.182	0.274	1.01	1.12
		4.0		0.0762	0.116	1.02	1.36
	10	0.1		0.0800	0.0976	0.287	0.318
		0.7		0.179	0.186	0.477	0.651
		4.0		0.0745	0.0777	0.304	0.861
	20	0.1		0.0842	0.0888	0.217	0.267
		0.7		0.174	0.176	0.306	0.596
		4.0		0.0722	0.0729	0.142	0.751
CK _{ang} / ($\Delta p L^3 D$)	3	0.1		0.00614	0.0108	0.0426	0.0585
		0.7		0.0240	0.0260	0.0533	0.0717
		4.0		0.0294	0.0307	0.0644	0.0844
	10	0.1		0.00990	0.0101	0.0144	0.0193
		0.7		0.0263	0.0263	0.0282	0.0364
		4.0		0.0295	0.0296	0.0350	0.0503
	20	0.1		0.0110	0.0110	0.0116	0.0151
		0.7		0.0261	0.0261	0.0263	0.0323
		4.0		0.0287	0.0287	0.0303	0.0454
$R / (\mu L (\frac{R}{C})^3)$	3	0.1		17.7	13.9	0.787	0.0142
		0.7		14.6	13.2	1.25	0.0182
		4.0		10.8	10.4	2.53	0.0485
	10	0.1		14.4	13.3	1.61	0.0223
		0.7		13.2	13.0	5.01	0.0789
		4.0		11.0	10.9	7.81	0.311
	20	0.1		13.4	13.1	3.78	0.0531
		0.7		13.1	13.0	9.15	0.278
		4.0		11.0	11.0	9.95	1.01
$R_{ang} / (\mu L^3 (\frac{R}{C})^3)$	3	0.1		0.672	0.562	0.1883	0.00221
		0.7		0.413	0.383	0.0913	0.00242
		4.0		0.401	0.389	0.111	0.00267
	10	0.1		0.241	0.232	0.0901	0.00272
		0.7		0.110	0.110	0.0844	0.00514
		4.0		0.274	0.273	0.198	0.00851
	20	0.1		0.0661	0.0668	0.0748	0.00435
		0.7		0.0642	0.0642	0.0658	0.0133
		4.0		0.259	0.259	0.236	0.0262

Table 5 Dynamic Data, $L/D = 1$, Double Row

Parameter	P/P_0	Λ	σ	0.01	1.0	10.	100.
$CK/(\Delta p L D)$	3	0.1		0.160	0.192	0.685	0.852
		0.7		0.447	0.459	0.907	1.26
		4.0		0.139	0.142	0.338	1.43
	10	0.1		0.201	0.212	0.297	0.372
		0.7		0.422	0.422	0.482	0.784
		4.0		0.133	0.133	0.150	0.704
	20	0.1		0.216	0.217	0.246	0.325
		0.7		0.408	0.408	0.424	0.692
		4.0		0.128	0.128	0.132	0.399
$CK_{aug}/(\Delta p L^3 D)$	3	0.1		0.00943	0.00966	0.0242	0.0575
		0.7		0.0319	0.0320	0.0396	0.0795
		4.0		0.0229	0.0229	0.0255	0.0861
	10	0.1		0.0135	0.0135	0.0147	0.0229
		0.7		0.0321	0.0321	0.0325	0.0454
		4.0		0.0224	0.0224	0.0226	0.0364
	20	0.1		0.0144	0.0144	0.0147	0.0193
		0.7		0.0314	0.0314	0.0315	0.0379
		4.0		0.0217	0.0217	0.0217	0.0259
$B/(\mu L (\frac{R}{C})^3)$	3	0.1		7.01	6.65	1.18	0.0306
		0.7		4.60	4.53	1.82	0.0463
		4.0		2.67	2.66	2.23	0.197
	10	0.1		3.83	3.79	1.69	0.0431
		0.7		3.55	3.56	2.99	0.193
		4.0		2.68	2.70	2.65	0.965
	20	0.1		3.06	3.08	2.25	0.0895
		0.7		3.37	3.45	3.30	0.600
		4.0		2.66	2.70	2.69	1.81
$B_{aug}/(\mu L^3 (\frac{R}{C})^3)$	3	0.1		0.154	0.154	0.101	0.00585
		0.7		0.102	0.101	0.0654	0.00707
		4.0		0.0720	0.0720	0.0698	0.0170
	10	0.1		0.0799	0.0800	0.0701	0.00713
		0.7		0.0646	0.0651	0.0634	0.0183
		4.0		0.0662	0.0671	0.0668	0.0482
	20	0.1		0.0568	0.0576	0.0552	0.0116
		0.7		0.0578	0.0605	0.0601	0.0358
		4.0		0.0649	0.0666	0.0665	0.0605

Table 6 Dynamic Data, L/D = 2, Double Row

Parameter	$\frac{P}{P_s}$	$\frac{L}{L_s}$	σ	0.01	1.0	10.	100.
CK/ (ΔpLD)	3	0.1	0.0888	0.0888	0.230	0.794	0.878
		0.7	0.271	0.271	0.347	1.13	1.28
		4.0	0.111	0.111	0.133	0.925	1.60
	10	0.1	0.117	0.117	0.131	0.333	0.378
		0.7	0.255	0.255	0.260	0.535	0.805
		4.0	0.105	0.105	0.107	0.243	1.03
	20	0.1	0.120	0.120	0.124	0.253	0.329
		0.7	0.246	0.246	0.248	0.354	0.739
		4.0	0.102	0.102	0.102	0.139	0.825
CK _{eng} / (ΔpL^3D)	3	0.1	0.00749	0.00749	0.00980	0.0463	0.0641
		0.7	0.0260	0.0260	0.0271	0.0620	0.0866
		4.0	0.0207	0.0207	0.0211	0.0462	0.105
	10	0.1	0.0108	0.0108	0.0109	0.0181	0.0246
		0.7	0.0262	0.0262	0.0262	0.0316	0.0502
		4.0	0.0202	0.0202	0.0202	0.0227	0.0632
	20	0.1	0.0115	0.0115	0.0115	0.0143	0.0206
		0.7	0.0256	0.0256	0.0271	0.0271	0.0449
		4.0	0.0196	0.0196	0.0196	0.0202	0.0470
B/ ($\mu L (\frac{R}{C})^3$)	3	0.1	17.2	17.2	13.7	0.0842	0.0167
		0.7	13.5	13.5	12.4	1.54	0.0248
		4.0	8.38	8.38	8.24	3.31	0.0815
	10	0.1	13.4	13.4	12.7	1.98	0.0302
		0.7	12.2	12.2	12.0	5.96	0.121
		4.0	8.49	8.49	8.48	7.23	0.574
	20	0.1	12.6	12.6	12.4	4.59	0.0763
		0.7	12.0	12.0	12.0	9.48	0.438
		4.0	8.48	8.48	8.51	8.14	1.76
B _{eng} / ($\mu L^3 (\frac{R}{C})^3$)	3	0.1	0.517	0.517	0.491	0.100	0.00306
		0.7	0.377	0.377	0.370	0.130	0.00359
		4.0	0.267	0.267	0.266	0.187	0.00716
	10	0.1	0.332	0.332	0.328	0.140	0.00397
		0.7	0.282	0.282	0.281	0.220	0.0103
		4.0	0.251	0.251	0.252	0.240	0.0401
	20	0.1	0.276	0.276	0.276	0.192	0.00729
		0.7	0.268	0.268	0.270	0.252	0.0323
		4.0	0.249	0.249	0.250	0.247	0.107

CHAPTER IV
EXPERIMENTAL EVALUATION OF THREE STEAM
PROCESSING UNITS

CHAPTER IV
TABLE OF CONTENTS

	PAGE
INTRODUCTION	129
DESCRIPTION OF UNITS TESTED	130
The Double-Concentric Tube, Long, Spiral-Finned Processor	130
The Single Tube, Short, Spiral-Finned Processor	130
Commercial Separator	133
TEST APPARATUS	137
TEST PROCEDURE	143
RESULTS	145
DISCUSSION OF RESULTS	146
DISCUSSION AND CONCLUSIONS	152
REFERENCES	155
APPENDIX	156

INTRODUCTION

Experiments have shown that steam-lubricated bearings can be operated satisfactorily with a saturated or high-quality steam supply, [IV-1]*. However, a most critical problem in the design and operation of these bearings is the elimination of steam hammer instability. The mechanism for this instability is believed to be associated with evaporation of entrained moisture in the bearing film - the moisture being carried into the film through the restrictor from a wet steam supply. Stable operation has resulted when the moisture fraction in the supply steam was kept below a limiting level which has been between 0.5 and 1.5 percent in bearing experiments.

In order to minimize the entrained moisture in the steam supplied to the bearing film, in spite of a higher than tolerable moisture content in the steam line supply, several types of processing units have been evaluated. These processors function either by evaporating entrained moisture, using throttling and reheat processes,** or by separating and removing entrained moisture by mechanical action or by a combination of these approaches. The processing devices were tested by measuring the quality of the steam they delivered. The first processor tested is the most expensive and largest, but also the most flexible. This processor is a long, (4-ft.), spiral-finned, double-concentric tube design and has been discussed fully in Ref. IV-1. The second processor tested is a short, (6-in), spiral-finned, single-tube design. The third processor tested is a relatively inexpensive, commercially available separator.

This chapter of the manual discusses these three processors and their experimental evaluation.

*Bracketed numbers refer to identically numbered references in the Reference section.

**Electrical heaters would certainly serve the purpose. However, the electrical energy is not necessarily available in all applications and therefore not considered an acceptable solution.

DESCRIPTION OF UNITS TESTED

In the actual steam bearing application, these three processing devices would be used in conjunction with properly designed heating and supply manifolds. See Fig. IV-1 for an illustration of a steam bearing employing a dual-manifold design. The jacketing header in this design is used to supply the heat load to all bearing walls, including the wall of the journal. The supply header is thus protected from such heat losses and supplies a high quality steam to the supply holes in the bearing wall.

The three steam processors that were tested are described below.

The Double-Concentric Tube, Long, Spiral-Finned Processor

The steam supply system for the double-concentric tube spiral-finned processor is shown schematically in Fig. IV-2. The steam flow is divided into bearing supply and jacketing header supplies with throttling valves in both legs. The steam enters a vertical section with the supply header steam passing through an inner tube and the jacketing steam in an outer, concentric tube. A cylindrical insert with spiral fins was installed in the inner tube forcing the steam to flow in an upward spiraling path of about 40 feet total flow path length. The intent of this design was to dry the supply steam by a process of throttling followed by reheat (assuming the jacketing header supply is not throttled). The spiraling flow path induced by the insert fins throws water droplets onto the outside, hot wall of the inner tube where they can evaporate. Also, this spiral path was relatively long, and consequently more effective in reheating of the supply steam. At the exit of the processor, the jacketing and supply steam flows pass through concentric supply tubes to the bearing inlet. The bearing supply steam flows through the inner supply tube with the jacketing steam in the outer tube.

The Single Tube, Short, Spiral-Finned Processor

The short spiral-finned processor is illustrated by a detailed sketch in

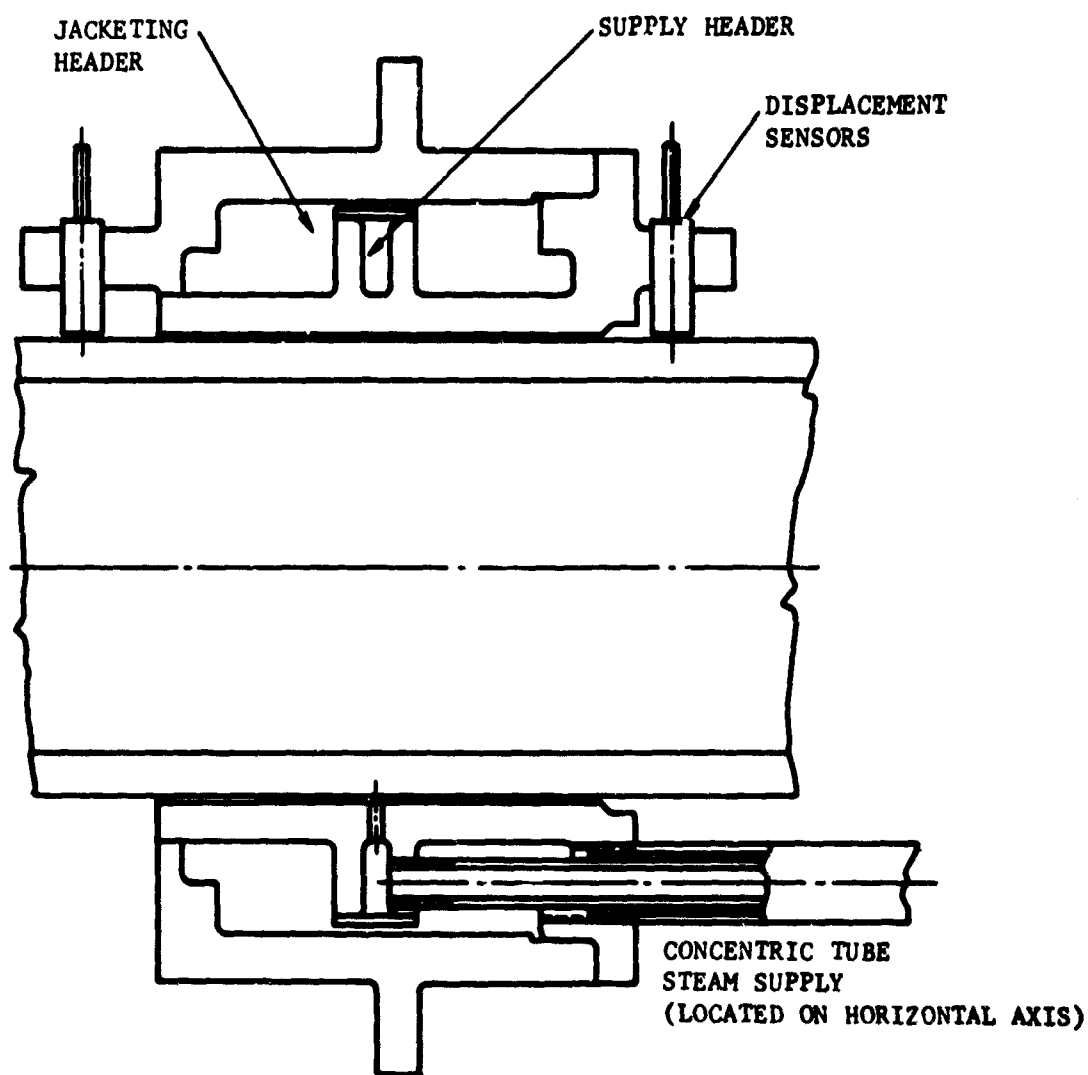


Fig. IV-1 Cross Sectional View of Dual-Manifold Steam Bearing

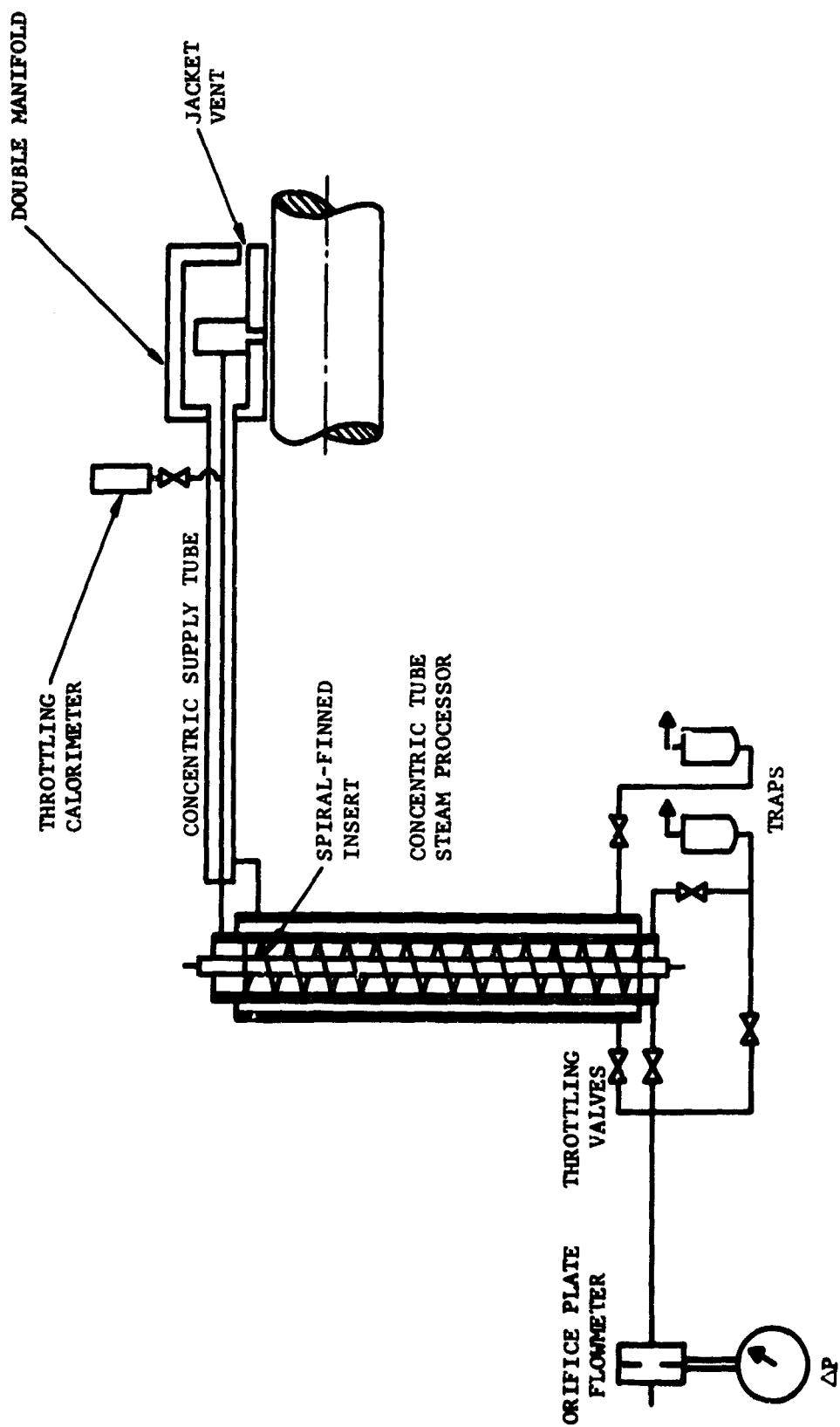


Fig. IV-2 Double-Tube, Spiral-Finned Steam Processing Unit Including Steam Supply System for Test Bearing

Fig. IV-3. The operation of this processor is similar to that of the long spiral-finned processor. It was anticipated that this processor could effectively replace the long processor by separating the dirt and moisture content from a saturated bearing steam supply by a spiraling action over a short compact six-inch section, although this short processor would lack the flexibility of a double-tube design.

The operation of this processor may be clearly understood by examining Fig. IV-3. Note that the steam inlet directs the wet steam to the spiral flow section. At the end of the spiral-flow section the moisture is collected and then trapped, or drained. The dry steam is then directed out of the processor at the axial center line of the flow path.

Commercial Separator

The commercial separator is illustrated in Fig. IV-4 and consists of a carbon steel housing with three ports and an internal, stainless steel baffle plate. A top port provides for the inlet of wet unprocessed steam. The bottom-side port provides an exhaust or drain for separated condensate. The bottom port provides the outlet for processed, high quality, clean steam.

The operation of this separator is extremely simple but efficient. Entrained moisture and any entrained solids in the inlet steam are separated from the main steam flow upon striking a stationary baffle plate. This baffle plate provides a centrifugal action casting the heavier elements to the outside of the flow path. These elements composed of condensate, and dirt particles are collected on the housing wall and rejected from the processor through the bottom-side drain. The dry, clean steam is in the center of the flow path and is collected by a tube near the center of the centrifugal separator element. This tube delivers the processed steam to the bottom, outlet port.

These separators are available as stock items in many sizes withstanding pressures to 400 psig, and temperatures as high as 500°F. The small, 1/2" port, size is capable of passing flows sufficient to supply either two steam

journal bearings, or a double-acting steam, thrust bearing. Higher pressure and temperature separators may also be obtained upon special request.

The spiraling action used to mechanically separate and trap the finely dispersed condensate has the additional advantage that it also tends to separate dirt particles, if any, from the bearing supply steam thereby generating high quality, clean steam.

In all steam processing systems effective separation and trapping (draining) of moisture in the steam supply at the processor and ahead of the bearing inlet is clearly important for high quality control.

For moisture separation to be effective, it is necessary to trap or drain the separated liquid from the system in order to prevent re-entrainment. Ordinarily, this was done from the drain line at the bottom of the processor by connection to a steam trap (This is a float-controlled valve which opens to discharge water when the accumulation reaches a certain level and then closes to keep steam from escaping).

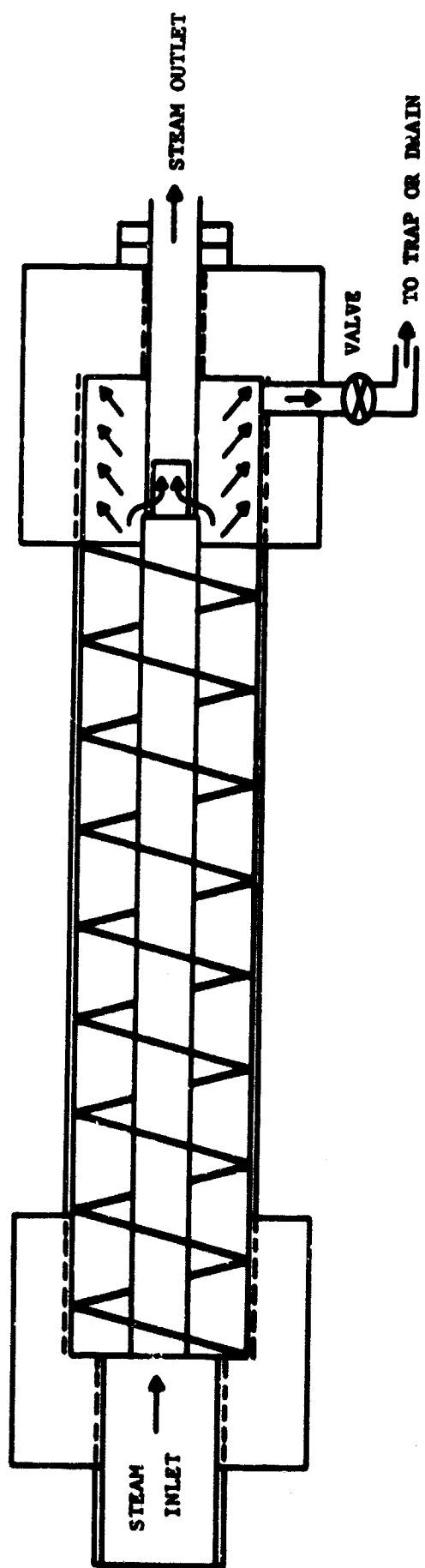


Fig. IV-3 Sketch of Short, Single-Tube, Spiral-finned Steam Processor

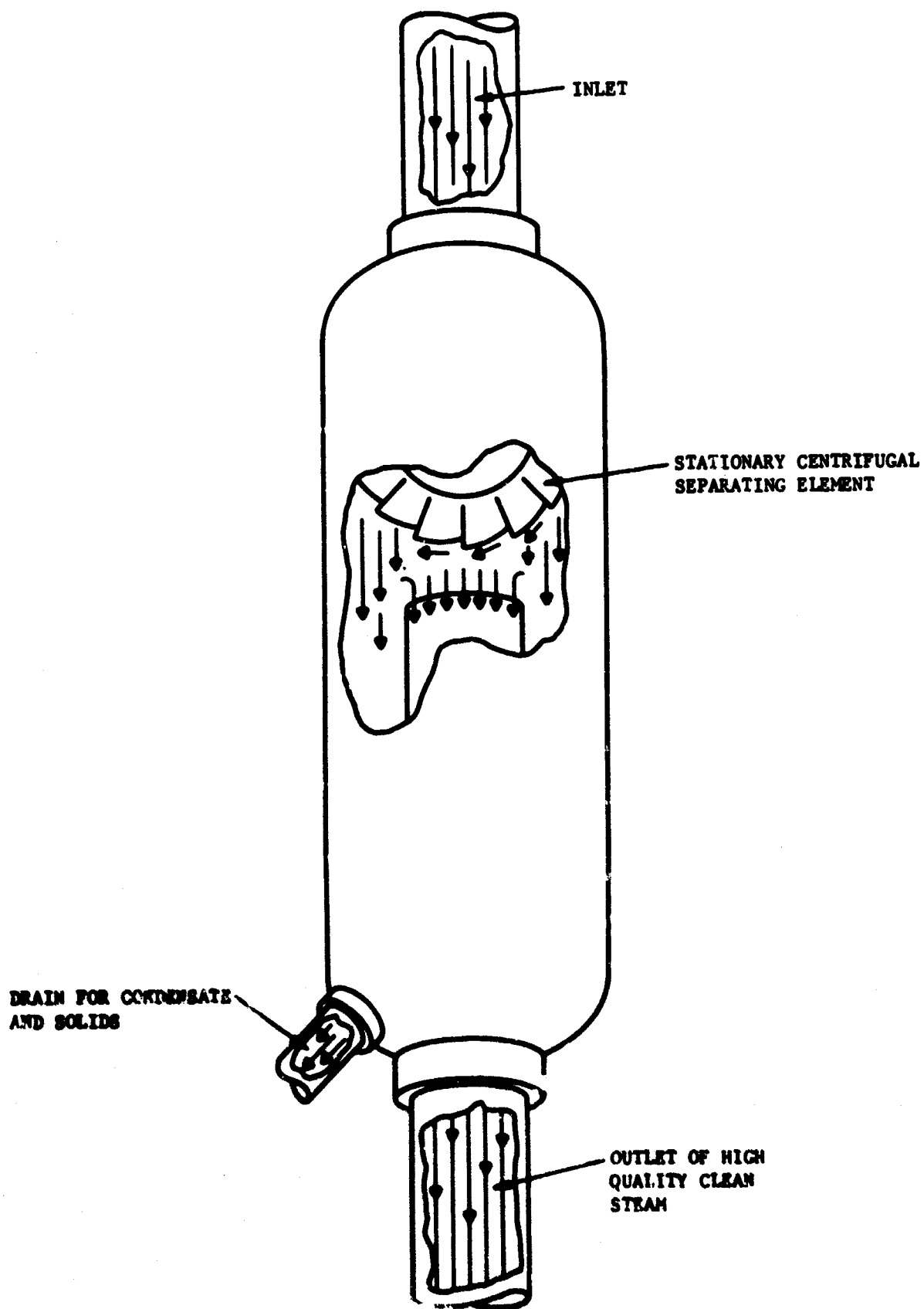


Fig. IV-4 Commercial Separator

TEST APPARATUS

A schematic of the apparatus used to test the three steam processors is shown in Fig. IV-5. This test apparatus consists of three main elements namely, the steam processor, the throttling calorimeter and the electric-heating calorimeter.

The steam processors have been discussed fully in the previous section. The plumbing of these three processors was the only change made in the line during the course of the tests.

The throttling calorimeter has been reported on [IV-1] and the description of this particular minaturized U-path type calorimeter, shown in Fig. IV-6 will, also be described in this report for completeness.

In this calorimeter, the steam is expanded through a 0.044 inch diameter orifice into a mixing chamber; then passes down the outside of the mixing chamber and exhausts to the atmosphere. Heat losses are minimized by the outer chamber, by installing the entire calorimeter in a small tube furnace, and by keeping the steam feed tube very short and well insulated. Two thermocouples are located in the mixing chamber to measure the temperature of the steam following expansion through the orifice plate. A third thermocouple is mounted on the outer wall of the calorimeter, next to the furnace tube. The furnace power is adjusted with an autotransformer to maintain an outer wall temperature about 10 degrees below the mixing chamber temperature. Steam quality is determined from the measured temperature (superheat) after throttling to atmospheric pressure and from the measured line pressure, by assuming a constant enthalpy throttling process.

The electric-heating calorimeter comprises of a number of items, namely, a highly insulated electric heating device, a flow measuring device and two pressure-temperature indicators.

A spiral-finned, electrical resistance heater of 2000 watt maximum capacity was used to supply the heat to the saturated steam, which flowed along its 20 inch spiral path. A wattmeter was used to measure the power input. At the outlet of this highly insulated heater and just before the thermocouple and pressure tap, stainless-steel wool was used to steady the turbulent flow of steam. This system was calibrated to obtain a heat loss to surroundings by using nitrogen and a rotometer and comparing the measured power input with the power input calculated from the measured flow and temperature rise. These results were confirmed by obtaining a similar comparison of results with superheated steam as the process gas. It was determined that an average of 65 watts could be assumed lost to the surroundings.

The flow measuring device used is sometimes called a "hot-well". The principle of this device is that of measuring the saturated steam condensing in a given period of time. The "hot-well" consisted of a standard hot water tank with a 3" O.D., stand pipe and 1/2" O.D., sight gauge. Initially, before tests, the tank was filled with cold water and the level marked. Superheated steam was directed into this tank where it condensed. Over a period of recorded time, this condensate would increase the level of water in the stand pipe. At the end of the test this final water level was recorded. Thus, for a given period of time the height increase of water in the stand pipe indicated the steam flow. [See Appendix]

Pressure gauges and thermocouples were used to measure the saturated steam conditions before the heating element and the superheated steam conditions after the heating element.

A description of the steam flow path might better illustrate the principle of operation of the electric-heating calorimeter. Again consider the schematic of the test apparatus, (Fig. IV-5).

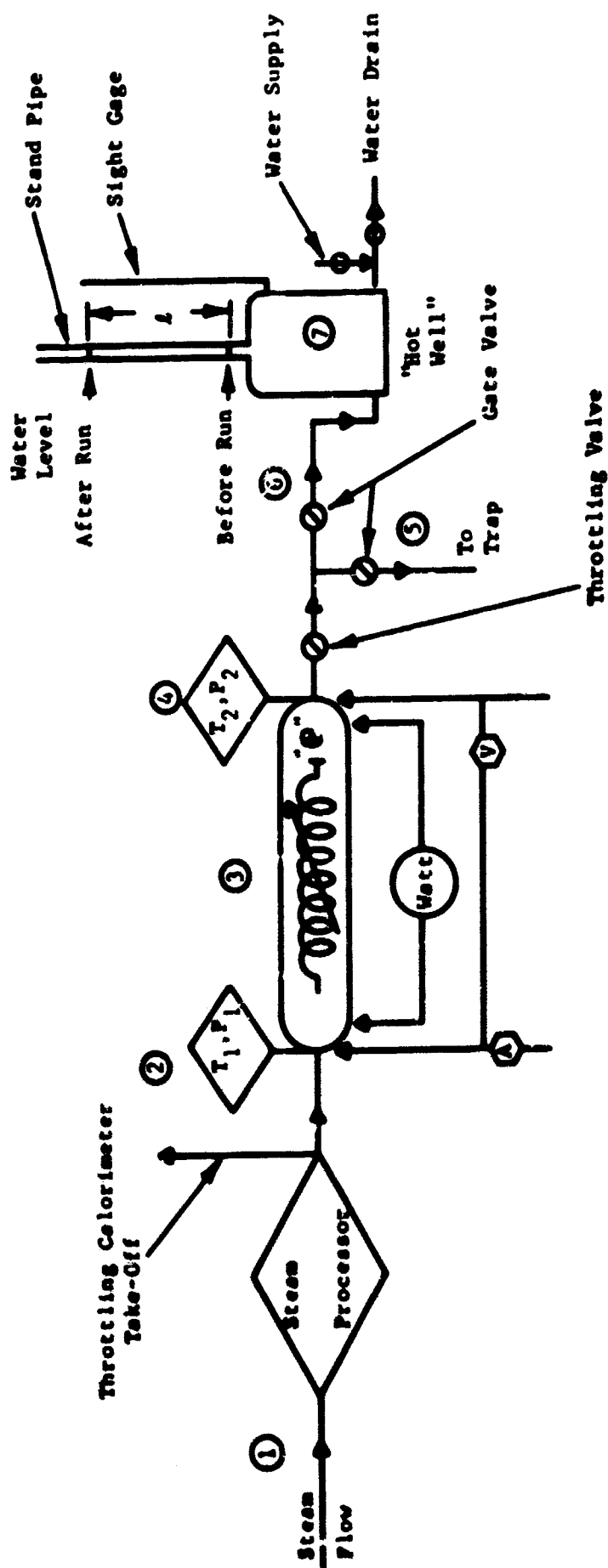


Fig. IV-5 Schematic of Electric Heating Calorimeter and "Hot-Well" Set up for Testing Steam Processors

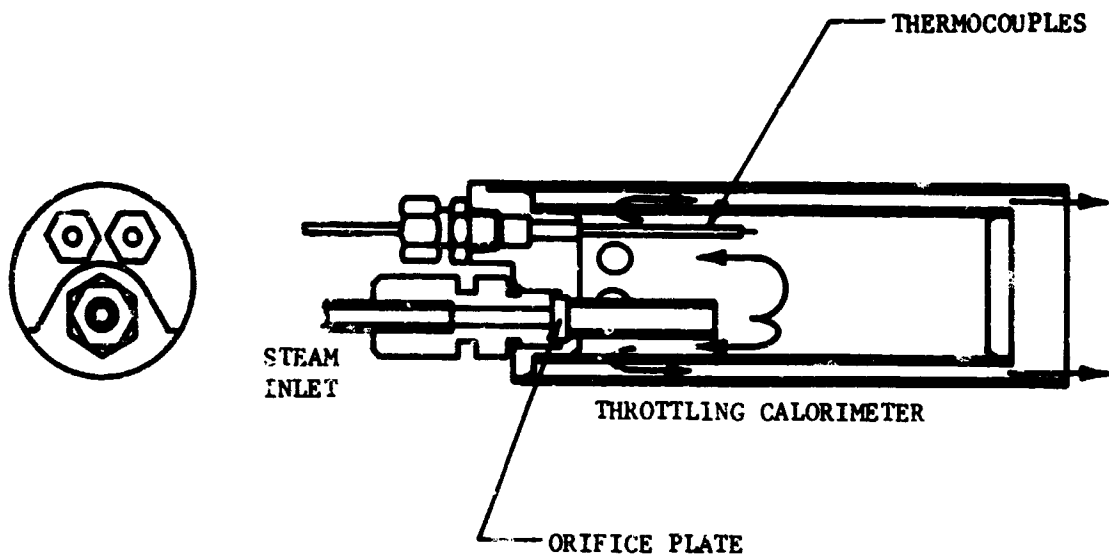


Fig. IV-6 Throttling Calorimeter

MTI-6311

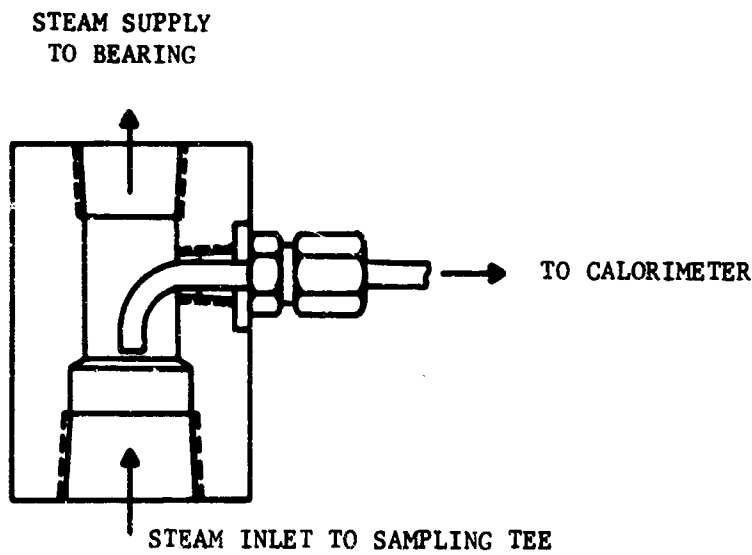


Fig. IV-7 Arrangement for Sampling from Steam Line

MTI-6312

The steam flows from the steam generator into the steam processor at point ①. A sampling tee is located downstream from the steam processor and is used to deliver a sample of the steam to a throttling calorimeter. Details of the throttling calorimeter are shown in Fig. IV-6 and details of the sampling tee are shown in Fig. IV-7. A separate main line delivers steam to a highly-insulated, spiral-finned electrical heater at point ②. At this point, both the pressure and temperature are measured and recorded. At point ③, a measured amount of heat is supplied to the saturated steam in order to superheat it. At point ④, the outlet of the electrical heating unit, both the temperature and pressure of this superheated steam are measured and recorded. The normal flow path during a test run is through valve ⑥ and into the "hot-well", ⑦. However, for a period of time preceding each run the flow is directed through valve ⑤ and to a trap, or drain. This period is necessary to obtain a steady state temperature equilibrium throughout the steam-flow system. The amount of condensate is measured by the rise in water level in the hot-well stand pipe over a given period of time. Usually 5 and 10 minute runs were made.

By recording the pressure and temperature of the superheated steam at point ④, measuring the power input to the saturated steam in order to get it to a superheated state measuring the mass flow of steam and finally by recording the measurement of pressure of the saturated steam at the point ②, one has the ingredients to determine the state of the saturated steam, and thus its quality. The steady state energy equation describing this process may be expressed symbolically as,

$$h_1 = h_2 - Q,$$

where,

h_1 = enthalpy of saturated steam at point ② in Btu/lb

h_2 = enthalpy of superheated steam at point ④ in Btu/lb

and Q = Heat Supplied to Steam, Btu/lb. [See Appendix]

The enthalpy, h_2 , of the superheated steam is defined by knowing the pressure, p_2 , and temperature, T_2 . The heat energy supplied, Q , is determined first by measuring with a wattmeter the power supplied by the electrical-resistance heater, and modifying this input by the power loss to surroundings, and second converting this heat energy by incorporating the steam flow measurement obtained by utilization of the "hot-well". The steady-state energy equation is then used to calculate the enthalpy of the saturated steam. Knowing this enthalpy and the pressure, p_1 , of this saturated steam one can determine its quality.

TEST PROCEDURE

The following test procedure was used in testing the three steam processors.

Steam was supplied to the particular steam processor in the line at a pressure p_1 , and flowed along the path points (1), (2), (3), (4) and (5). (See Fig.IV-5). Heat was then supplied to the saturated steam at point (3). After an initial "warm-up" period, say 20 minutes, all temperatures of the system reached steady-state equilibrium and the flow was then measured by incorporating the "hot-well" technique.

The steam flow path during the flow measurement was along the path, points (1), (2), (3), (4) and (6). The following data was taken:

p_1 - pressure of saturated steam, psi

T_1 - temperature of saturated steam, $^{\circ}\text{F}$

p_2 - pressure of superheated steam, psi

T_2 - temperature of superheated steam, $^{\circ}\text{F}$

\mathcal{P} - Electrical Power Input, Watts

h - total rise of water in stand pipe, in

t - elapsed time during the rise of water in stand pipe, min.

and, T_c - temperature of steam following expansion through the orifice plate in throttling calorimeter, $^{\circ}\text{F}$.

Note that at points ⑤ and ⑥, gate valves, or on-off valves were used to change the flow path and that the flow system was made flexible in the sense that the flow setting could be changed with the globe valve. This flexibility was necessary in order to better simulate actual bearing, pressure-flow conditions.

This procedure was followed for all pressures, p_1 , from 90 to 210 psig in increments of 30 psig. All processors were tested using this procedure. The double-concentric tube processor was also tested to study the effect on quality of having a pressure difference between the inner and outer tubes.

Most of the experiments were performed with the steam generator supplying the steam operating under conditions which produced very low quality steam (typically 8-10 percent moisture). This was done by using a reduced firing rate and supplying cold (about 60F) feedwater. This is regarded as an abnormally high moisture content - ordinarily, saturated steam line supply qualities are believed to be 2 - 3 percent moisture which is in line with the experimental system supply when operating with normal firing rate and preheated (120-130F) feedwater. However, this procedure permitted an evaluation of processor performance under very severe conditions.

The results of the tests are presented in the next section.

RESULTS

The results of the processor tests are summarized and presented as two tables and two graphs.

The notation of processors α , β and γ are used in presenting the results. Processor α is the double-concentric tube, long spiral-finned unit, processor β is the single tube, short spiral-finned unit, and processor γ is the 1/2" (pipe connection) commercial processing unit.

The results presented in Table IV-1 for processor α indicate the comparison of moisture content measured by both the throttling and heating calorimeters as a function of supply pressure, p_1 , and the jacketing tube pressures.

The results presented in Fig. IV-8 are also for processor α and show the relationship between the moisture content measured by the throttling calorimeter and that measured by the heating calorimeter.

In Table IV-2, the comparison of the performance of the three processors is shown as a function of supply pressure, p_1 . Also, the results using no processor are presented to show the effectiveness of the processors in reducing the steam moisture content.

Fig. IV-9 shows the data for processor γ in which the % moisture measured by the heating calorimeter is plotted as a function of flow rate. This curve illustrates the effect of flow rate on the efficiency of processor γ .

DISCUSSION OF RESULTS

The data presented in Table IV-1 show that there is a definite advantage at all supply pressures to have the jacketing pressure set at a higher pressure than that of the supply. A 20 to 30 psi pressure differential between jacketing and supply tubes delivers the highest quality steam compared to that delivered when the differential is 10 psi, or zero psi. The outer wall temperature of the supply tube will approach that of the jacketing saturation temperature and provide a drying mechanism to lower pressure, lower temperature supply steam. Thus, besides a spiral-action which causes the entrained moisture to be directed outward to the wall of the supply where it is drained and trapped, this processor also provides an added drying feature.

One should note that in Table IV-1 the data indicate a definite trend for the % moisture content measured by the heating calorimeter to be higher than that measured by the throttling calorimeter. This is typical of the results for all three processors.

The heating calorimeter is regarded as the more accurate measurement device, especially when the moisture may not be evenly distributed in the steam. All of the steam passes through the heating calorimeter while the throttling calorimeter draws a sample from the line which may not be representative. The sampling connection used with the throttling calorimeter, shown in Fig. IV-7, was designed to give a representative midstream sample. The comparison between qualities measured by throttling and heating calorimeters for processor α is shown in Fig. IV-8. The results show no consistent relationship. The throttling calorimeter generally indicates a lower moisture content than the heating calorimeter, but there is no fixed relationship. Probably, this situation reflects the variability due to sampling errors.

Comparison of results from throttling and heating calorimeters for the other two processors (Table IV-2) shows a more consistent relationship. These data indicate that the moisture fractions measured by the throttling calorimeter

TABLE IV-1

Comparison of Results for Processor - α with Various
Pressures in Jacketing Tube

<u>PRESSURE</u> <u>PSI</u>		<u>FLOW</u> <u>LB/HR</u>	<u>T*</u> <u>% MOISTURE</u>	<u>H*</u>
<u>P₁</u>	<u>Jacket</u>			
90	120	31.5	1° _s **	0.9
90	120	32.8	1° _s **	1.0
90	110	30.9	0.1	0.9
90	110	33.2	0.1	0.5
90	100	33.8	0.6	0.7
90	90	33.2	0.9	0.9
120	150	39.8	2° _s **	0.3
120	140	43.6	0.2	0.1
120	130	45.0	0.4	0.3
120	120	46.4	0.7	0.7
150	180	52.6	0	0.3
150	170	37.3	0.3	0.5
150	160	35.5	0.5	1.0
150	150	34.5	0.7	1.5
180	210	50.7	2° _s **	0.7
180	200	46.2	0.1	1.2
180	190	42.8	0.3	1.3
180	180	42.8	0.7-2.5	1.2

*T % moisture measured by throttling calorimeter

*H % moisture measured by heating calorimeter

** Indicates degrees superheat

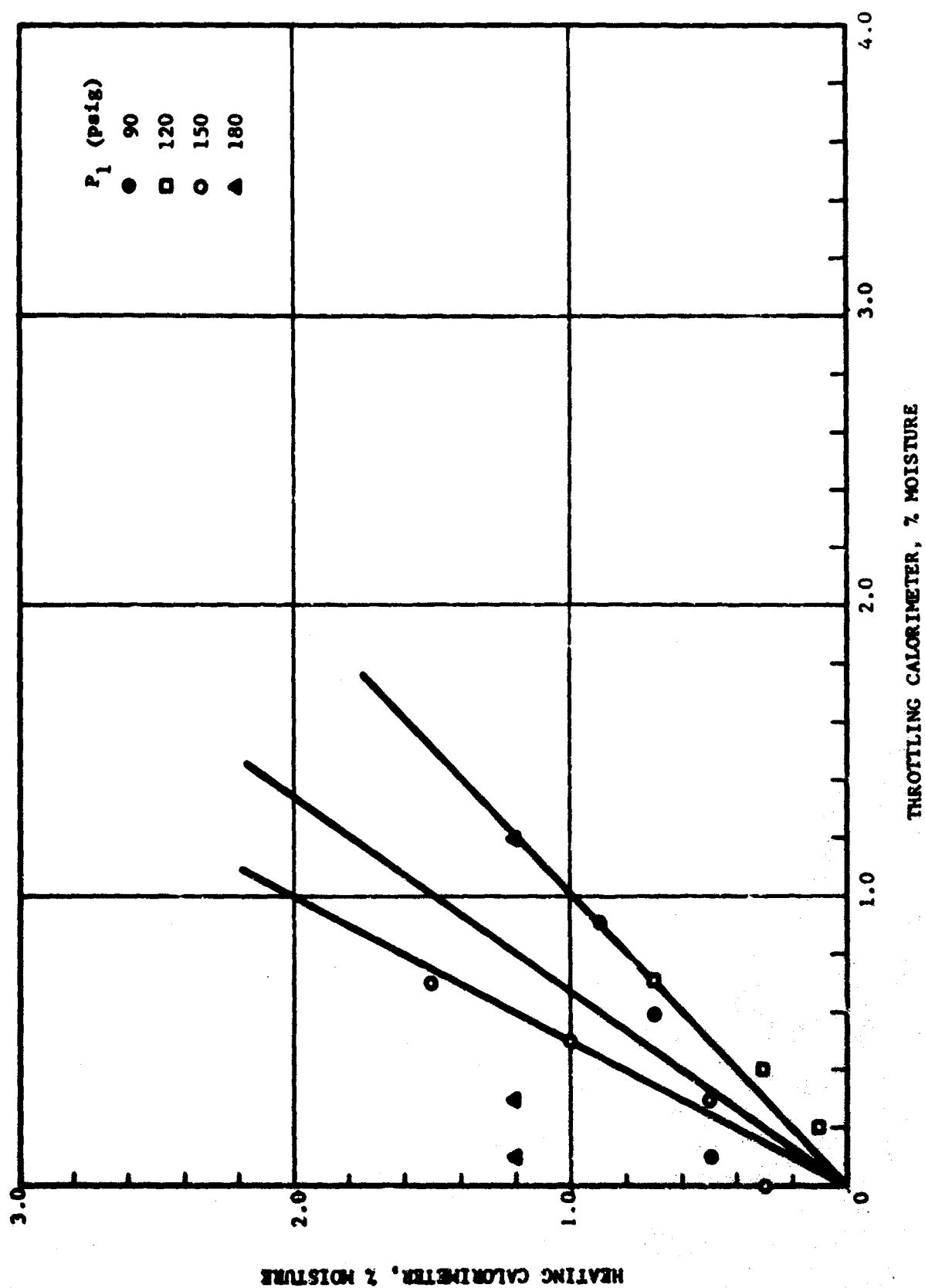


Fig. IV-8 Comparison of Measured Moisture Content: Heating Calorimeter versus Throttling Calorimeter

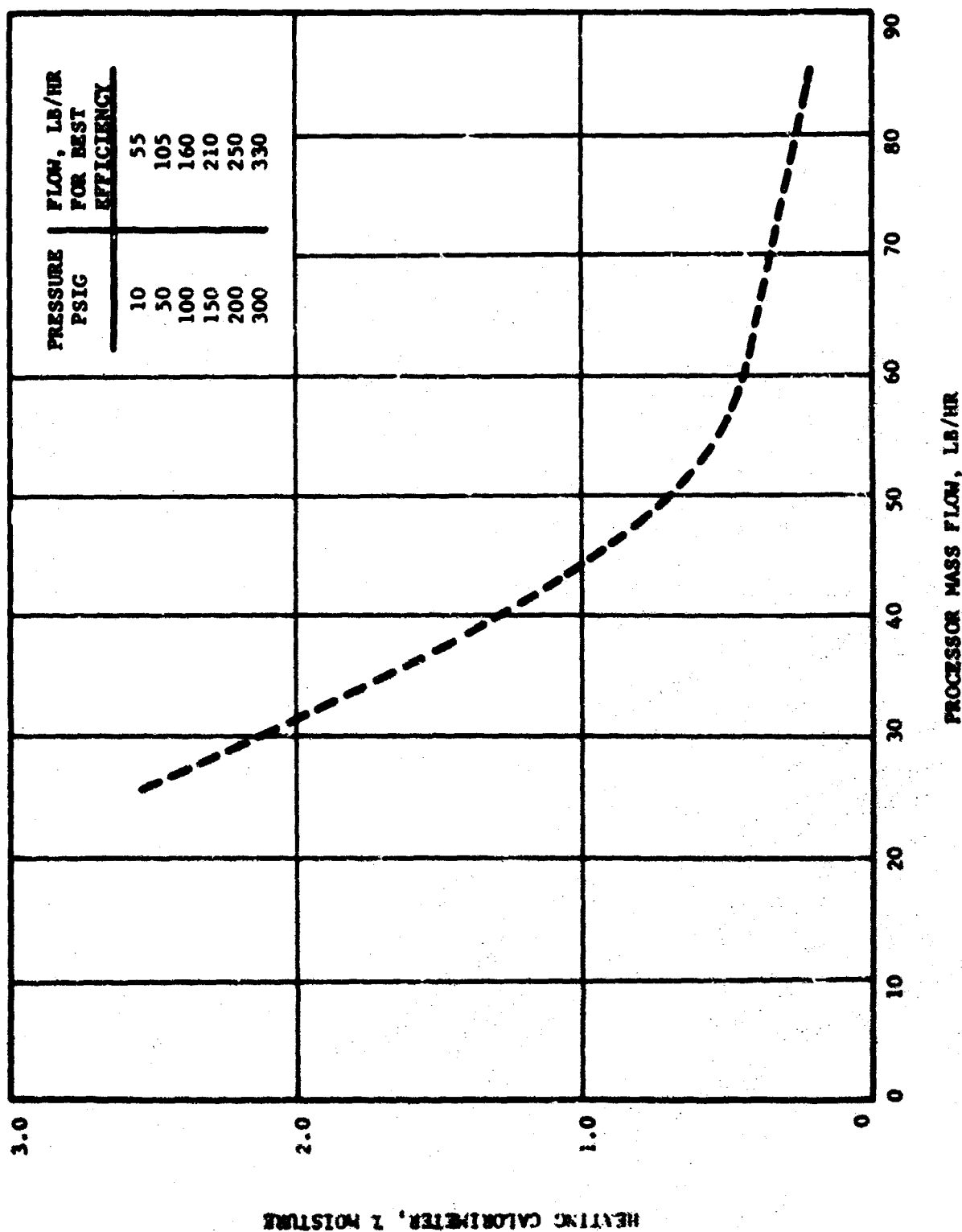


Fig. IV-9 Percent Moisture Measured by Heating Calorimeter versus Flow Rate for Commercial Processor

TABLE IV-2
Comparison of Results of Three Processors

Pressure P_1 Psi	PROCESSOR- α			PROCESSOR- β			PROCESSOR- γ			NO PROCESSOR		
	Flow lb/hr	T $^{\circ}$	H $^{\circ}$	Flow lb/hr	T	H	Flow lb/hr	T	H	Flow lb/hr	T	H
90	33.	0.9	0.9	28.	1.1	2.3	31.	0.8	2.2	23.	2.0	7.0
120	46.	0.7	0.7	38.	0.6	2.6	43.	0.6	1.6	37.	2.0	9.5
150	34.5	0.7	1.5	43.	0.6	3.2	48.	0.6	1.6	32.	> 5.3	10.3
180	30.5	0.7-2.5	1.2	47.	0.7	4.1	53.	0.7	1.9	35.	> 5.5	11.6
210				35.	1.0	2.5	62.	0.5	1.4	41.	> 5.8	11.1

PROCESSOR- α Double-concentric tube, long spiral-finned unit
PROCESSOR- β Single tube, short spiral-finned unit
PROCESSOR- γ Commercial Unit

- *T % moisture measured by throttling calorimeter
- *H % moisture measured by heating calorimeter
- ** Results for pressure of jacketing tube equal to P_1

The pressure drop across the electrical resistance heating unit ranged from 3 to 6 psi.

are lower than those measured by the heating calorimeter by a factor of 2.5 to 3.

In Table IV-2, a comparison of the results of the three processors are presented, along with data taken with no processor in the steam line. These comparative results indicate that the concentric tube, long spiral-finned processor (α) performs better than the others, particularly when the bearing supply is throttled below the jacketing supply. The commercial, mechanical separator (γ) is next in order of merit and, according to the results given in Table IV-2 it should probably be adequate even for the very high inlet steam moisture fractions used in these tests. The short-path spiral-finned processor (β) is least effective. All of these processors removed substantial amounts of entrained moisture from the wet steam supply.

The commercial separator offers distinct advantages over the concentric tube, long spiral-finned processor with respect to size, simplicity and cost. Therefore, additional experiments were performed with this separator using normal steam generator operating conditions to produce more representative inlet steam conditions. The effect of steam flow rate was investigated during these experiments. The performance of this type of separator should be flow dependent; improving with increased flow. The manufacturer's recommended flow levels for the model used are 160 lb/hr at 100 psig pressure to 250 lb/hr at 200 psig. These levels are well above those used in the initial tests. The effect of flow rate on the processor performance, as measured by heating calorimeter and using normal steam generator operating conditions, is shown in Fig. 21-2. As expected, the outlet steam moisture fraction falls significantly as the flow increases. The rate of improvement levels off around 35 percent of the manufacturer's specified flow for best efficiency, and well above the flow rate used in the earlier tests - indicating that the performance of this processor, (γ) indicated in Table IV-2 would have been improved considerably if higher flow rates had been used.

DISCUSSION AND CONCLUSIONS

The concentric tube long spiral-finned processor has been used in the steam supply lines for experiments with externally-pressurized, steam-lubricated journal bearings [IV-1] and with a thrust-bearing model configuration consisting of three circular pads, each with a single, centered feedhole, [IV-2]. Satisfactory, stable operation was achieved in both cases. Under some conditions, it was necessary to operate with a small (10 to 20 psig) difference between jacketing and supply pressures in order to have stability. Recently, the commercial separator has been used with the three-pad bearing model and this processor also performed satisfactorily, producing stable bearing operation [IV-2].

Evaluation of the three processors has brought out the following:

- 1) The performance ranking of the three processors for comparable flows and at all supply pressures is, from best to worst, the double-concentric tube, spiral-finned processor, the commercial processor, and finally the single-tube, spiral-finned processor.
- 2) The performance of the commercial processor improves considerably at high flows and, although this processor delivers a lower quality steam than the double-concentric tube spiral finned processor at low flow rates, it does deliver steam which is adequate for use in a steam bearing system. Moreover, at high flow rates, indications are that its performance is comparable with the concentric tube, long spiral-finned processor. The moisture content, measured by the heating calorimeter, is equal to or less than 0.5% for flows greater than 50 lb/hr.
- 3) The heating calorimeter measurements indicate that the steam is of lower quality than that measured by the throttling calorimeter. For the double-concentric tube spiral finned processor the relationship between the two types of measurements varied rather widely with the heating calorimeter indicating, on the average, 1.5 times the moisture content measured by the throttling calorimeter. For the commercial processor the ratio was on the average 2.5 to 1.0.

In order to fairly judge the three processors, it is not only important to compare their ability to deliver clean, dry steam, but also other items that should be considered are:

- a) initial cost
- b) cost to fabricate and/or install
- c) ease of implementation into the overall steam system
- d) compactness in size
- e) flexibility and/or adjustability
- f) amount of preventive maintenance required or reliability
- g) useful life and
- h) availability

The following rating table can then be prepared for the three processors (Rating of 1 is best or more desirable).

Consideration →	Processor →	α	β	γ
Performance (ability to deliver clean, dry steam)		1	3	2
a) Initial cost		3	2	1
b) Fabrication, installation cost		3	2	1
c) Ease of implementation		2	1	1
d) Size		3	1	2
e) Flexibility		1	3	3
f) Reliability		3	2	1
g) Life		2	2	1
h) Availability		<u>3</u>	<u>2</u>	<u>1</u>
Total		21	18	13

From these considerations, it appears that processor - γ , the commercial processor, is the best choice and it is recommended for future steam bearing system designs.

There is little doubt that the method of the heating calorimeter employed in these tests is a better or more accurate method for determining the quality of steam in comparison with the throttling calorimetry method. However, the heating calorimeter is also much more difficult to apply and to operate, it requires physical space, and interpretation of results is considerably more difficult. In particular, use of the heating calorimeter requires a very accurate flow measurement which is extremely difficult in an in-line, continuously operating system. Also, it would be necessary to use a sampling arrangement with the heating calorimeter also if it were applied to a bearing supply system and this would adversely affect its performance.

The comparative results obtained in these experiments indicate that the moisture fraction measured by the throttling calorimeter can be expected to be low by a factor of 1.5 to 2.5.

REFERENCES

- IV-1 Orcutt, F.K., Dougherty, D.E. and Malanoski, S.B., "Steam Lubrication Studies, Part I - Experimental Investigation of a Steam Lubricated Journal Bearing" prepared under Contract N00014-66-C0214 for the Office of Naval Research, MTI-67TR76, Nov. 1967. A similar manuscript, by the same authors written above and also Pan, C.H.T., entitled, "Investigation of Externally Pressurized Steam-Lubricated Journal Bearing" was presented at the ASME Lubrication Symposium, Las Vegas, Nevada, June 17-20, 1968. Paper No. 68-LubS-24.
- IV-2 Orcutt, F.K. and Malanoski, S.B., "Experimental Study of an Externally-Pressurized, Steam Lubricated, Single-Restrictor, Prepared for U.S. Atomic Energy Commission under Contract AT(30-1)-3839. Report NYO-3839-3, MTI-68TR35, August 1968.

APPENDIX

This appendix contains the equations necessary for calculating the flow Eq. (1) and heat input Eq. (2) from the data obtained from the heating calorimeter tests.

The total volume of the stand pipe, including the sight pipe is:

$$\text{Volume} = V = \text{Area} \times \text{height of water} = A \times l.$$

The inner diameter of the stand pipe is 2.848 in. The inner diameter of the sight pipe is 0.375 in. The total cross-sectional area is therefore $A = 6.48 \text{ in}^2$.

The flow may then be calculated by using an average density of the water of $\rho = 0.0361 \text{ lb/in}^3$. The flow equation is then written as:

$$\begin{aligned} \text{Flow} &= V\rho/(\text{minutes}) = 6.48l \times 0.0361/t \\ \text{Flow (lb/min)} &= 0.234l/t \\ \text{Flow (lb/hr)} &= 14l/t, \end{aligned} \tag{1}$$

where l = height of water, in.

t = time, min.

Using a conversion constant of 1 watt = 3.42 Btu/hr., the heat input, Q may be calculated as:

$$\begin{aligned} Q(\text{Btu/lb}) &= \text{Watts} \times 3.42/\text{Flow (lb/hr)} = 3.42P/\text{Flow} \\ Q(\text{Btu/lb}) &= \frac{P}{4} \times \frac{t}{l} \end{aligned} \tag{2}$$

CHAPTER V
THERMAL DESIGN GUIDE

CHAPTER V
TABLE OF CONTENTS

	<u>PAGE</u>
INTRODUCTION	159
DISCUSSION OF DUAL-HEADER BEARING DESIGN	162
THEORETICAL APPROACH	166
THEORETICAL RESULTS AND GUIDELINES	171
REFERENCES	176
NOMENCLATURE	177

INTRODUCTION

In the design of gas bearings for use in rotating machinery such as turbo-equipment, motors and generators, thermal gradients must be anticipated and the question arises concerning practical limits for gradients in the bearing region. Utilizing standard thermal analysis techniques the radial, axial and circumferential gradients existing in the bearing region may be computed. The resulting thermal distortions of the bearing may result in out-of-roundness, misalignment and tapers of the bearing components. It is distortions of this nature that the gas bearing designer should be concerned with in regards to their effect on bearing performance. Certainly distortions must be limited to within the clearance limits of the bearing. But the question arises as to what effect these distortions might have on the load capacity and stability characteristics of the bearing. It is possible to analytically examine some of these distortions by introducing the local variations in film clearances in the governing Reynolds' equation for pressure generation in the bearing. Considerable experimental work has been done, however, which can provide sufficient design direction for many design applications. In general, imperfections of the journal such as surface finish and out-of-roundness are averaged out by the bearing. This implies that the average clearance can be utilized to predict bearing performance. Results proving this point have been reported in Ref. V-1, and essentially can be used in the design of steam-lubricated journal bearings.

Steam lubrication implies elevated operating temperatures and also raises the possibility of phase change with very large accompanying change in specific volume of the lubricant as it passes through the bearing. There have been numerous laboratory investigations and practical applications of gas-lubricated bearings operating at elevated temperatures. Prior to recent work on steam-lubricated journal bearings, there was very little experience with phase change effects other than a brief investigation of steam-lubricated, self-acting bearings, (Ref. V-2), and some investigation of the effects of severe bearing surface cooling on thin-film pressure flow in a configuration resembling a thrust bearing, (Ref. V-3). Both of these investigations

indicated that phase change effects can be significant.

The most critical thermal design problem associated with steam-lubricated bearings, is not that of high temperature gas bearings - thermal distortions, but that of steam-hammer instability brought about by phase changes in the lubricant. Steam hammer is manifested as a vibration of the shaft within the bearing clearance which can be quite violent, resulting in impact of journal and bearing surfaces. Steam hammer is associated, only, with the use of a condensable vapor lubricant. That is, there is no evidence of instability when using hot air instead of steam as the lubricant. The experimental findings led to analytical investigation of two-phase flow in thin films, aimed at providing insight into the nature and cause of steam-hammer instability. A generalized solution of the problem was formulated and a limited numerical analysis was carried out (Ref. V-5). The analysis indicated that evaporation of entrained moisture in the film is most likely the cause of steam-hammer instability. Entrained droplets of saturated water entering the bearing film evaporate by boiling at the droplet surface under the influence of the film pressure gradient (as the droplet moves through the film, it experiences a steadily falling ambient pressure). The heat of vaporization is supplied principally from the internal energy of the remaining liquid within the droplet. Droplet evaporation alters the film pressure distribution and instability can result. The experimental findings support this hypothetical explanation of steam-hammer instability. There is a correlation between the supply steam quality and bearing stability.

Consistently stable operation was obtained with externally-pressurized journal bearings by using a steam processor and a dual-manifold bearing design. The steam processor is to dry the steam supplied to the bearing film. The dual-manifold arrangement includes a jacketing header to control the bearing and shaft temperature with very little loss of heat from the steam in the separate header which supplies the bearing film. The jacketing header is filled with steam at or above the supply header pressure. The shaft and bearing temperatures are maintained close to the supply steam saturation temperature by condensation of steam in the jacketing header to supply the heat losses. With these features, the bearings have consistently operated stably in a room temperature environment and with no source of heat other than the steam supply.

The evaluation of various steam processors has been carried out in another chapter of this manual. Accordingly, this chapter is a design guide which discusses the dual-manifold (header) bearing features illustrating the typical temperature fields of the bearing sleeve, lubrication film and the shaft. Design variables such as length to diameter ratio, clearance ratio, thermal conductivity, shaft diameter and wall thickness, bearing wall thickness, etc. are discussed with reference to how these may be changed to prevent or minimize condensation within the bearing film which in turn will eliminate evaporation. Recommendations are given on the necessary manifold pressures and shrouding requirements for stable operation.

DISCUSSION OF DUAL-HEADER BEARING DESIGN

Schematic diagrams of the dual-manifold, single-admission-plane, steam journal bearing is shown in Fig. V-1a and the dual-manifold, double-admission-plane, bearing is shown in Fig. V-1b. Both designs feature a dual-header system with an inner header which supplies steam to the inherently compensated restrictors (feed holes) and an outer header, covering most of the bearing axial length. The bearing sleeve surrounding the shaft has a wall thickness as small as possible. The walls of the inner manifold are also made purposely thin to provide a maximum amount of heat transfer. The outer, or jacketing, header is intended to supply the heat load represented by conduction across the flexible mount to the bearing housing, convection to the environment, and by conduction across the clearance space to the shaft with conduction along the shaft. The objective is to supply this heat load by condensation of the steam in the jacketing header with the least possible heat loss from the steam feeding the bearing film. The condensing steam must either be vented from the jacketing header to the housing cavity from a small fixed orifice, or bled to an external trapping arrangement. The orifice or trap take-off is located on one end at the lowest point on the jacketing header. The inner, supply, header and the outer, jacketing, header are supplied with steam from separate lines and they are sealed so that it is possible to operate with different, independently controlled pressures. The entire bearing is also enclosed by housing walls separating it from the ambient air. Axial shaft clearance seals installed in the housing are used in this design. The clearances may be of the order of ten times the bearing clearance.

As indicated in Ref. V-4 and V-6, this type of dual-manifold arrangement for a wide range of operating conditions, provides for an isothermal vapor film and the needed flexibility for control of steam-hammer instability. By jacketing the vapor lubrication film with a manifold of condensing supply steam, one can maintain the bearing and shaft surfaces of the vapor lubrication film superheated with respect to the local saturation temperature of the film. This superheated film condition can be obtained with standard bearing-shaft configurations and materials. This type of manifold jacketing will prevent condensation from occurring in the lubrication film if properly designed. Figure V-2 taken from

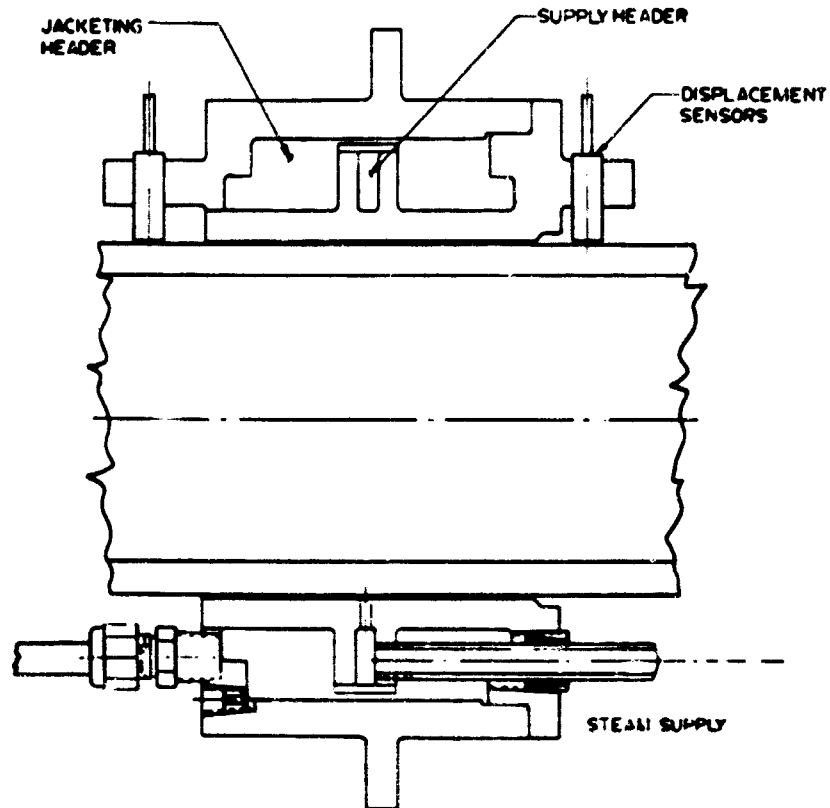


Figure V-1a Schematic Diagram of a dual Manifold Single Admission Plane Steam Journal Bearing

WT1-6271

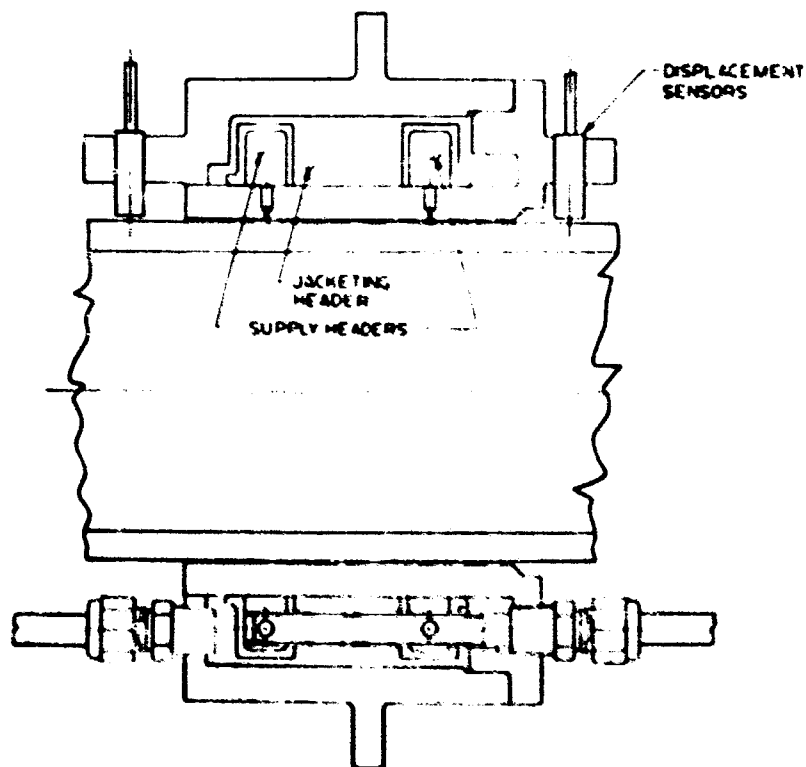


Figure V-1b Schematic Diagram of a Dual Manifold Double Admission Plane Steam Journal Bearing

WT1-6271

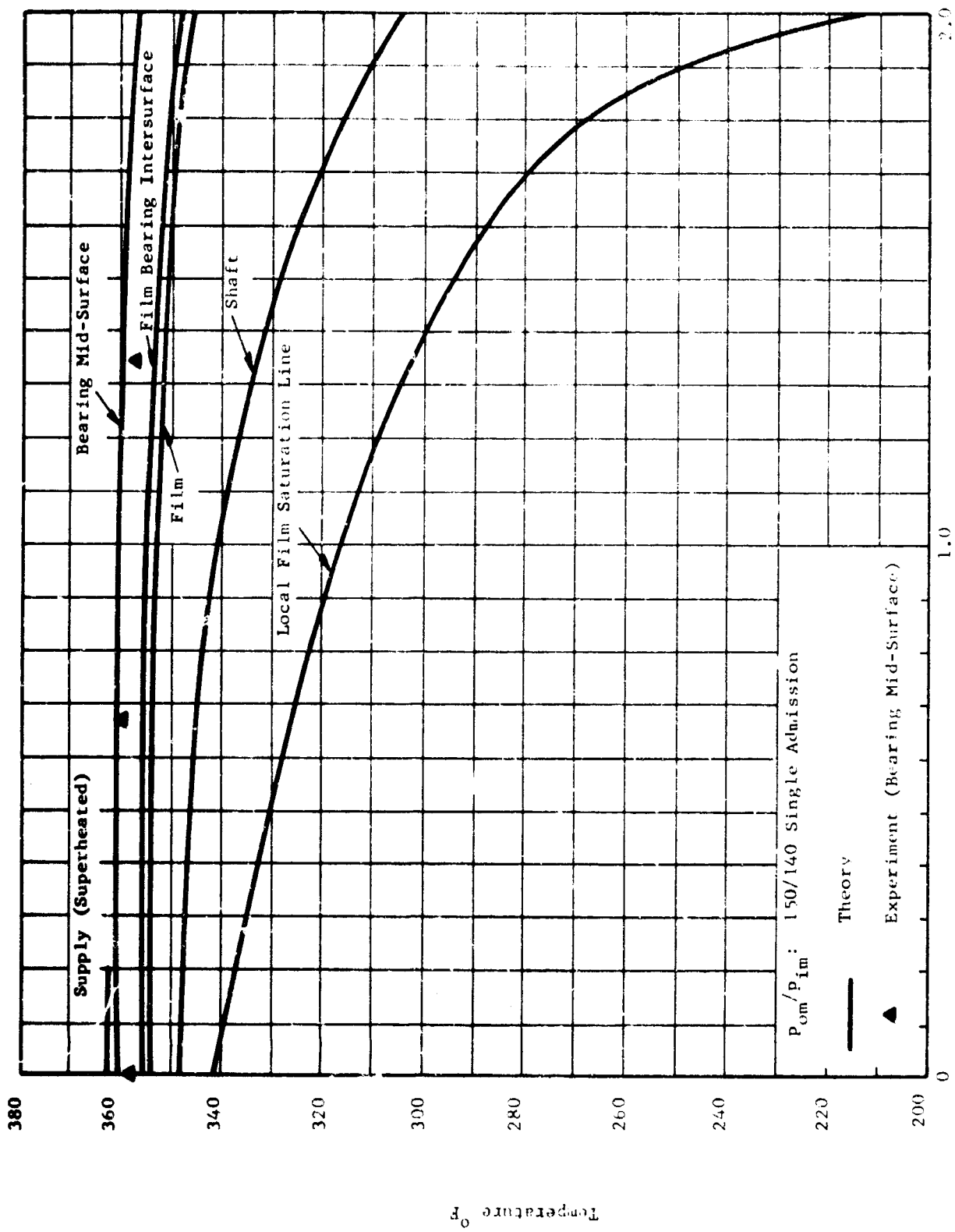


Fig. V-2 Typical Temperature Distributions in Steam Journal Bearing

Ref. V-6 illustrates that the film is essentially isothermal, and further indicates that the point of most concern is at the entrance to the bearing film. Notice that the shaft temperature has the least margin over the local film saturation temperature at this point. Thus, if the engineer can design the dual-header bearing such that the shaft temperature at the entrance to the film has a value somewhat higher than the local saturation film temperature at this point, he should have a stable design.

Recent experimental investigations (Ref. V-7) of the dual-header bearing design indicate that the stability of this steam-lubricated journal bearing is definitely load sensitive. A larger load-carrying capacity requires a larger Δp between jacketing and supply manifolds. Under zero-load applications usually a $\Delta p < 10$ psi is sufficient, however, for maximum load applications a $\Delta p \approx 30$ psi is recommended.

THEORETICAL APPROACH

The basic assumptions and equations for studying the thermal environmental problem are completely covered in Ref. V-6, and will not be repeated. However, design data has not been generated in this reference and that will be the main objective here.

The steam bearing thermal model is illustrated in Fig. V-3. This figure presents the nomenclature, temperature conditions, and energy balance. By making one more assumption, i.e. that in the so called flow region the flow is considered negligible, or $\frac{d\dot{H}}{dx} = w c_p \frac{dT}{dx} \rightarrow 0$, where w is the mass flow and \dot{H} is the time rate of change of the total enthalpy, the solution of the problem becomes greatly simplified and more amenable for design calculations.

Thus, for the trapped region the solution to the problem as indicated in Ref. V-6 is,

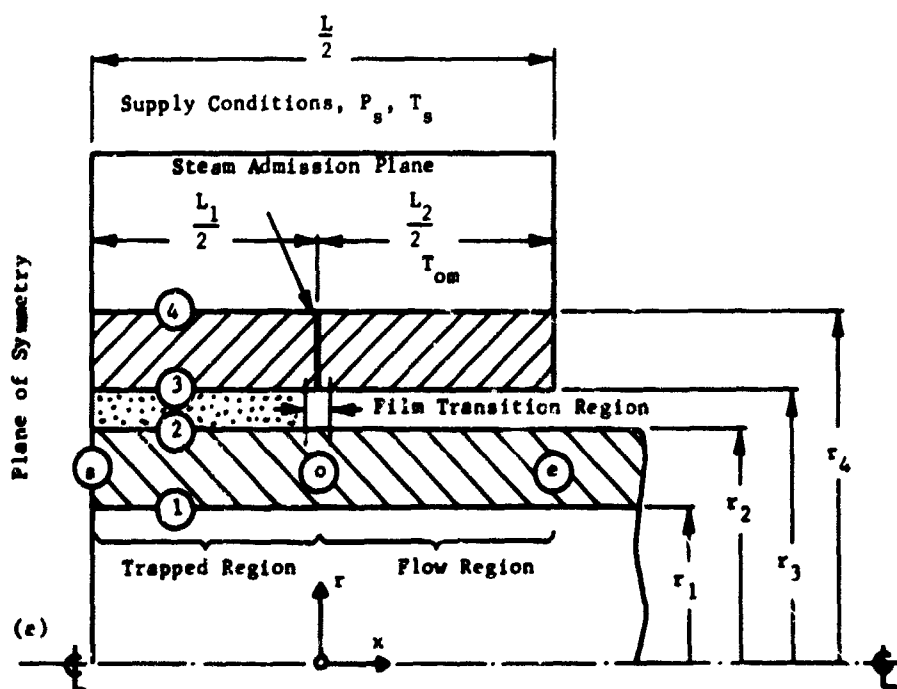
$$\theta_s = \theta_{so} \frac{\cosh \left[\sqrt{\beta} \left(\frac{L_1}{D} + \frac{2x}{D} \right) \right]}{\cosh \frac{L}{D} \sqrt{\beta}} \quad (1)$$

which satisfies the boundary conditions that $\theta_s (x = 0) = \theta_{so}$ and $D \theta_s (x = -\frac{L_1}{2}) = 0$, where D denotes $\frac{d}{dx}$.

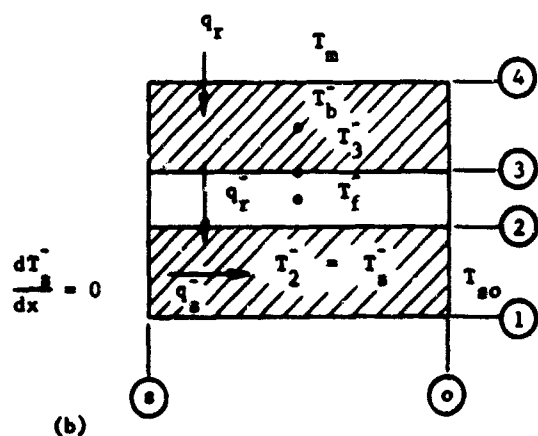
For the flow region the steady-state equations reduce to a second order, ordinary differential equation with constant coefficients similar to the trapped region. Thus, for the flow region

$$(D^2 - \Delta) \theta_s = 0 \quad (2a)$$

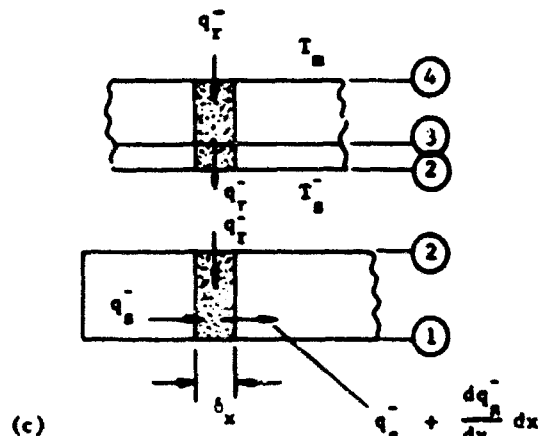
with the boundary conditions,



Steam Bearing Thermal Model

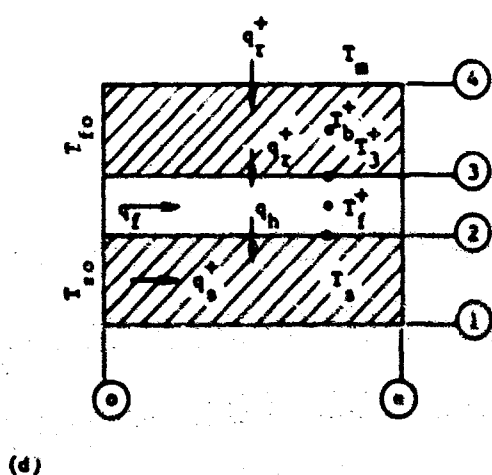


(b)

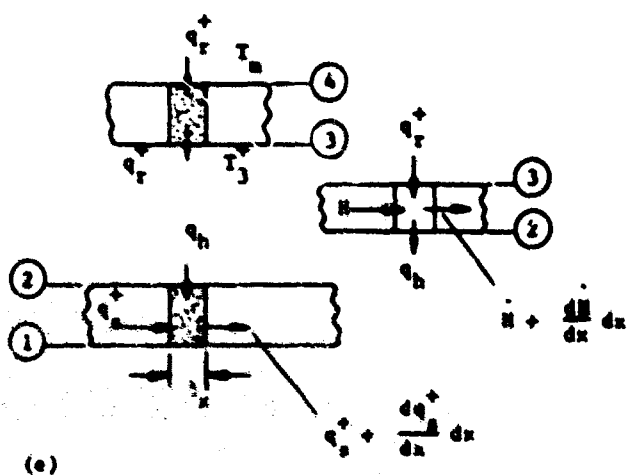


(c)

Trapped Region Temperature Fields and Energy Balance



(d)



(e)

Flow Region Temperature Fields and Energy Balance

Fig. V-3 Thermal Model, Temperature Fields and Energy Balance

$$\left. \begin{aligned} \theta_s \left(x = \frac{L_2}{2} \right) &= 1 \\ D \theta_s (x \rightarrow 0)_{\text{Eq. 2a}} &= D \theta_s (x \rightarrow 0)_{\text{Eq. 1}} \\ \theta_s (x = 0) &= \theta_{s0} \end{aligned} \right\} \quad (2b)$$

In Eq. (1) β is defined as,

$$\beta = \frac{2}{\left[1 - \left(\frac{r_1}{r_2} \right)^2 \right]} \left\{ \frac{1}{\frac{k_s}{k_b} \ln \frac{r_4}{r_3} + \frac{k_s}{k_f} \ln \frac{r_3}{r_2}} \right\} \quad (3)$$

In Eq. (2a) Δ is defined as,

$$\Delta = \frac{2}{\left[1 - \left(\frac{r_1}{r_2} \right)^2 \right]} \left\{ \frac{1}{\frac{k_s}{r_2 h_{fs}} + \frac{k_s}{k_b} \ln \frac{r_4}{r_3} + \frac{k_s}{r_3 h_{bf}}} \right\} \quad (4)$$

For all practical purposes $h_{bf} = h_{fs} = \frac{k_f}{C/2}$. Also note that $r_s = r_2 + C$, so that $\ln \frac{r_3}{r_2} = \frac{C}{R}$ and that $\frac{k_s}{r_2 h_{fs}} + \frac{k_s}{r_3 h_{bf}} = \frac{C}{R} \left(\frac{k_s}{k_f} \right)$, where $r_2 = R$. Therefore,

$$\beta = \Delta = \frac{2}{\left[1 - \left(\frac{r_1}{r_2} \right)^2 \right]} \left\{ \frac{1}{\frac{k_s}{k_b} \ln \frac{r_4}{r_3} + \frac{C}{R} \frac{k_s}{k_f}} \right\} \quad (5)$$

Now, the general solution to Eq. (2a) is written as

$$\theta_s = C_1 e^{\sqrt{\Delta} \bar{x}} + C_2 e^{-\sqrt{\Delta} \bar{x}} \quad (6)$$

where $\bar{x} = \frac{2x}{D}$.

The constants C_1 , C_2 and θ_{s0} are determined from the three conditions stated as

Eq. (2b).

The solution is

$$\theta_s = \theta_{so} \left[\cosh \left(\sqrt{\Delta} \frac{2}{D} x \right) + \tanh \left(\frac{L_1}{D} \sqrt{\Delta} \right) \sinh \left(\sqrt{\Delta} \frac{2}{D} x \right) \right], \quad (7)$$

$$\text{where } \theta_{so} = \left[\cosh \frac{L_2}{D} \sqrt{\Delta} + \tanh \left(\frac{L_1}{D} \sqrt{\Delta} \right) \sinh \frac{L_2}{D} \sqrt{\Delta} \right]^{-1}. \quad (8)$$

In the above equation θ_s is the temperature difference ratio, $(T_m - T_s)/(T_m - T_{se})$ where T_m is the known jacketing manifold temperature, T_s is the unknown shaft temperature and T_{se} is the assumed known temperature of the shaft at the exit of the bearing. In most applications the designer would not necessarily know the value of T_{se} but could probably determine a value or range of values for the heat transfer from this point either along the shaft and/or to the ambient. Thus, another form of the solution would be to eliminate the temperature difference, $T_m - T_{se}$, and include the heat transfer rate, q_{se} .

Thus,

$$q_{se} = (T_m - T_{se}) \pi (r_2^2 - r_1^2) k_s D \theta_s \left(x = \frac{L_2}{2} \right). \quad (9)$$

Using Eqs. (7), (8) & (9) one obtains the following result,

$$\theta_{so} = \frac{2\pi(r_2^2 - r_1^2) k_s (T_m - T_{so})}{q_{se} L} = \left\{ \frac{L}{D} \sqrt{\Delta} \left[\sinh \frac{L_2}{D} \sqrt{\Delta} + \tanh \left(\frac{L_1}{D} \sqrt{\Delta} \right) x \right] \right. \\ \left. \times \cosh \sqrt{\Delta} \frac{L_2}{D} \right\}^{-1}. \quad (10)$$

There are two usual design configurations: namely, the single-row design where

$$\frac{L_1}{2} = 0 \text{ and } \frac{L_2}{2} = \frac{L}{2}, \text{ and the double-row design where } \frac{L_1}{2} = \frac{L_2}{2} \text{ and } \frac{L}{2} = \frac{L_1}{2} + \frac{L_2}{2} = L_2. \text{ For these two cases Eq. (10) reduces to}$$

$$\tau_{so} = \begin{cases} \left[\frac{L}{D} \sqrt{\Delta} \sinh \left(\frac{L}{D} \sqrt{\Delta} \right) \right]^{-1}, & \text{single-row} \\ \left[2 \frac{L}{D} \sqrt{\Delta} \sinh \left(\frac{L}{2D} \sqrt{\Delta} \right) \right]^{-1}, & \text{double-row.} \end{cases} \quad (11)$$

These equations have been plotted in Fig. V-4 and the discussion of this figure follows.

THEORETICAL RESULTS AND GUIDELINES

Figure V-4 illustrates the variation of ψ_{so} with $\frac{L}{D}\sqrt{\Delta}$ for both the single-row (solid line) and double-row (dotted line) dual-header bearing design. Figure V-5 is a plot of pressure versus the corresponding steam saturation temperature. This plot is used in conjunction with Fig. V-4 when making design calculations. Some general and specific observations can be made.

General Guidelines

In general, for a given heat transfer rate, ψ_{so} should be made as small as possible such that the difference, $(T_m - T_{so})$ is minimized. This will provide the largest potential for satisfying that T_{so} be larger than the local film saturation temperature and thus minimize the possibility for condensation at the entrance to the film. Naturally, this is accomplished by making $\frac{L}{D}\sqrt{\Delta}$ as large as possible. By further examination of Fig. V-4 one notes that for a fixed $\frac{L}{D}\sqrt{\Delta}$ the double-row design has a larger value of ψ_{so} than the single-row design, indicating that the single-row design would provide the larger margin of safety against the formation of condensation.

The complete heat transfer analysis developed in Ref. V-6 has been used to run extensive checks on this simplified theory. Typical values of C/R, L/D, τ_g , τ_b , D, k_g and k_b , such as tabulated in the table below, have been used in order to establish the normal design range of $L/D\sqrt{\Delta}$ and a comparison of this simplified analysis with the more exact analysis presented in Ref. V-6.

TABLE OF VALUES

<u>Parameter</u>	<u>Min. Value</u>	<u>Max. Value</u>
C/R (mils/in.)	0.5	1.5
L/D	0.5	2.0
τ_g (in.)	0.125	0.5
τ_b (in.)	0.125	0.5
D (in.)	2.0	6.0
k_b [Btu/(hr-in. - °F)]	0.0833	8.33
k_g [Btu/(hr-in. - °F)]	0.0833	8.33

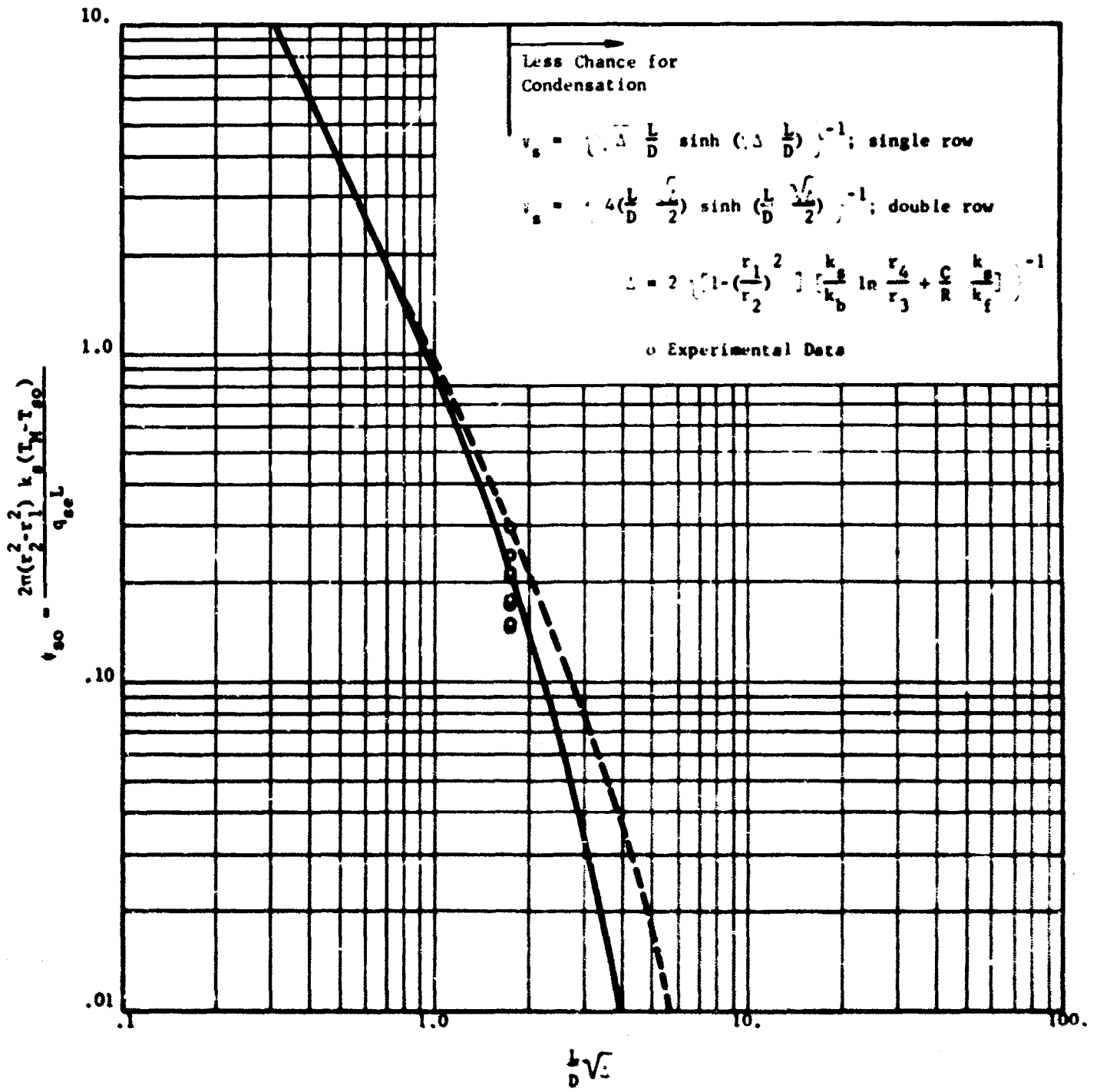


Fig. V-4 Thermal Design Chart: r_{so} versus $L/D\sqrt{\Delta T}$

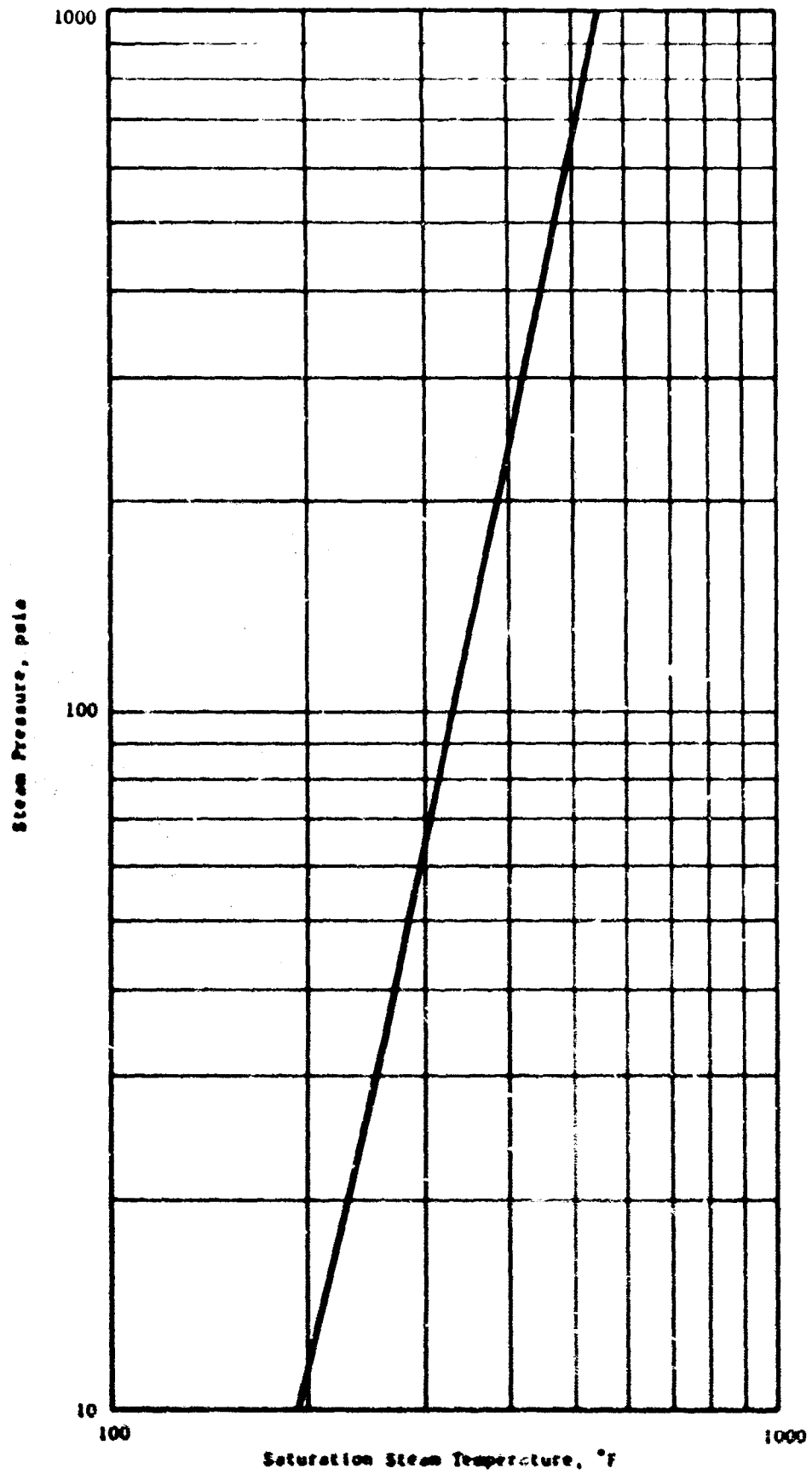


Fig. V-3 Steam Pressure Versus Corresponding Saturation Temperature

By making numerous computations with the minimum and maximum values of the parameters listed, one comes to the conclusion that the normal operating range for $\frac{L}{D}\sqrt{\Delta}$ is, $0.75 \leq \frac{L}{D}\sqrt{\Delta} \leq 4.0$. However, experience indicates that to have some assurance that condensation will not form at the film entrance $\frac{L}{D}\sqrt{\Delta}$ should be greater than 1.75 for a single-row design and $\frac{L}{D}\sqrt{\Delta}$ should be greater than 2.0 for a double-row design. Experimental data for the single-row, dual-header journal bearing discussed in Chapter II of this manual are superimposed on this figure illustrating this point.

For a given value of $\frac{L}{D}\sqrt{\Delta} \leq 2.5$ the simplified theory predicts either an equal or a larger value for \dot{V}_{so} than the more complete analysis of Ref. V-6. Thus, the simplified theory has a built-in safety factor.

A general guide to minimize the formation of condensation and enhance the protection against steam-hammer instability is to: 1) minimize $\frac{C}{R}$, τ_a , τ_b and k_g with, k_g having the strongest effect, and 2) maximize k_b and $\frac{L}{D}$ with $\frac{L}{D}$ having the stronger effect.

Specific Guidelines and Recommendations

Further indications are that the variation of $\frac{C}{R}$ from its minimum to maximum value has little effect on the change in the temperature difference, $(T_m - T_{so})$ and usually the smaller value of $\frac{C}{R}$ is best. Since smaller values of $\frac{C}{R}$ can usually bring about other problems it is recommended that $\frac{C}{R} = 1.0$ mil/in. be used whenever possible as a first design choice.

Within the range of values indicated in the table for the shaft wall thickness, τ_a , and bearing wall thickness, τ_b , there is a minor influence on the change in the temperature difference, $(T_m - T_{so})$. The smaller the thickness the better but certainly other design considerations such as shaft weight and rigidity must be factored into the overall design. It is recommended that the ratio of $\tau/D = 3/32$ be considered first. For a journal diameter of two inches this would make $\tau_b = \tau_a = 3/16$ in. for a four inch diameter $\tau_b = \tau_a = 3/8$ in. As the journal size is increased above a four inch diameter it is recommended that a maximum value of say, $\tau_b = \tau_a = 1/2$ inch be used.

Once a rotor layout is available the rotor diameter and bearing reactions can be obtained. Usually the load-capacity or stiffness requirements fix the bearing length and thus the L/D . One normally tries to design using an $L/D = 1$. However, in some instances it might be necessary to decrease the bearing length because of axial spacing limitations. This could lead to higher bearing flows. From the thermal design standpoint the larger the L/D the better. Usually the range of L/D is from $1/2$ to 2 . It is recommended that one try the initial design setting $L/D = 1$ and if the margin of safety is still judged insufficient go to $L/D = 1-1/2$ as a maximum. One should normally try to avoid bearings with $L/D < 1$.

Another parameter which has a considerable effect in the thermal design is the thermal conductivity of the shaft, k_s . The thermal conductivity of the bearing, k_b , within the range of values in the table, has a minor effect. By designing with a stainless steel shaft rather than a plated, mild-steel shaft one gains considerably in the thermal design. It is recommended, therefore, that for the initial design one should try to use a 400 series stainless steel which has an average thermal conductivity of $1.1 \text{ Btu/(hr-in.-}^{\circ}\text{F)}$.

REFERENCES

- V-1 "Design of Gas Bearings," Vol. 2, Design Notes, Section 6.5, Self-Acting Bearings, Non-Isothermal Operation, Design Manual for RPI-MTI Gas Bearing Design Course, (1966).
- V-2 Unterberg, W., and Ausman, J. S., "Condensing Vapor Lubrication of Self-Acting Long Journal Bearings," Journal of Basic Engr., Trans. ASME, Vol. 88, Series D, 1966.
- V-3 Orcutt, F. K., "Experimental Investigation of Condensing Vapor-Lubricated Thrust Bearing," ASLE Trans., Vol. 7, No. 2, p. 168 (April 1964).
- V-4 Orcutt, F. K., Dougherty, D. E., and Malanoski, S. B., "Steam Lubrication Studies, Part I - Experimental Investigation of a Steam-Lubricated Journal Bearing," prepared under Contract N00014-66-C0214 for the Office of Naval Research, MTI-67TR76, November 1967. A similar manuscript, by the same authors written above and also Pan, C.H.T., entitled "Investigation of Externally-Pressurized Steam-Lubricated Journal Bearing," was presented at the ASME Lubrication Symposium, Las Vegas, Nevada, June 17-20, 1968. Paper No. 68-LUBS-24.
- V-5 Zuber, N., and Dougherty, D. E., "Fluid Dynamics of Dispersed Two-Phase Vapor-Liquid Flow in Lubricant Films, Part I and II, Topical Report #2, prepared under Contract AT(30-1)-3839, Steam Lubrication of Turbo-Machinery, for the U. S. Atomic Energy Commission, MTI-68TR30, March 1968.
- V-6 Hsing, F. and Dougherty, D. E., "Steam Lubrication Studies, Part II, Thermal Environmental Analysis of an Externally Pressurized Steam Bearing," MTI-67TR77, Contract N00014-66-C0214, 1967.
- V-7 Experimental Investigation of a Steam-Lubricated, Multi-Bearing, Rotor System. Work presently in progress at Mechanical Technology Incorporated for the U. S. Atomic Energy Commission.

NOMENCLATURE

C	=	bearing radial clearance, in.
$C_{1,2}$	=	constants defined by Eqs. (2b) and (6)
c_p	=	specific heat at constant pressure, Btu/(lb-°F)
D	=	differential operator = $\frac{d}{dx}$, also journal diameter, in.
H	=	total enthalpy, (Btu/hr)
h	=	specific enthalpy, (Btu/lb)
h_{ij}	=	film coefficient between mediums i and j, Btu/(hr-in ² -°F)
k_l	=	thermal conductivity of medium l, Btu/(hr-in.-°F)
L	=	total length of journal bearing, in.
L_1	=	distance between admission planes ($L_1 = 0$ for single plane admission), in.
L_2	=	$L - L_1$, in.
q	=	heat rate, Btu/hr
R	=	journal radius, in.
r_1, r_2, r_3, r_4	=	inner and outer radii of shaft and bearing, in.
T	=	temperature, °F
t_l	=	thickness of wall of item "l", in.
w	=	mass flow rate, lb/hr
\bar{x}	=	$2x/D$
x	=	axial coordinate, in.
β	=	defined by Eqs. (3) and (5)
Δ	=	defined by Eqs. (4) and (5)
ψ_{so}	=	defined by Eqs. (10) and (11)
ϕ_s	=	$\frac{T_m - T_s}{T_m - T_{se}}$

Subscripts

b	=	bearing
f	=	film
m	=	jacketing manifold
s	=	shaft
se	=	shaft condition at film exit
so	=	shaft condition at film entrance

CHAPTER VI
SUGGESTED MATERIALS

CHAPTER VITABLE OF CONTENTS

	<u>Page</u>
INTRODUCTION	180
SUMMARY OF RESULTS FROM REF. VI-4	185
CONCLUSIONS	193
REFERENCES--	195

INTRODUCTION

A number of requirements must be considered in the selection of any process fluid-lubricated bearing materials. These include the following:

- Dimensional stability to both external stresses and internal metallurgical changes.
- Matched coefficients of thermal expansion between the journal and the bearings to maintain design clearances.
- Corrosion resistance to the environment.
- Erosion resistance (in the case of externally pressurized bearings).
- Good sliding compatibility to prevent surface damage or excessive wear during sliding contacts at both low and high sliding velocities.
- Ease of fabrication.

Past experience in the design and fabrication of bearing systems which must operate over a wide temperature range, has shown that a step-by-step approach in material selection is preferable to reconcile all of the system requirements. If one attempts to select a given shaft and bearing combination to satisfy all of these requirements in one package, the problems are almost insurmountable. The most logical breakdown in material selection is to choose one base material with the required bulk properties such as adequate strength, stability and corrosion resistance. Having established the identity and characteristics of this base material, coating or surface modifications can then be used, if necessary, for improved surface characteristics such as erosion resistance and sliding compatibility. This approach also eliminates the problem of matching thermal expansion characteristics since the same base material can be used for both the journal and bearings.

There are a number of dimensionally stable, high strength alloys, with good corrosion resistance to steam in this temperature range, which could be used as the base material for the journal and bearings. These include cobalt or nickel-base superalloys and a number of stainless steels. In the following table, the dimensional changes which resulted from exposure of typical alloys to steam are shown.

<u>Material</u>	<u>Temperature 600 C</u>		<u>Temperature 700 C</u>	
	<u>Thickness Increase- mils</u>	<u>Exposure Time- days</u>	<u>Thickness Increase mils</u>	<u>Exposure Time- days</u>
Type 347 Stainless Steel	+ 0.5	312	+ 1.3	371
Stellite 6	- 0.1	371	- 0.3	371
Inconel 600	+ 0.1	371	+ 1.1	371
Type 446 Stainless Steel	+ 0.1	90	---	---

With the possible exception of Stellite, none of these alloys would have good sliding characteristics in steam.

To improve the sliding behavior of these alloys, there are many coatings or surface modifications available. In general, these surface coatings can be classified into two categories:

- Soft, self-lubricating films.
- Hard, wear-resistant coatings.

The former category, self-lubricating films, has very limited applicability to the steam bearing problem. Few, if any, of these soft coatings would be able to withstand the steam environment, even at moderate temperatures.

The latter category of hard, wear-resistant coatings includes both diffusion coatings such as nitriding, chromizing, etc., and surface coatings such as platings and plasma-sprayed coatings. MTI has had considerable success in gas bearing applications with plasma-sprayed coatings and has also used these coatings successfully in short-time steam bearing tests. Combinations of these coatings have been found which have excellent sliding behavior during starts and stops and for high speed runs (Refs. VI-1,2). They are far superior to the diffusion coatings, such as nitriding, as far as resistance to sliding damage is concerned.

In addition, they can be applied to almost any metallic surface. Previous work has also demonstrated that many of these plasma coatings are very corrosion resistant, can withstand high temperature steam exposure, and have

good adherence to the substrate in air at temperatures up to at least 1600 F (Ref. VI-2). The major questions in the use of these coatings 1. their ability to withstand erosion damage in long time steam service.

Erosion damage can occur in the vicinity of the restrictors of externally pressurized steam-lubricated bearings. In this type of bearing, the pressure in the bearing film which is necessary to "float" the rotor is produced by supplying pressurized steam to the film through feedholes, or restrictors, in the bearing wall. The steam is supplied through the restrictors in order to give the bearing stiffness. Part of the supply steam pressure is expended by expansion through the restrictor with the remainder of the expansion taken across the bearing film. Figure VI-1 illustrates the restrictor-film geometry (for inherent restriction which is normally used in steam-lubricated bearings) and shows the steam pressure distribution. As the steam expands outward through the annular restrictor area, it accelerates to high velocities and erosion may occur on the bounding surfaces.

Even small changes in feedhole size at the exit or a slight degradation of the shaft surface may, over a long period of time, result in significant changes in the bearing characteristics. Erosion can result from the introduction of small, gas-borne particles from the delivery piping, or it can be a chemical and/or physical effect. The former problem can be alleviated by proper choice and corrosion protection of piping materials, good housekeeping in assembly and the use of filters. For the latter problem, corrosion-resistant materials must be used, since corrosion-resistance generally implies some measure of erosion resistance.

As noted earlier, there are a variety of materials available with suitable corrosion resistance to high temperature steam. To improve the sliding behavior of these materials, there are plasma-sprayed coatings which can be used to prevent surface damage during rubbing contacts. These coatings have been found to be suitable for use in high temperature steam environments. This leaves erosion damage as the major unknown. If it could be shown that the combination of a substrate material and a plasma-sprayed coating was

sufficiently resistant to erosion damage, then the problem of material selection would be greatly simplified. Otherwise, it would be necessary to fabricate the bearing components out of some solid alloy, such as Stellite 6B, which is generally considered to have adequate erosion resistance and sliding compatibility. Even this approach is open to question because of a lack of reliable test data to show that alloys of this type are actually suitable for this particular application as far as sliding behavior is concerned.

Considerable work has already been done to evaluate the corrosion and erosion resistance of materials in steam (e.g. Ref. VI-3), but most of this effort has been concentrated on specialized applications, such as turbine blade erosion by wet steam. The results are of limited value as far as the problem of steam-lubricated bearings is concerned. In turbine blade erosion, the loss of a mil or two of surface material is of minor consequence. In steam lubricated bearings, this would be considered as catastrophic damage. Similarly, adherent corrosion films would probably not cause any problems in most applications, but in steam bearings the thickness of these films could represent a large percentage of the bearing clearances.

To evaluate the severity of this problem of material selection for steam bearings, an exploratory program was conducted at MII. Based on past experience, a limited number of corrosion-resistant substrate materials and hard coatings, with potential capabilities for resisting sliding damage, were selected and evaluated in static tests to determine their ability to resist damage from steam erosion. From the results of these tests, two of the best combinations were then evaluated as thrust bearings in high speed rub tests.

The approach used in evaluating the materials and the results of the tests are reported fully in Ref. VI-4 and are summarized in the following section of this manual.

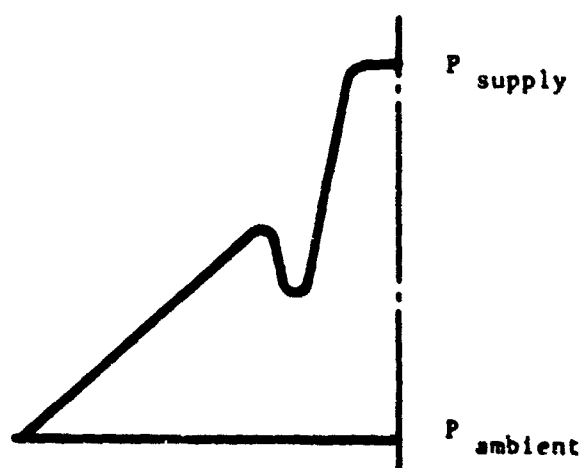
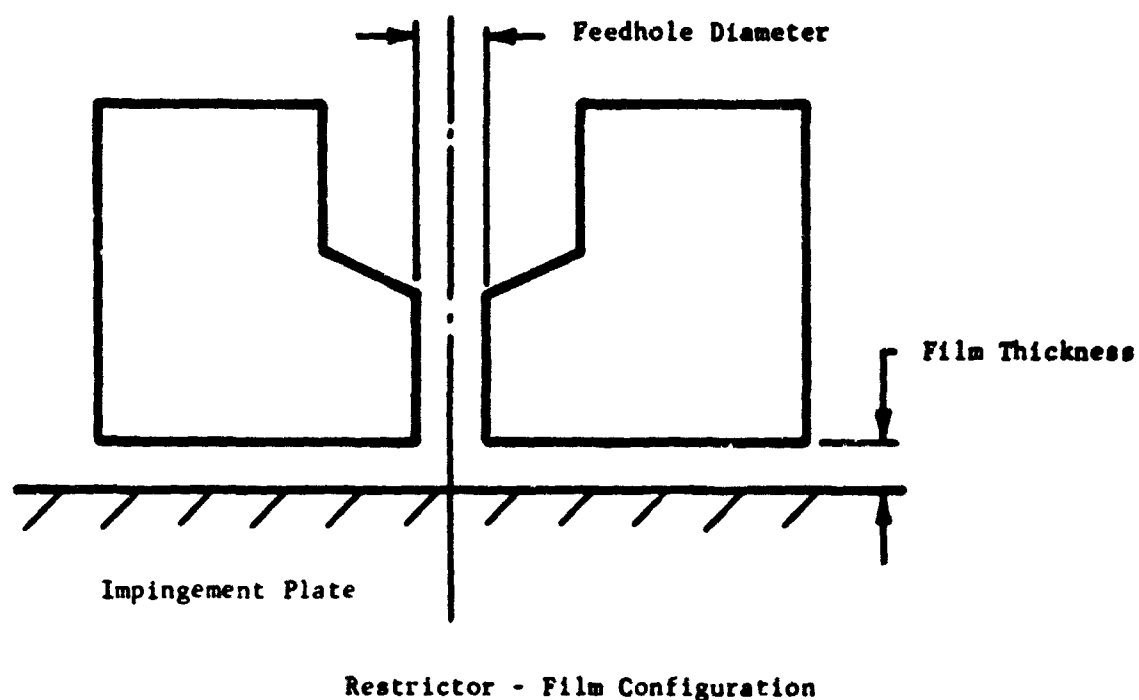


Fig. VI-1 Pressure Distribution in Restrictor-Film Configuration

SUMMARY OF RESULTS FROM REFERENCE VI-4

Problem Approach

The approach which was used consisted of the following phases:

1. The selection of a limited number of corrosion-resistant substrate materials and plasma-sprayed coatings which had known capabilities for resisting surface damage during sliding contacts.
2. The evaluation of these materials in a static erosion test to assess their resistance to erosion damage.
3. The selection of the most promising combinations and the evaluation of these combinations for high speed sliding compatibility in the steam environment.

Selection of Materials for Erosion Tests

In general, cobalt-base alloys, such as Stellite 6B, are prime candidates for any water or steam lubricated applications. These alloys have been reported by many investigators to have good erosion and corrosion resistance as well as reasonable sliding behavior. For this reason, Stellite 6B was an obvious choice as a candidate material. However, it should be noted that if it did prove to be necessary to use solid Stellite, this would remove much of the design and fabrication simplification which the use of plasma-sprayed coatings offered. Both the bearings and the journals would have to be made of solid Stellite sleeves, attached in some manner to the rest of the structure. This would present many difficulties in fabricating the bearings, especially as far as drilling feedholes was concerned. In addition, while Stellites have been used successfully in some water lubricated applications, there was still a question as to whether the sliding compatibility of these materials was good enough for a steam bearing. Experience gained on water and steam sliding evaluations at MTI (Ref. VI-5) indicated that there were better combinations available. Therefore, although solid Stellite was selected as one candidate, it was more in the line of a "back-up" material in the event that nothing else was found suitable. Also, it was considered to be a good standard to use for erosion tests.

Because Stellite coatings appeared to offer many of the advantages of solid Stellite, and eliminated some of the disadvantages, one Stellite coating, Stellite 6, was also selected for evaluation. This coating was applied by an arc-spray process.

In the category of hard, plasma-sprayed coatings, two cemented carbide compositions, nickel chrome-bonded chrome carbide and nickel-bonded tungsten carbide, were both known to have good sliding behavior and satisfactory corrosion resistance to steam. (Cobalt-bonded tungsten carbide was not considered as a candidate because the cobalt binder has been found lacking as far as corrosion resistance to high temperature steam is concerned.) Coatings of nickel-chrome bonded chrome carbide have been evaluated on gas bearing surfaces by MTI at temperatures from 100 F to 1400 F in both air (Ref. VI-2) and in argon (Ref. VI-6). These coatings were found to be very resistant to surface damage during high speed rubs. Nickel-bonded tungsten carbide is being used in the MTI NaK lubricated bearing test rig and has run very satisfactorily on water, alcohol and NaK lubrication (Ref. VI-7). This carbide coating was also used in steam bearing tests for the Office of Naval Research (Ref. VI-8).

Two plasma-sprayed, self-bonded oxide coatings were also selected for evaluation. These were chrome oxide (Cr_2O_3) and aluminum oxide (Al_2O_3). Previous gas bearing material studies had shown that both of these coatings would resist sliding damage during high speed rubs. This was particularly true of chrome oxide which has been used very successfully in a number of gas bearing machines, as well as in water lubricated bearings. Unlike Cr_2O_3 , self-mated Al_2O_3 is not a good combination, but coatings have been found which can slide effectively against Al_2O_3 .

Finally, one specimen of uncoated, annealed 410 stainless steel was included to evaluate the performance of a straight metallic alloy, even though it was known that this material would not have satisfactory sliding behavior.

Since one of the test variables was the composition of the substrate material, these coatings were applied on four different alloys to determine if this would have an obvious influence on the results. An attempt was also made to determine the effect of substrate hardness by applying the nickel-bonded tungsten carbide to both hardened and annealed 410 stainless.

The actual combinations of coatings and substrate materials which were evaluated in these tests at steam supply pressures of 60 and 150 psig are listed in Table VI-1.

Results from Erosion Tests

The order of effectiveness of these materials with 60 psig supply steam appeared to be as follows:

<u>Feedhole Plate</u>	<u>Best</u>	<u>Impingement Specimen</u>
Chrome carbide on 347 stainless		Annealed 410 stainless, no coating
Annealed 410 stainless, no coating		Stellite 6B (solid)
Tungsten carbide on hardened 410 stainless		Stellite coating on 17-4 PH stainless
Stellite 6B (solid)		Chrome oxide on 347 stainless
Tungsten carbide on annealed 410 stainless		Tungsten carbide on hardened 410 stainless
Stellite coating on 17-4 PH stainless		Tungsten carbide on annealed 410 stainless
Chrome oxide on 303 stainless		Chrome oxide on 303 stainless
	<u>Worst</u>	

In certain cases, especially on the impingement plates, this ranking is somewhat arbitrary since the difference between specimens were rather slight.

The same combinations, with the exception of the chrome oxide coated specimens, were again set up in the erosion test.

The second part of the test was run for 95 hours with an inlet steam supply of 150 psig in order to determine the effect of higher steam pressure.

The most obvious effect of increasing the inlet steam pressure from 60 to 150 psig was to increase the damage around the feedhole exit. The impingement surfaces showed slightly more damage at 150 psig, but the differences were small. This indicated that the velocity and flow pattern of the steam was much more important than the impact forces. Again, damage on the impingement surfaces was in the form of annular rings.

The order of effectiveness of these materials with 150 psig supply steam appeared to be as follows:

<u>Feedhole Plate</u>	<u>Best</u>	<u>Impingement Specimen</u>
Annealed 410 SS, no coating	↓	Annealed 410 SS, no coating
Tungsten carbide on hardened 410 stainless		Solid Stellite
Chrome carbide on 347 stainless		Stellite coating on 17-4 PH
Tungsten carbide on annealed 410 stainless		Chrome carbide on 347 stainless
Solid Stellite		Tungsten carbide on hardened 410 stainless
Stellite coating		Tungsten carbide on annealed 410 stainless
	<u>Worst</u>	

All of these material combinations showed some erosion damage. This was the intent of the tests -- to run accelerated evaluations which would make it possible to rank the materials on a relative basis. Yet, the results

TABLE VI-1 - MATERIAL COMBINATIONS EVALUATED IN STATIC EROSION TESTS
AT STEAM SUPPLY PRESSURES OF 60 AND 150 PSIG

<u>Feedhole Plate</u>	<u>Impingement Specimen</u>
Tungsten carbide coating (a) (25% WC, 7% Ni, bal. W-Cr carbides) on annealed 410 SS (16-18Rc)	Same as feedhole plate.
Tungsten carbide coating (25% WC, 7% Ni, bal. W-Cr carbides) on hardened 410 SS (40-42Rc)	Same as feedhole plate.
Ni-Cr bonded chrome carbide coating on 347 SS (40-42Rc)	Same as feedhole plate.
Stellite coating on 17-4 PH stainless (40-41Rc)	Same as feedhole plate.
(b) Chrome oxide on 303 SS (5Rc)	Same as feedhole plate.
(c) Aluminum Oxide coating on 347 SS (17-19Rc)	Ni-Cr bonded chrome carbide on 347 Stainless (17-20Rc)
Solid Stellite 6B (36-38Rc)	Same as feedhole plate.
Annealed 410 SS (16Rc), Uncoated	Same as feedhole plate

(a) All coatings ground and lapped, 0.003 inches thick.

(b) This coating failed because of feedhole edge chipping in 95 hour test at 60 psig.

(c) This coating failed because of feedhole edge chipping in 50 hour test at 150 psig.

raised the question as to whether any of the materials were suitable for long term bearing applications in steam.

To help resolve this question, an examination was made of the shaft which was used in the steam-lubricated journal bearing tests performed for the Office of Naval Research (Ref.VI-8). This shaft had a nickel-bonded tungsten carbide coating on a nickel-plated mild steel substrate. It was, therefore, comparable to the tungsten carbide-coated, annealed 410 stainless specimen which had been used in the static erosion tests. This shaft had about fifty hours of operating time over a wide range of conditions. In the erosion tests, fifty hours was certainly long enough to cause measurable erosion damage.

Since the shaft was large and bulky, replica techniques were used to examine the surface. The journal areas had one deep scratch, just outside of the restrictor region, which had been caused by an abrasive particle being trapped in the bearing. Adjacent to this scratch, the restrictor area was visible as a faint, polished, circumferential ring. Two replicas were made, 180° apart on the journal. For all practical purposes there was no indication of any surface damage or material removal from the carbide coated journal surface.

There are at least two reasons why the journal surface should not show as much damage as the static erosion test specimens. First, the journal surface is normally moving under the feedholes. Thus, the impingement area is constantly changing as the journal moves or rotates. Secondly, in the actual bearing, only about 25 percent of the total pressure drop takes place across the annular restriction formed by the feedhole circumference and the clearance gap of the shaft. In the static erosion test, about 65 percent of the total pressure drop takes place in this area. This results in choked restrictor flows in the erosion test, while subsonic flows are normal in bearings. Thus, it is apparent that the static erosion test conditions are appreciably more severe than the conditions in the bearing.

Selection of Erosion Resistant Materials for Sliding Tests

Aside from the results obtained with the uncoated 410 stainless, the best overall materials found in these static erosion tests were chrome carbide and tungsten carbide coatings. The solid Stellite 6B and the Stellite coating were both satisfactory for the impingement surface, but very questionable for use around the feedholes.

Because other gas bearing material studies had shown that self-mated chrome carbide coatings had good sliding compatibility, this was one of the combinations which was selected for the evaluation of sliding behavior in steam.

The second combination selected was the tungsten carbide coating running against the Stellite coating. If this combination did prove to be effective in sliding, it was planned that the tungsten carbide could be used on the bearing because of its resistance to erosion around the feedholes, while the Stellite could be applied to the journal for resistance to impingement erosion.

Results from Sliding Tests

The first combination which was evaluated was the nickel chrome-bonded carbide sliding against itself. This coating was sprayed on hardened 410 stainless substrates. The coating on the thrust runner was 0.003 inches thick. The thrust bearing spiral-grooved pattern was made by spraying the coating through a stainless steel mask and then grinding the coating back to form a groove depth of 0.001 inch.

This self-mated coating survived the complete series of impact loads. If anything, the hydrodynamic performance of the bearing was better at the end of the test. The contact areas were polished and no evidence of welding or tearing could be detected.

The second combination was a Stellite coated thrust bearing sliding against a tungsten carbide coated runner. This combination gave very poor results. The edges of the Stellite grooves were almost completely wiped out in the preliminary start-up runs, even before any impact loads had been applied. This wear destroyed the hydrodynamic capability of the bearing.

Since the chrome carbide had survived, not only these preliminary start-up runs but also the complete series of impact tests, this coating was selected as the most promising material to use on the actual steam bearing.

CONCLUSIONS

The experimental study reported in Ref. VI-4 was made to select material combinations for use in steam-lubricated bearings. Major emphasis was placed on the use of wear-resistant plasma coatings, sprayed on corrosion resistant substrates. These coatings have outstanding resistance to damage during high speed rubs, simplify design and fabrication problems, and have shown promise in actual steam bearings.

The work was divided into three phases:

1. A number of candidate materials and coatings, which were believed to have good sliding behavior in steam, were selected for evaluation.
2. These materials were screened in a static erosion test under conditions which accelerated damage, thus permitting a relative ranking of materials.
3. The most promising candidates from the erosion tests were then evaluated to determine their resistance to damage during high speed rubs.

The test materials included: solid Stellite 6B, a sprayed Stellite 6 coating, two metal-bonded carbides, two self-bonded oxides, and plain annealed 410 stainless. These materials showed varying degrees of damage in the erosion tests.

Uncoated, annealed 410 stainless showed outstanding resistance to erosion damage, but the sliding behavior of this alloy was known to be poor. On the impingement surfaces, solid Stellite 6B and the Stellite 6 coating were resistant to erosion, but both were damaged badly around the edge of the feedhole. Of those materials which would be most suitable for use in the steam bearing, a nickel chrome-bonded chrome carbide coating gave the best overall results. Nickel-bonded tungsten carbide on a hardened steel substrate showed good resistance to erosion damage around the feedhole, while the Stellite 6 coating was promising for the impingement surface.

An examination was also made of the surface of a tungsten carbide coated journal which had been operated for about 50 hours under a variety of test conditions in steam-lubricated bearing experiments. The results showed that the static erosion tests were actually much more severe than the application.

For the sliding evaluations, two combinations were selected. These were:

- (a) Nickel chrome-bonded chrome carbide versus itself.
- (b) Stellite coating versus nickel-bonded tungsten carbide.

These two combinations were evaluated in a hydrodynamic thrust bearing test in a steam environment to determine their resistance to damage during high speed runs. The self-mated chrome carbide showed outstanding resistance. The Stellite versus tungsten carbide combination failed in the preliminary shakedown tests.

Based on the overall results of this work, the chrome carbide coating sprayed on 410 or 416 stainless substrate appears to be the best choice for steam bearing design at this date in the development of the "state of the art".

REFERENCES

- VI-1 Murray, S.F., "Material Combinations for Hydrodynamic Inert Gas-Lubricated Bearings". Trans. ASME, Journal of Lubrication Technology, Jan. 1968, p. 49.
- VI-2 Wilson, D. and Murray S.F., "Gas Lubrication Research for 1900 F Non-Isothermal Operation". AFAPL-TR-67-57, Part I, May 1967.
- VI-3 Cataldi, H.A., Cheng, C.F., and Musick, V.S., "Investigation of Erosion and Corrosion of Turbine Materials in Wet Oxygenated Steam". Trans. ASME Oct. 1958, p. 1465
- VI-4 Murray, S.F., and Orcutt, F.K., "The Selection and Evaluation of Materials for Steam Lubricated Bearings", Topical Report No. 1, Prepared under Contract AT(30-1)-3839, Steam Lubrication of Turbomachinery, for the U.S. Atomic Energy Commission, MTI-68TR13, February 1968.
- VI-5 Peterson, M.B., and Ling, F.F., "Bearing Materials for Process Fluid Lubricants". Progress Report III, MTI-63TR41, December 1963. Contract NONR-3731(00) FBM. Task NR 391-348. For ONR.
- VI-6 "Research and Development of High-Temperature Gas Bearings". NASA Contract NAS3-9433, work in progress.
- VI-7 Murray, S.F., "Bearing and Seal Materials for Liquid Metal Lubrication". Proceedings of Technical Meeting on Super-Laminar Flow Bearings and Seals for Process Fluid Lubricated Turbomachinery, Nov. 1 and 2, 1966, Albany, New York NYO3363-6, MTI-66TR66, Contract AT(30-1)-3363.
- VI-8 Orcutt, F.K., Dougherty, D.E., and Malanoski, S.B., "Steam Lubrication Studies, Part I. Experimental Investigation of a Steam Lubricated Journal Bearing". MTI-67TR75, Nov. 1967, Contract N00014-66-C0214.

UNCLASSIFIED

Security Classification

DOCUMENT CONTROL DATA - R&D

(Security classification of title, body of abstract and indexing annotation must be entered when the overall report is classified)

1. ORIGINATING ACTIVITY (Corporate author)		2a. REPORT SECURITY CLASSIFICATION	
Mechanical Technology Incorporated		None	
		2b. GROUP	
		N/A	
3. REPORT TITLE			
Design Manual: Externally-Pressurized, Steam-Lubricated, Journal Bearings			
4. DESCRIPTIVE NOTES (Type of report and inclusive dates)			
Design Manual (Periods during 1967-1968)			
5. KNOWLEDGE/KNOWLEDGE/KNOWLEDGE/KNOWLEDGE/KNOWLEDGE Contributors:			
Bjerklie, John Malanoski, Stan B. Orcutt, Fred, K. Lund, Jorgen Murray, S. Frank Pan, Coda H.I.			
6. REPORT DATE		7a. TOTAL NO. OF PAGES	7b. NO. OF REFS
November 1968		195	35
8a. CONTRACT OR GRANT NO.		9a. ORIGINATOR'S REPORT NUMBER(S)	
N00014-66-C0214		MTI-68TR61	
b. PROJECT NO.			
c.		9b. OTHER REPORT NO(S) (Any other numbers that may be assigned to report)	
d.			
10. AVAILABILITY/LIMITATION NOTES			
No Limitations			
11. SUPPLEMENTARY NOTES		12. SPONSORING MILITARY ACTIVITY	
Gas Bearings (Steam-Lubricated)		Office of Naval Research	
13. ABSTRACT			
<p>This manual consolidates the pertinent up-to-date findings related to the design of steam-lubricated, externally-pressurized, journal bearings. It consists of six chapters:</p> <ul style="list-style-type: none"> • Design Procedures • Summary of Experimental Results • Bearing Design Methods and Data • Experimental Evaluation of Three Steam Processing Units • Thermal Design Guide • Suggested Materials 			

DD FORM 1473

1 JAN 64

UNCLASSIFIED

Security Classification

MTI-2548

UNCLASSIFIED
Security Classification

14. KEY WORDS	LINK A		LINK B		LINK C	
	ROLE	WT	ROLE	WT	ROLE	WT
Bearings, Journal, Steam-Lubricated, Externally-pressurized, Thermal, Materials, Processing, Design						

INSTRUCTIONS

1. **ORIGINATING ACTIVITY:** Enter the name and address of the contractor, subcontractor, grantee, Department of Defense activity or other organization (*corporate author*) issuing the report.

2a. **REPORT SECURITY CLASSIFICATION:** Enter the overall security classification of the report. Indicate whether "Restricted Data" is included. Marking is to be in accordance with appropriate security regulations.

2b. **GROUP:** Automatic downgrading is specified in DoD Directive 5200.10 and Armed Forces Industrial Manual. Enter the group number. Also, when applicable, show that optional markings have been used for Group 3 and Group 4 as authorized.

3. **REPORT TITLE:** Enter the complete report title in all capital letters. Titles in all cases should be unclassified. If a meaningful title cannot be selected without classification, show title classification in all capitals in parenthesis immediately following the title.

4. **DESCRIPTIVE NOTES:** If appropriate, enter the type of report, e.g., interim, progress, summary, annual, or final. Give the inclusive dates when a specific reporting period is covered.

5. **AUTHOR(S):** Enter the name(s) of author(s) as shown on or in the report. Enter last name, first name, middle initial. If military, show rank and branch of service. The name of the principal author is an absolute minimum requirement.

6. **REPORT DATE:** Enter the date of the report as day, month, year; or month, year. If more than one date appears on the report, use date of publication.

7a. **TOTAL NUMBER OF PAGES:** The total page count should follow normal pagination procedures, i.e., enter the number of pages containing information.

7b. **NUMBER OF REFERENCES:** Enter the total number of references cited in the report.

8a. **CONTRACT OR GRANT NUMBER:** If appropriate, enter the applicable number of the contract or grant under which the report was written.

8b, 8c, & 8d. **PROJECT NUMBER:** Enter the appropriate military department identification, such as project number, subproject number, system numbers, task number, etc.

9a. **ORIGINATOR'S REPORT NUMBER(S):** Enter the official report number by which the document will be identified and controlled by the originating activity. This number must be unique to this report.

9b. **OTHER REPORT NUMBER(S):** If the report has been assigned any other report numbers (*either by the originator or by the sponsor*), also enter this number(s).

10. **AVAILABILITY/LIMITATION NOTICES:** Enter any limitations on further dissemination of the report, other than those

imposed by security classification, using standard statements such as:

- (1) "Qualified requesters may obtain copies of this report from DDC."
- (2) "Foreign announcement and dissemination of this report by DDC is not authorized."
- (3) "U. S. Government agencies may obtain copies of this report directly from DDC. Other qualified DDC users shall request through _____."
- (4) "U. S. military agencies may obtain copies of this report directly from DDC. Other qualified users shall request through _____."
- (5) "All distribution of this report is controlled. Qualified DDC users shall request through _____."

If the report has been furnished to the Office of Technical Services, Department of Commerce, for sale to the public, indicate this fact and enter the price, if known.

11. **SUPPLEMENTARY NOTES:** Use for additional explanatory notes.

12. **SPONSORING MILITARY ACTIVITY:** Enter the name of the departmental project office or laboratory sponsoring (*paying for*) the research and development. Include address.

13. **ABSTRACT:** Enter an abstract giving a brief and factual summary of the document indicative of the report, even though it may also appear elsewhere in the body of the technical report. If additional space is required, a continuation sheet shall be attached.

It is highly desirable that the abstract of classified reports be unclassified. Each paragraph of the abstract shall end with an indication of the military security classification of the information in the paragraph, represented as (TS), (C), (S), or (U).

There is no limitation on the length of the abstract. However, the suggested length is from 150 to 225 words.

14. **KEY WORDS:** Key words are technically meaningful terms or short phrases that characterize a report and may be used as index entries for cataloging the report. Key words must be selected so that no security classification is required. Identifiers, such as equipment model designation, trade name, military project code name, geographic location, may be used as key words but will be followed by an indication of technical context. The assignment of links, roles, and weights is optional.

UNCLASSIFIED

Security Classification